SENSOR CHARACTERIZATION FOR LONG-TERM REMOTE MONITORING OF BRIDGE PIERS

A Thesis presented to the Faculty of the Graduate School of the

University of Missouri – Columbia

In Partial Fulfillment of the Requirements for the Degree

Master of Science

By

JOSEPH CALEB PHILIPPS

Dr. Glenn Washer, Graduate Advisor

DECEMBER 2007

The undersigned, appointed by the Dean of the Graduate School, have examined the thesis entitled

SENSOR CHARACTERIZATION FOR LONG-TERM REMOTE MONITORING OF BRIDGE PIERS

Presented by Joseph Caleb Philipps,

A candidate for the degree of Master of Science,

And hereby certify that, in their opinion, it is worthy of acceptance.

_____

Professor Glenn Washer

_____

Professor Hani Salim

_____

Professor Steven Neal

ACKNOWLEDGEMENTS

I would like to thank my advisor, Dr. Glenn Washer, Assistant Professor of the Department of Civil and Environmental Engineering at the University of Missouri–Columbia. Dr. Washer's knowledge and oversight was critical in all of the progress made on this project.

I would like to thank Paul Fuchs for his skill and shared wisdom in electronics. Thanks to Kathy Masterson, who has assisted with the majority of the project and will continue the work. Thanks to Brian Samuels, Rex Gish and Rich Oberto for their technical expertise. Finally, thanks to Patrick Earney for the use of his temperature chamber.

TABLE OF CONTENTS

LIST OF FIGURES

LIST OF TABLES

ABSTRACT

Structural instability of bridge piers resulting from scour or other natural hazards can lead to bridge collapse. A monitoring system that analyzes bridge pier behavior could prevent this type of failure by detecting conditions, such as pier tilt, that may lead to instability. The sensor system developed during this project consists of an array of low cost tilt sensors, deployed on both the pier and superstructure of a bridge, to monitor structural behavior of a bridge pier. The goal of the research presented in this thesis is to characterize the behavior of the sensors that are to be used in this system. Characterization of the sensors required analysis of several distinct sensor attributes that can often be specific to individual sensors. For example, this analysis included sensor calibration, drift analysis, characterization of temperature effects, in-situ sensor behavior, and characterization of the sensor system's resolution.

This thesis will describe the process of designing test systems required to complete the sensor characterization. The experiments performed to characterize the sensors using these test systems will be defined. Finally, the results of the testing conducted to characterize sensor behavior, and the implications of sensor characteristics on the final system's operational capability will be discussed.

1: Introduction

1.1. Overview

Structural instability of bridge piers resulting from the effects of scour or other factors has led to bridge collapse in the past. An effective monitoring system that analyzes bridge pier behavior could prevent this type of failure. This thesis outlines the progress made in developing such a monitoring system. The system will utilize an array of low cost tilt sensors, deployed on both the pier and superstructure of a bridge, to monitor structural behavior of a bridge pier. Changes in the tilt measured directly from tilt sensor output and vertical pier displacement found geometrically from the tilt sensor output are being explored. This could allow for a more complete understanding of a bridge pier's behavior than is currently possible using available technology. Signal processing algorithms, which will provide correlation of data from multiple sensors, are being developed in a separate project. These algorithms will use density of sensor groups and group locations to better measure and understand the long-term tilt and displacements of the pier.

To begin development of the monitoring system, sensors with sufficient precision were identified and their behavior was characterized. This characterization is important to the development of algorithms that will interpret sensor output into a reliable

representation of structural behavior. The project reported herein has evaluated the sensors, characterized their behavior, and developed test systems to support the system development in the laboratory.

1.2. Goals and Objectives

The goal of the research presented in this thesis is to characterize the behavior of the sensors that are to be used for long-term monitoring of bridge piers. Characterization of the sensors requires analysis of several distinct sensor attributes that can often be specific to individual sensors. For example, this analysis included:

- Operational testing of sensors
- Sensor calibration
- Stationary drift analysis
- Characterization of temperature effects
- In-situ sensor behavior on test bridge
- Long-term stationary drift characterization at controlled temperature
- Simulated long-term measurements
- Characterization of sensor system resolution

This thesis will describe the process of designing test systems, such as calibration devices, required to complete the sensor characterization. The experiments performed to characterize the sensors using these test systems will be defined. Finally, the results of the testing conducted to characterize sensor behavior, and the implications of sensor characteristics on the final system's operational capability will be discussed.

2: Background

2.1. Monitoring Systems

Natural hazards such as scour at the base of bridge piers can undermine the stability of piers in highway bridges. The term scour describes erosion of soil around a bridge foundation by water. The most common cause of bridge failures is from floods scouring bed material from around bridge foundations (FHWA 2001). Presently, there are more than 26,000 bridges in the U.S. identified as scour critical (Richardson 2003; Schall 2004). More than 3,700 bridges were damaged by scour during the period of 1985 to 1995 (Mueller 2005). Instability in bridge piers resulting from scour has been the cause of bridge failure in many cases and significant research has been to address this problem.

There is a significant number of technologies that have been developed to analyze the effects of natural hazards on pier foundations. Some of the technologies used for scour monitoring include sounding rods, fathometers and ground penetrating radar (GPR). Sounding rods consist of a rod with a large foot that rests on the streambed. As the streambed drops during a scour condition, so does the foot. This drop in height is recorded to determine scour depth. Fathometers use seismic (acoustic) waves that propagate through the water. The time required for these waves to reflect off the

streambed and travel back to the source provides a depth measurement if wave velocity in water is known. GPR uses electromagnetic signals that reflect from the interface of two different materials such as water and soil.

There are several reasons why scour monitoring systems can be ineffective. These systems will evaluate the potential causes of damage by detecting scour holes, but are not capable of determining if damage to the bridge pier has actually occurred. A relatively large scour hole can develop without the structure becoming unstable. On the other hand, a small scour hole that may be undetectable can cause structural instability under certain circumstances. Additionally, because many scour monitoring systems typically need to be partially submerged, these monitoring systems are susceptible to the high water flow and debris that is inevitable during a flood event. This can cause the systems to be damaged or destroyed at a time when their function is most critical. For these reasons, a system that can monitor structural behavior to determine any structural instability is more advantageous than a system that detects scour.

In addition to scour issues, the structural stability of piers can be undermined by unpredicted behavior of subsurface soils and by unexpected behavior of superstructure elements such as bearings. This was the case in the near-collapse of the I-787 Bridge near Albany, New York in August, 2005 (Alampalli 2005). In this case, a failure of the bearing system to perform as designed contributed to significant tilting of a pier, and one section of a steel-beam bridge nearly fell from the top of the pier. This bridge section fell to a final bearing on one inch of the pier, and a catastrophe was only averted by the fast actions of the NYSDOT. A summary of the near-collapse is contained in Chapter 3.

Systems have been developed to determine the tilt in bridge piers. These systems typically consist of very few, costly tiltmeters. Because so few sensors are used, an overall structural behavior must be assumed with only the localized behavior measurements. This behavior may not be representative of the overall bridge pier. For this reason, the actual movements cannot be determined and rigid body behavior of the pier is assumed. The low number of sensors, typically placed on the pier alone, also prevents the system from determining vertical pier displacement that may occur without significant tilt in the pier. In order to determine the vertical tilt of the structure, sensors would also need to be placed on the superstructure of the bridge to determine tilt in the bridge girders caused by vertical pier movement. Systems with a small number of sensors are also susceptible to deleterious effects from diurnal and seasonal temperature changes, sensor drift over long periods, and sensor failure.

Some states have used the measurement of tilt of an abutment or pier as an indication of scour conditions. A remote monitoring system consisting of inclinometers was tested on a bridge in California in 1999 (Marron 2000). This system consisted of two inclinometers mounted on each face of the pier, wired to a central data acquisition system that collected tilt data from each of the 18 piers on an hourly basis. This data was made available to State personnel by dialing into the system using the program *pc anywhere* (Marron 2000). Initial results from outputs of these sensors indicated that significant diurnal variations in inclinometer output were experienced, making interpretation of data difficult. A system that can compensate for these diurnal variations would make accurate interpretation of the structural behavior possible.

The instrumentation of a multistory underground parking structure used tiltmeters in an effort to measure and understand structural movements (Iskander 2001). In this case, tiltmeters were mounted on walls where motion was expected, with the goal of converting tilt measurements to structural displacements. The temperature-dependant outputs of the tiltmeters resulted in significant scatter, and as a result it was difficult to determine if the structural movements suggested by the data were actually occurring, or were simply temperature effects. The authors also indicated that the relatively short monitoring time and small number of tiltmeters used in the project presented challenges in the analysis of data, and that all possible structural motions needed to be considered in an effective instrumentation plan (Iskander 2001). The effects of diurnal temperature variations on tiltmeter response was addressed by estimating temperature effects using a sine wave function, although this method has many limitations(Schuyler 2000). The fundamental problem is that the temperatures experienced by the sensors are significantly different than the temperatures experienced within an instrumented structure. The thermal behavior of the sensors is dominated by the physical location of the sensor, i.e. in the sun, shade, adjacent to water etc. The thermal behavior of the structure is dominated by its tremendous mass, and as a result, the relationship between actual thermal movements and thermal behavior of the sensors is difficult to separate and model (Schuyler 2000).

These previous long-term monitoring systems have involved a limited number of tilt sensors on a pier and have not seen widespread use. A major shortcoming of this technique is the inability to detect the downward movement of a pier. For some cases, the downward movement of a pier undermined by scour may not be accompanied by tilt

of the pier, or the tilt may occur between measurement periods. As a result, it is desirable to design a sensor system that is capable of measuring both the tilt of the piers and any vertical motion of the pier, i.e. settlement. The vertical displacement of a pier could be monitored using tiltmeters mounted on the girders of the bridge. Under this scenario, the relative displacement of a pier would result in overall tilt of the superstructure, and this approach has been used in the past to monitor the effects of compaction grouting (Schuyler 2000). Again, temperature effects presented challenges to this application, as noted above, and long-term measurements require a more sophisticated instrumentation scheme to become effective.

Another difficulty with previous implementations of tilt meters for structural monitoring is the high cost of the inclinometers used for determining tilt of the structure. Due to the high cost of these precision sensors, a relatively small number of sensors have been used. As a result, the systems are susceptible to failure of a single sensor and have little redundancy to confirm sensor outputs through multiple measurements. The sensors used for this project are less than two hundred dollars for each unit. Some additional cost for suitable environmental enclosures is required for field application. This relatively low cost makes the use of multiple sensors more feasible.

2.2. Project Instrument Description

The monitoring system developed during this research is intended to analyze the structural behavior of bridge piers. It will utilize multiple sensors arranged along the structure in high-density clusters. The strategic placement of these clusters will allow the network of sensors to provide data of the local and overall structural behavior as well as

provide more reliable long term measurements. Sensor arrays will be combined to form a Tilt and Displacement Sensor (TDS) system that will utilize sensor groups on both the pier structure and the superstructure of the bridge. Sensor groups on the superstructure will provide vertical displacement measurements by geometrically relating the angle of the superstructure to pier movements. These are referred to as the Pier Sensor Array (PSA) and the Superstructure Sensor Array (SSA). A schematic diagram of the system concept can be seen in Figure 2-1. This shows sensor placement along the length of the bridge pier as well as on the bridge girders. A commercial system that has the ability to encompass all of these different structural behaviors is not currently available.

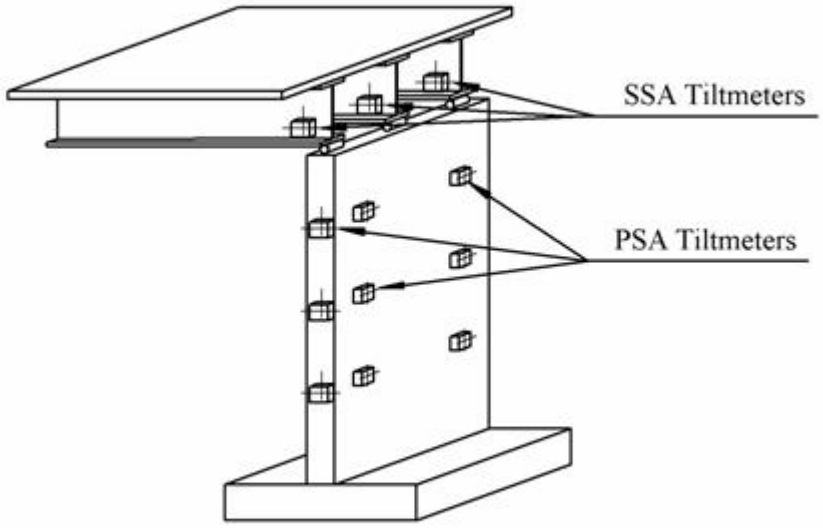

Figure 2-1: Schematic diagram of the PSA and SSA on a bridge.

The TDS system is being designed to measure long-term changes in tilt-angle and displacement of a pier, making it capable of measuring changes that may occur from not only scour, but also unbalanced superstructure loading, bridge bearing failure, long-term creep of a substructure and corrosion damage that may undermine the structural stability of a pier or column.

By understanding individual sensor behavior, a relationship between sensors in each cluster as well as in the entire network can be made. The thermal effects on the sensor, sensor drift, and resolution of the individual sensor units need to be fully understood. Characterizing the behavior of the sensors is the critical first step in developing an integrated system. The research reported here characterizes the behavior of these sensors under a variety of conditions in the laboratory, including thermal effects, erroneous readings, drift and resolution. Each sensor has a unique output due to slight variations in their manufacturing. Individual sensor characteristics create a need for calibration of their voltage outputs to determine their voltage per angle of tilt correlation.

Once the sensors' individual characteristics have been fully evaluated, the information can be used to create algorithms that improve the overall system functionality. By comparing the outputs of sensors that have been grouped together, the errors that the individual sensor will encounter can be reduced. Correlations of sensor results can increase certainty of measurements and signal to noise ratios. This research is part of the larger project of creating a long-term remote monitoring system for bridge piers. An overview of the entire project is included in the following section.

2.3. Task Descriptions

The overall project is to develop a long-term remote monitoring system for bridge piers. This includes development of instrumentation, laboratory sensor characterization, preliminary system testing, field testing, and final system development. For the overall project, there are six main tasks to be completed. These tasks provide a general path that will be followed throughout the project. They also provide milestones that are to be achieved according to the project timeline. These tasks are not all fully developed under the research presented in this thesis, but are part of the overall scope of the project and provide the context for the work completed. Following is a description of the main tasks and the activities each will encompass.

Task 1 considers the system design. During this task, the architecture and design of the integrated tilt and displacement sensor (TDS) system was completed. Initial sensor selections were made for preliminary performance evaluation, along with supporting electronics and signal conditioning.

A laboratory test fixture was designed at MU to support testing of the TDS system. The test fixture supports the evaluation of system hardware and testing of signal processing correlation algorithms. The fixture was designed to simulate controlled pier tilt and displacement such that algorithm performance can be fully evaluated, to model behavior similar to an actual bridge pier, and to provide appropriate mounting for sensors. A conceptual design of such a fixture is shown in Figure 2-2 as originally proposed. This design was modified significantly during the course of the research. Test fixtures were also designed for calibration of the tilt sensors. Calibration requires appropriate precision tilt stages that the sensors can be tested on. Both of these lab

fixtures required original designs, prototype development, testing, and development of evaluation algorithms. These portions of the project have been completed and are discussed in this report.

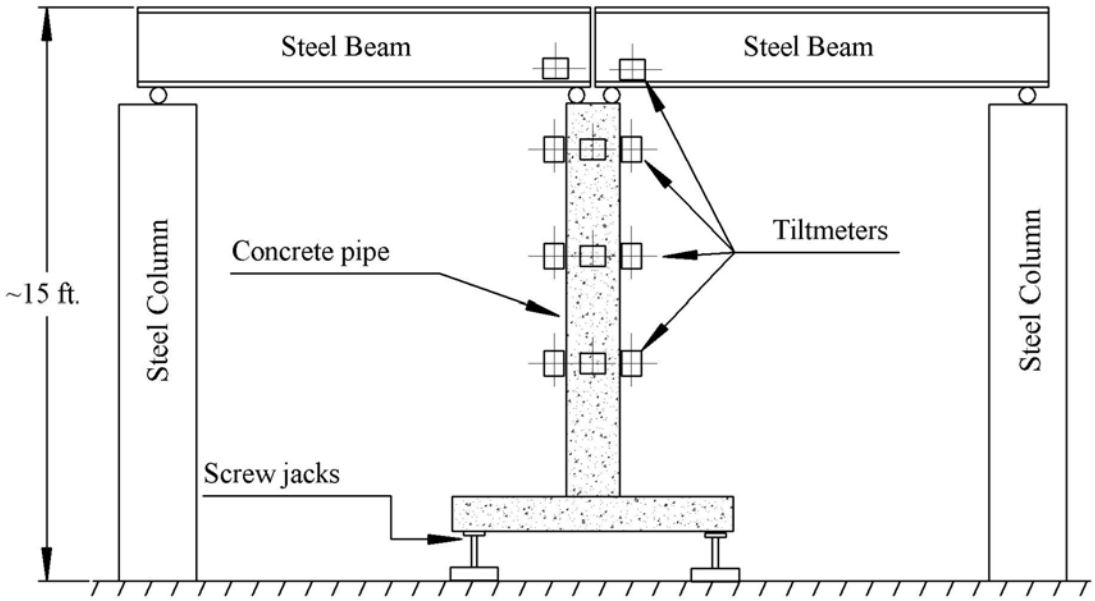

Figure 2-2: Conceptual design of test bridge for evaluation of sensor array.

Task 2 consisted of the manufacturing and construction of the sensor system and laboratory test fixtures. The manufacturing of the on-site data acquisition system was completed by Fuchs Consulting, Inc. (FCI). This system was used in the majority of the laboratory testing. It can collect data from two axes of ten sensors simultaneously. A photograph of the system can be seen in Figure 2-3.

Figure 2-3: Photograph of data acquisition system designed and manufactured by Fuchs Consulting, Inc.

This system supplies the power to the tiltmeters, logs the outputs from the sensors at a specified rate, provides temperature measurements, and provides a computer interface for analyzing data. Ten sensors with the associated electrical wirings were provided. This included 20 foot sensor cables with connectors for tilt modules and a 20 foot temperature sensor cable with sensor. Associated software was also designed by FCI. This software allows the user to collect data at various rates. These data collection rates with all ten sensors range from as fast as every 1.5 seconds to every 120 minutes. With a

single sensor only, the system can collect data as fast as every 0.2 seconds. Data is stored in a stand-alone mode within the instrument, independent of an external computer.

Construction of the test bridge and calibration stage was completed during this task. These completed systems will be used in the sensor characterization and are discussed in Sections 4.3.2 and 4.3.3.

Task 3 consists of several activities that are progressing at the same time in order to test the initial system, characterize sensors, evaluate performance and develop signal processing algorithms. The first of these activities involves testing the operation of the datalogging system provided by FCI. Data recorded by the instrument was compared to a rudimentary system consisting of a power supply, to power the sensors, and a precision multimeter. Sensor calibration was also completed in order to determine the correlation between sensor output (mV) and tilt angle for each individual sensor. The behavior of the sensors was analyzed during multiple tests. These tests determined sensor noise, drift, warm-up periods, temperature effects and resolution in order to create the appropriate algorithms for optimizing the TDS system output. A description of the experimental approach to sensor characterization can be found in Chapter 4. The results of the sensor characterization completed within this task are included in Chapter 5.

Under a separate research effort, algorithms are being developed to enable the sensors to provide reliable long-term measurements on bridge piers. These algorithms are expected to address problems such as sensor drift, sensor failure, diurnal temperature variations and low signal-to-noise ratios. The test bridge will be used to analyze the performance of these algorithms under a wide variety of pier motions that could be anticipated. These algorithms will be further refined to provide accurate and reliable data

on pier motions. A prototype TDS system, consisting of sensors, a data acquisition system and associated algorithms, will be completed by the end of this task.

Task 4 will be the responsibility of FCI and will consist of developing a finalized, field ready system that will be prepared for a field test site.

Task 5 will involve testing the prototype system at a field location. The system will be installed on an actual bridge and will be monitored during the operation.

Finally, during Task 6, a report that documents the activities and developments during the project will be completed. Tasks 4, 5 and 6 are outside the scope of the research reported here.

3: Case Scenario

3.1. Introduction

This section will provide an overview of the partial collapse of a bridge in upstate New York that involved the significant tilt and displacement of a highway bridge pier. In this example, the bridge superstructure fell from its rocker bearings as a result of displacements at the pier cap associated with a horizontal force applied to the pier from the bridge superstructure. This overview is included for three primary reasons:

- To provide a real-world example of the potential effects of pier tilt
- To provide context for the research described
- To illustrate the size, scale and type of highway bridge for which the proposed system could be utilized

This real situation, where significant tilting in a bridge pier may have caused bridge failure, is a potential application for the system being developed during this project.

The Dunn Bridge Memorial Interchange is located in the city of Albany, New York. On July 27, 2005, the bridge experienced a partial collapse of the superstructure onto a pier. Rocker bearings that support the superstructure and bear on the pier cap tipped, causing this collapse as seen in Figure 3-1. This either caused or was caused by

major deflection of a pier. After falling off the bearings, portions of the superstructure sheared the pedestal concrete and came to rest on the edge of a pier cap. The following summary will explain the structure's details; specifically the rocker bearings and pier involved in the collapse, and will define apparent failure processes that led to the collapse of the Dunn Bridge. This information is summarized directly from the NYSDOT Structural Forensic Investigation Report (NYSDOT 2005).

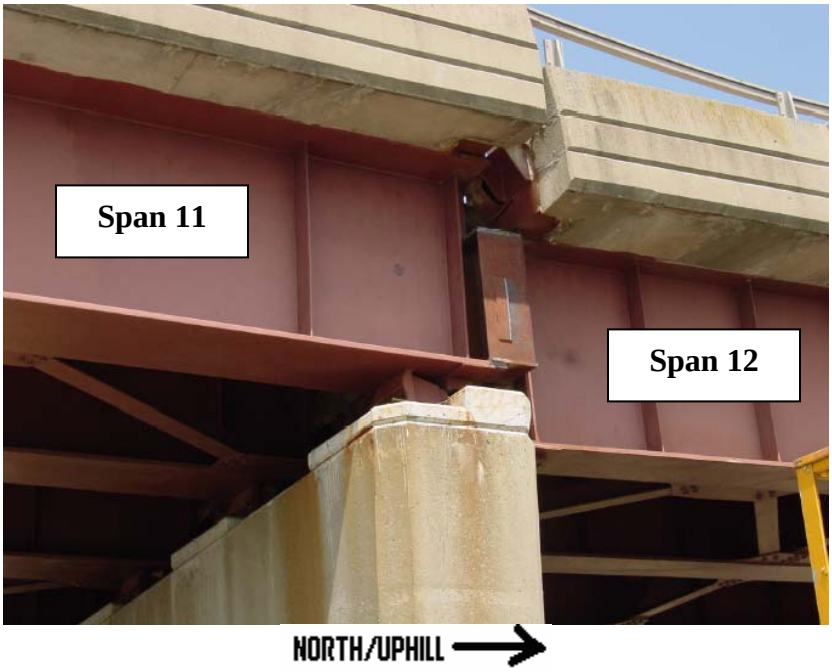

Figure 3-1: Photograph showing the fallen rocker bearings and girders after the collapse.

3.2. Structural Description

The Dunn Bridge is a ramp structure that consists of a 24 span "flyover" made up of one and two span steel girders. Single column hammerhead reinforced concrete piers support the majority of the spans. The spans involved in the collapse can be seen in Figure 3-2. Spans 10 and 11 are constructed from two span continuous girders that are 188 feet long. Spans 12 and 13 also consist of two span continuous steel girders that are

116-117 feet long (length difference due to a horizontal curve to the west after the first 50 feet of Span 12). Pier 11 is 82 feet tall, supports the ends of Span 11 and Span 12, and is the site of the accident.

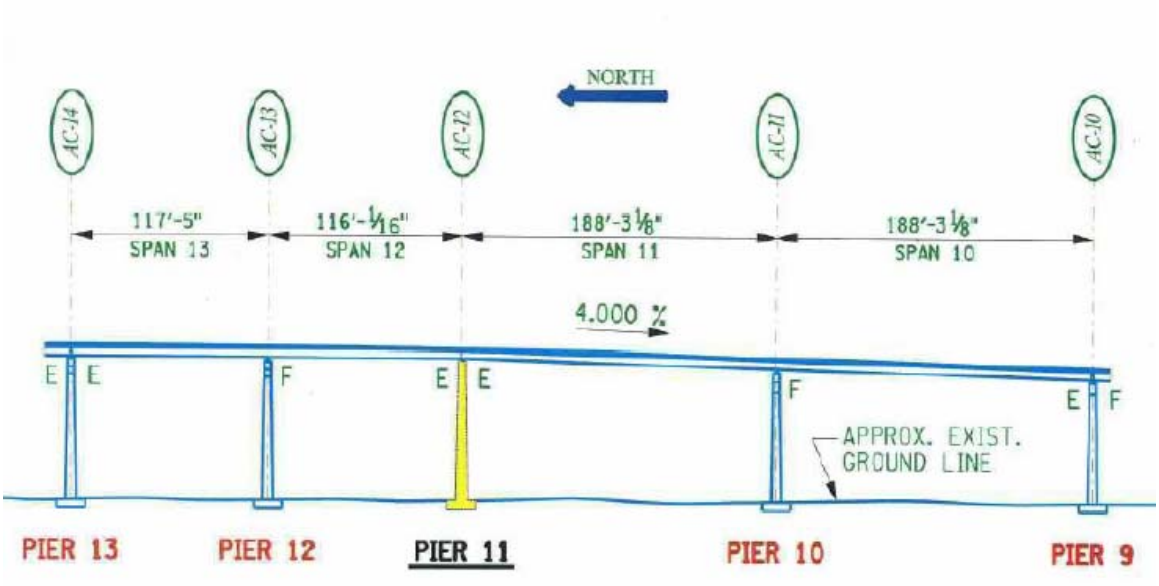

Figure 3-2: Bridge layout of the Dunn bridge, piers 9-13.

3.3. Rocker Bearing Analysis

The rocker bearings on Pier 11 were designed to allow longitudinal expansion and contraction of the structure due to thermal effects. The Span 12 rocker bearings are smaller than the Span 11 rocker bearings. This can be seen in Figure 3-3. The larger sized rocker bearings for Span 11 are due to the longer length of the span, thus larger thermal deflections. The radii and maximum displacements of these bearings are 9 inches and 2.5 inches from the centerline of the bearings for Span 12, and 13 inches and 3.25 inches for Span 11. These rocker bearings rest on a masonry plate that rests on a pedestal that is formed atop the pier cap.

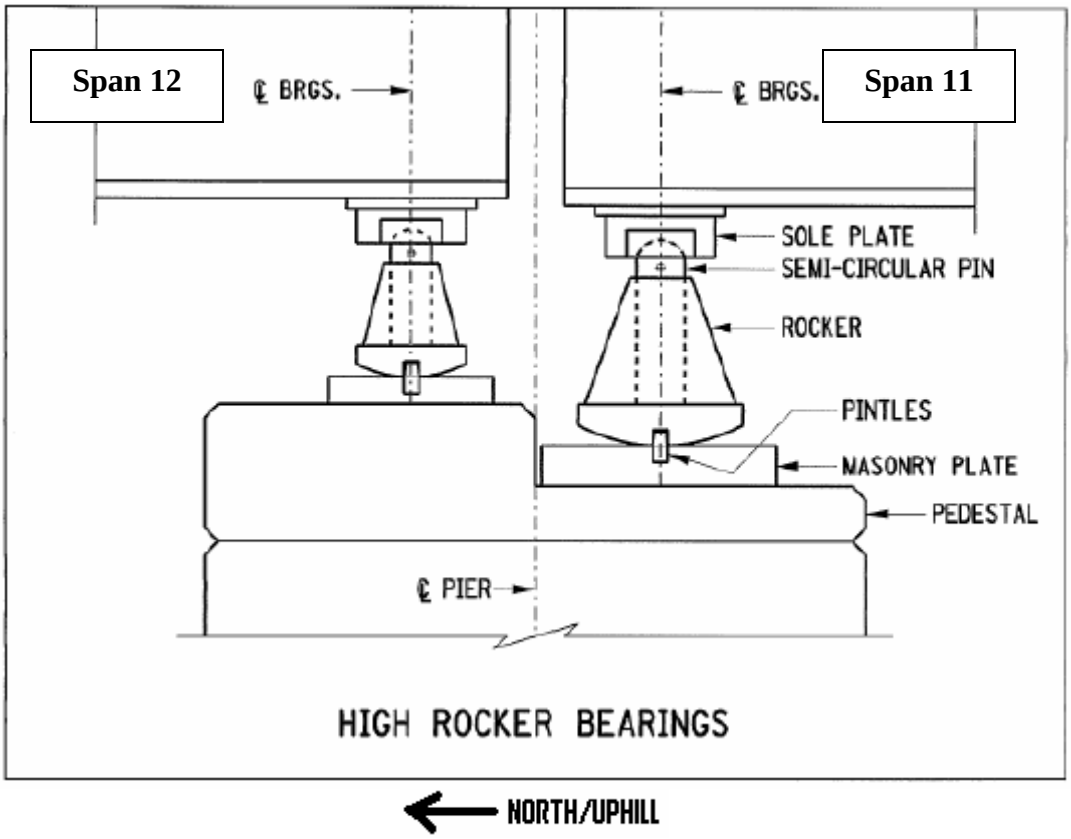

Figure 3-3: Diagram of the high rocker bearings atop Pier 11.

Tilt of the rocker bearings was detected early in the service life of the bridge during the routine bridge inspections required every other year. During the first inspection in 1985, both of the Pier 11 rocker bearings were tilted northward or uphill. At the ambient temperature during the bridge inspection, the rocker bearings should have been near vertical according to the bridge design. It should be noted that the tilting of both rocker bearings in the same direction could not have been caused by structural temperature changes. Temperature variations should cause the rocker bearings to tilt in opposite directions due to the independent expansion and contraction of the two spans. In other words, as the structure's temperature increases, Spans 11 and 12 will expand and cause the rocker bearings to tilt inward towards each other. Whenever the structure's

temperature is reduced, the spans will contract away from each other. The initial tilt was determined to have been caused by longitudinal braking forces from the northbound traffic on the ramp, which exerted a force in the uphill direction.

The tilt in the rocker bearings continued to increase through the 2003 inspection. In 2003, the Span 12 rocker bearings were overextending their design range by 0.9 inches. Although the rocker bearings were still geometrically stable, their design limit had been exceeded and they were trending towards a future geometric. A photograph from one of the inspections can be seen in Figure 3-4.

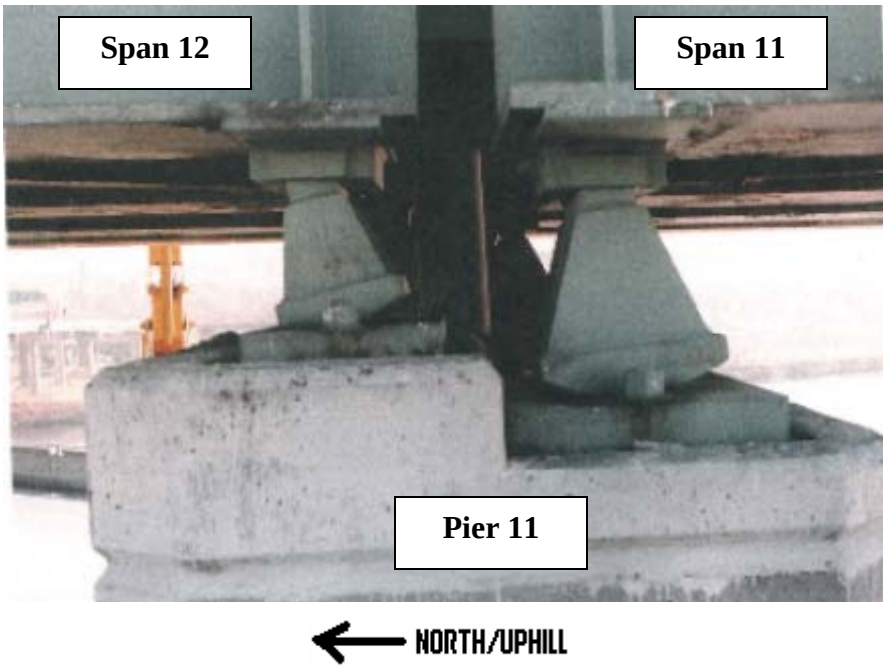

Figure 3-4: Photograph of the Pier 11 bearings during a 1989 inspection.

The rocker bearings were in the tilted position for at least the past 20 years, causing major corrosion buildup beneath them that can be seen in Figure 3-5. This corrosion prevented the rocker bearings from rotating back to their original position by forming a wedge beneath the rocker bearing. The corrosion also provided the proper amount of friction for the rocker bearings to exert large amounts of horizontal force onto

Pier 11. This force comes from the horizontal component of the vertical live and dead loads on the bridge. The transferred force made the pier susceptible to displacement rather than the bearings, thus causing a tilt of the pier originating from the applied force at its top surface.

Figure 3-5: Photograph of the corrosion in the rocker bearings.

3.4. Pier 11 Analysis

Pier 11 is a single column hammerhead pier that supports the rocker bearings for Spans 11 and 12. This pier reportedly had significantly less reinforcement than the other piers supporting the spans. The Pier 11 reinforcement ratio at its base was only 0.28 percent. This is below the minimum of 1 percent set by design codes. The lack of reinforcement made the pier more susceptible to large deflections under applied horizontal forces than a normally reinforced pier. Due to the applied force from the rocker bearings, a large deflection was created at the top of the pier and in turn became a major factor in the partial bridge collapse. This large deflection was considered to be a

failure by exceeding the designed parameters. Although unexpected horizontal forces from the rocker bearings did lead to the failure of this pier, it is notable that the overall condition of the pier, prior to failure, was very good, with a rating of 6 on a 7 point scale that is used by NYSDOT.

One of the causes of failure for Pier 11 was that the design considerations were such that they assumed the rocker bearings were always functioning properly. It has been noted that the rocker bearings were not functioning properly, causing large horizontal forces to be applied to the pier.

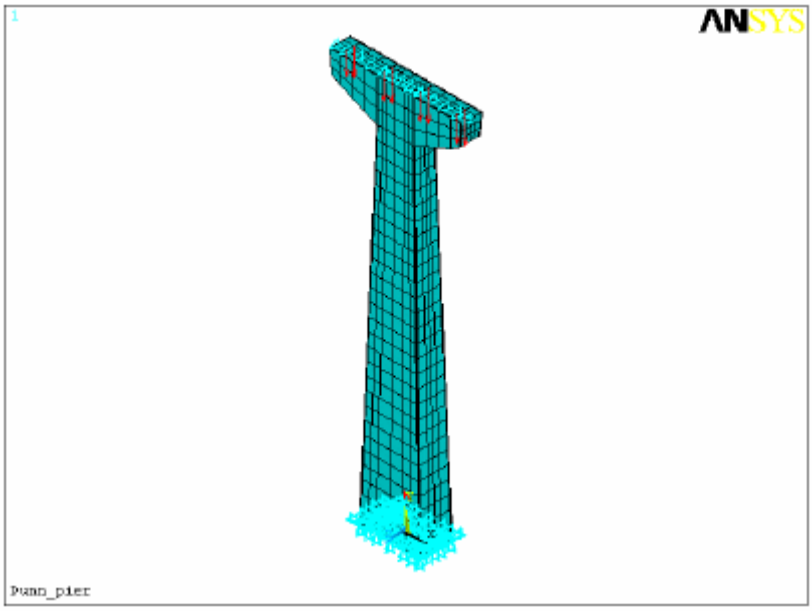

Figure 3-6: Model of Pier 11 used in finite element analysis.

After an in-depth finite element analysis of the pier was completed, a prediction of displacements at the top of the pier could be made when a given force was applied in the model. The model used during the finite element analysis can be seen in Figure 3-6. The graph in Figure 3-7 shows the displacement of the pier top as a function of increasing

applied horizontal force from the rocker bearings. It can be seen that the pier initially withstands a large force until approximately 141 kips where the concrete initially cracks. Once concrete cracking occurs, the steel begins to experience the tensile stress of the flexural mechanism.

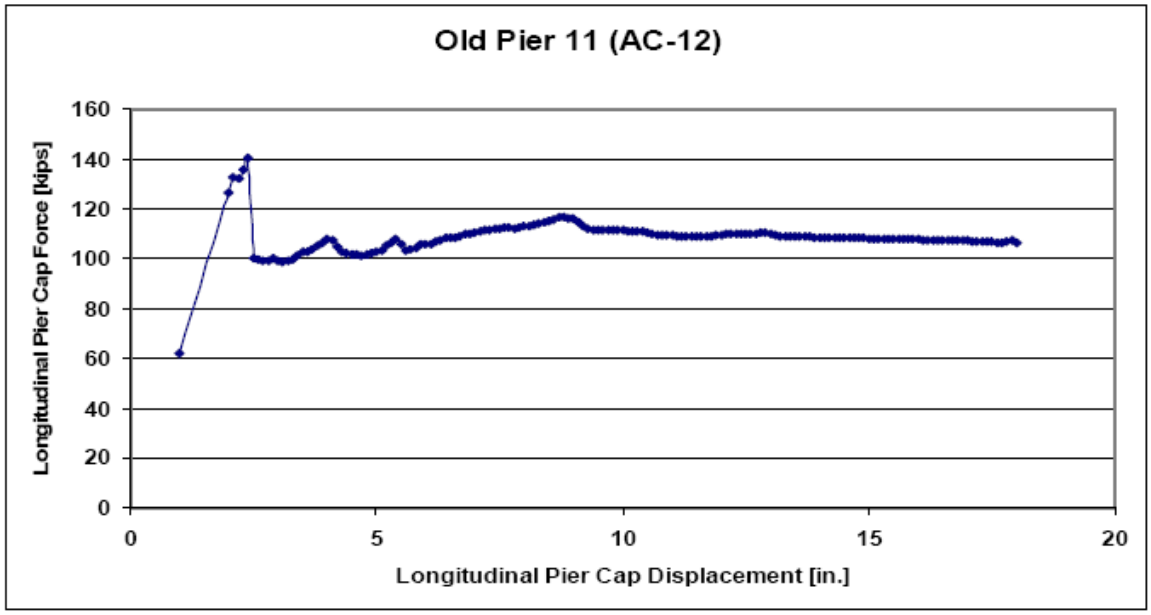

Figure 3-7: Graph of the horizontal force required to cause deflection at the top of Pier 11.

This analysis showed that the steel would begin to yield after a lateral displacement of 5.4 inches which corresponds to about 108 kips of horizontal force. This analysis was validated post-failure after restraining forces from the collapsed girders were lifted from the pier during repair. The pier deflected 5.5 inches thus exhibiting the elastic range predicted by the analysis. According to the report, the pier had very little ductility and would fail immediately after concrete cracking and subsequent steel yielding.

3.5. Failure Hypothesis

According to the NYSDOT report, the failure at of the Dunn Memorial Bridge was the combination of over-rotated Span 12 bearings as well as Pier 11 exceeding the designed displacement. It was proposed by the report that this leads to two possible failure scenarios. The difference in these failure modes is dependent upon when Pier 11 exceeded its displacement parameters.

According to the report, the first scenario is that the force exerted by the tilted bearings caused the column to fail in flexure. This caused a large southward deflection in the pier, allowing the bearings to overextend and tip. This scenario can be seen in Figure 3-8.

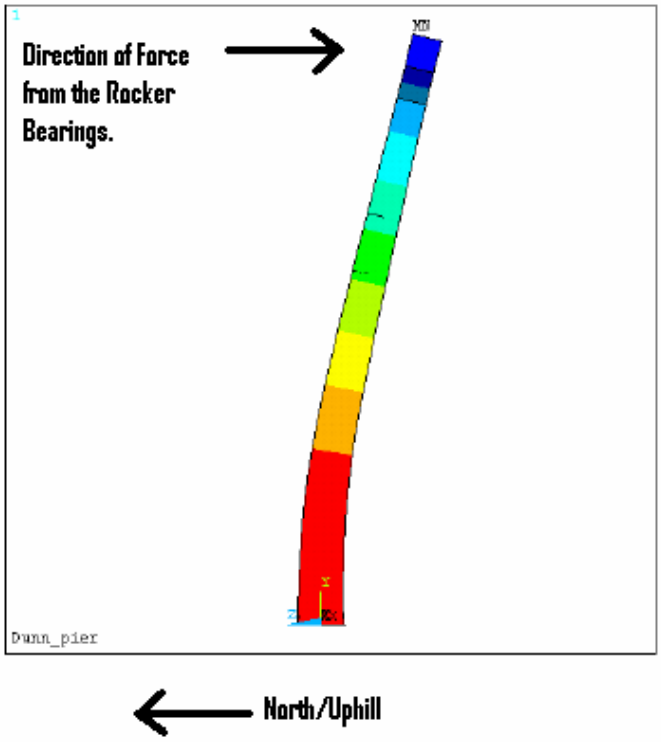

Figure 3-8: Diagram of Pier 11 deflecting from the horizontal load applied by the rocker bearings.

The second scenario is that the bearings, known to be overextended from the 2003 inspection, tipped first. This applied a sudden force onto Pier 11 immediately causing column failure.

3.6. Conclusion

According to the NYSDOT report, both scenarios described above are possible and a definitive conclusion could not be found. However, the factors leading up to either scenario exhibit problems of identical importance. Over-extension of the bearings led to the collapse of the two spans onto the top of Pier 11. The tilting pier allowed these bearings to reach their overextended state. The order of events is not of significant importance. Identifying and resolving the factors that led to the collapse is important so that future issues of similar nature can be investigated. Understanding this collapse could prevent future accidents that could end much more tragically.

The application of tiltmeter technology for a problematic bridge pier, such as the one described here, is one method of measuring movements exhibited by the structure. The data obtained by a tiltmeter sensor array could be analyzed to determine if a measured structural displacement is becoming worse or if the structure is remaining stable. With a system such as this available, a bridge owner could better analyze the changing condition of a structure, such as a bridge pier, and identify when abnormal behavior is exhibited. Monitoring the Dunn Bridge to detect pier displacements of high magnitude could have allowed officials to notice that a problem was developing such that actions could have been taken to prevent the collapse of the spans. If the failure scenario

was such that the pier exhibited measurable tilt beyond normal behavior, the bridge could have been closed for repairs.

4: Experimental

4.1. Introduction

The experimental section will provide a description of the sensor development, testing platform development and characterization test set-up that will be found in Sections 4.2. 4.3. and 4.4. respectively. Sensor development was the first step in the characterization of the sensor system and was the foundation for the ensuing tests. Development of testing platforms was necessary for the analysis of the sensors. Characterization tests were planned to analyze the sensors and will define the adequacy of the sensor system.

4.2. Sensor Development

The selection and testing of sensors that are to be used during the overall project was the first step in the experimental process. Sensors were selected based on their precision, durability, range, cost and potential to be practically applied to highway bridges. The sensors were tested to ensure that their function in the project was suitable. This section will further describe the sensor selection process.

4.2.1 Sensor Selection

A key component to the TDS system is the tilt sensor. Sensors that are inexpensive, reliable, durable, and precise are required. An electrolytic tilt sensor was selected over a MEMS-based technology due to the greater stability and precision allowed by electrolytic sensors. The initial sensor used was the EZ-TILT-2000-008-rev2 dual-axis electrolytic sensor and can be seen in Figure 4-1. The sensor was manufactured by Advanced Orientation Systems Inc. (AOSI). Specifications for this sensor are shown in Table 4-1. This sensor has an adjustable tilt range of +/- 15 arcdegrees and an analog output of 1-4 Volts giving the sensor 0.1 Volts/Degree. This sensor was used in several tests that will be described later in this thesis. To achieve high resolution with this sensor, which had outputs of only a 3 Volt range; a low angular range was required. The low angular range of this sensor made installation difficult. The sensor had to be leveled precisely so that it would not exceed the tilt range that it was capable of measuring. As a result of initial testing, a different sensor based on the same principles, but with different angular and voltage range values was selected for implementation in the laboratory system.

Figure 4-1: Photograph of the EZ-TILT-2000 rev-2 sensor.

Table 4-1: Specifications for EZ-TILT-2000 rev-2

Specification	Data	Description/units
RANGE	-15 to +15	Arcdeg
Analog Out	1Vdc to 4Vdc	adjustable gain for Full Scale
PWM Out	10% to 90% @	adjustable for Full Scale
2 Thresholds	0Vdc to 5Vdc	adjustable angle for each axis
SUPPLY	6 to 12	Vdc
RESOLUTION	12	bit
RESPONSE TIME	40 mS	10% - 90% Output *#
REPEATABILITY	<0.02 arcdeg	Typical
SYMMETRY	<0.3% @ 8°	after correction
LINEARITY	<0.3% @ 8°	after correction
SENSING ELEMENT	Dual axis DX-008	(Included)
CONSTRUCTION	Shatter proof	Hi Temp Advanced Polymer
TEMPERATURE	-40 to +60	degC
RS232	300-38Kbs,8,N,1	any standard COM port

The EZ-Tilt 3000 modules with DX-008 sensors that were chosen as the primary sensor for the project are also manufactured by (AOSI) and is shown in Figure 4-2. These sensors provide a larger voltage and angular range. The larger range allows for sensor placement without precision leveling of the module during the field installation process. The modules provide a dual axis angle measurement solution with an analog sensor output. The actual sensor, the DX-008 consists of a dual axis, five pin, electrolytic tilt sensor shown in Figure 4-3. The sensor can be removed from the module to be mounted separately from the supporting electronics. For example, mounting the sensors within a concrete structure would allow the sensor to react in accordance to the structure with respect to temperature changes. Specifications can be seen in Table 4-2. The total range of +/- 20 arcdegrees includes a linear range of +/-8 arcdegrees.

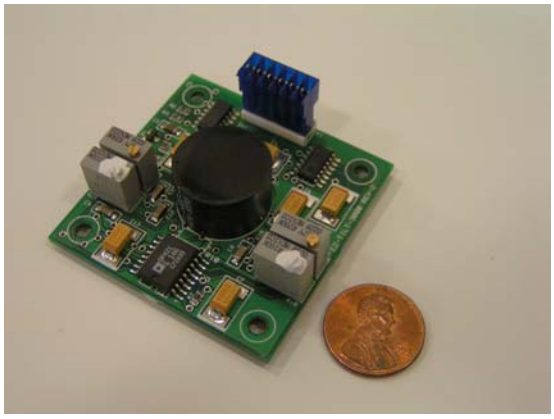

Figure 4-2: Photograph of an EZ-Tilt 3000 Module with a DX-008 Sensor.

Table 4-2: Specifications for EZ-TILT-3000 with a DX-008 Sensor.

Specification	Data	Description/units
RANGE	-20 to +20	Arcdeg monotonius
RANGE	-8 to +8	degrees Linear
SUPPLY	5 to 18	Vdc
CURRENT	2mA	@ 5Vdc Supply
RESPONSE TIME	40 mS	10% - 90% Output *#
NOISE	<1mVdc	Band Width 0Hz to 100Hz
LOAD (min. R)	3Kohm	On -X- and -Y- Outputs
REPEATABILITY	<0.02	arcdeg Typical
RESOLUTION	< 3 arcsec	Typical
SYMMETRY	<2% @4°	Typical
LINEARITY	<1% @ 8°	Typical
SENSING ELEMENT	Dual axis DX-008	(Included)
CONSTRUCTION	Shatter proof	Hi Temp Advanced Polymer
TEMPERATURE	-40 to +60	degC

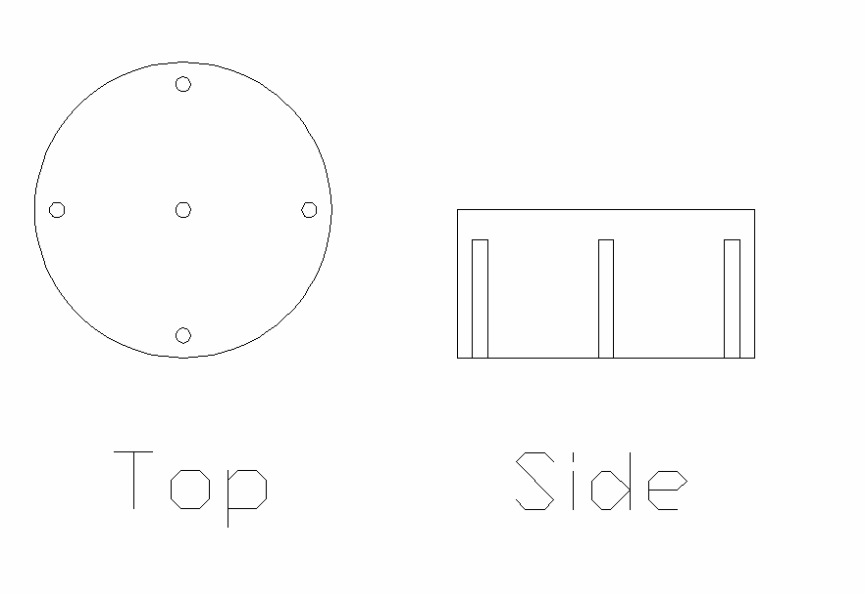

Figure 4-3: Diagram of a five pin electrolytic tilt sensor.

Electrolytic tilt sensors produce precision measurements of tilt with respect to the gravity vector. The sensor operates on the principle that an enclosed bubble always orients its surface perpendicular to gravity. The bubble is enclosed within an electrolytic, or electrically conductive, fluid. As the enclosure tilts, the bubble orients itself with respect to the gravity vector. A central pin conducts an alternating current between the outside four pins. Alternating current is necessary to prevent electrolysis of the sensor. The conductivity between the points is dependent upon the amount of fluid between them, and thus, an impedance variation results from the changes in the fluid level between pins. The changing angle of tilt produces an output voltage that is a function of the tilt angle of the sensor. It should also be noted that the DX-008 sensors exhibit a maximum range of positive twenty degrees to negative twenty degrees of which the linear range goes from positive eight degrees through negative eight degrees. A graph

displaying actual readings that show the linear and non-linear behavior of these sensors can be seen in Figure 4-4. This data was collected from testing of the sensors through + - 20 arcdegrees using a stepped process.

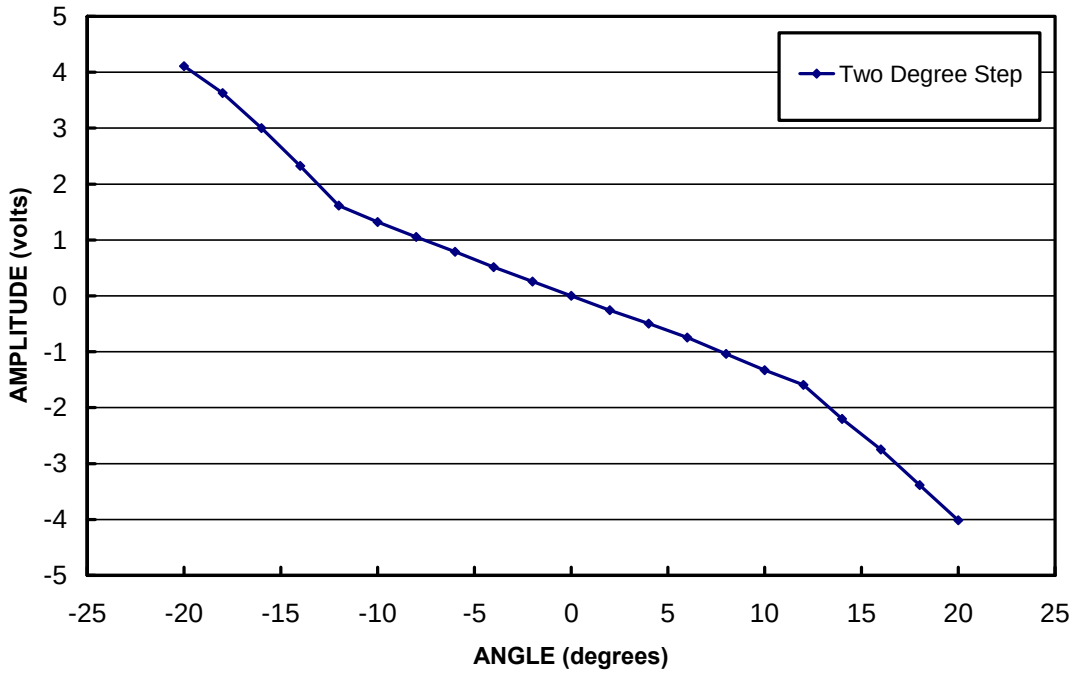

Figure 4-4: Graph showing the linear and the non-linear behavior of the DX-008 Sensors.

4.2.2 Wireless Sensor System

To begin the preliminary system development for the project, two wireless tilt monitoring devices were built. This gave the research group a better understanding of the EZ-TILT-2000-008-rev2 tilt sensors that were initially chosen and a representation of the problems that would be faced in creating the overall system. Wireless data acquisition was accomplished using a Microstrain™ V-Link 2.4 GHz Wireless Voltage Node.

The sensors were mounted in enclosures that provided appropriate leveling methods to accommodate for the narrow angular range of the sensors. The enclosures contained the necessary electrical system for both RS232 hard lines and wireless data transfer. One wireless system can be seen in Figure 4-5.

Figure 4-5: Photograph of the first wireless tilt monitoring system.

The resulting tests from these sensor systems led to reconsideration of the sensor to be used. The slow, unreliable method of leveling the sensor after initial placement, due to the narrow angular range, was not desired. For this reason, the EZ-Tilt 3000-008-op sensors were chosen for their larger angular range and increased voltage output.

The wireless sensors were used to verify the proper functioning of the tilt evaluation platform that will be discussed in the following section.

4.3. Testing Platform Development

This section describes the design and construction of a series of test platforms for analyzing the behavior of tilt sensors. These were original designs that had to accommodate the sensors and the characterization tests that were to be performed on them. The construction of prototype support systems to be utilized in the final test bridge design is described in Section 4.3.1. The design, development and construction of the test bridge platform that was used for the development of algorithms under other research efforts are described in Section 4.3.2. Finally, the design and construction of a precision sensor calibration device to be used in the testing is described in Section 4.3.3.

4.3.1 Tilt Sensor Evaluation Platform

This section describes the development of a platform for testing a single sensor. Testing of the tilt sensors requires an appropriate laboratory setup that can tilt in a three dimensional field. A fixture that was capable of these movements was designed and tested. This process is described in Sections 4.3.1.1 and 4.3.1.2. This fixture was considered a prototype for the test bridge design described in Section 4.3.2.

4.3.1.1 Mechanical Design

In order to most accurately represent the structural behavior of actual bridges, tilt in all directions must be considered. To satisfy this requirement, a tripod-style setup was designed that would allow for the necessary tilt angles. A three point setup is more advantageous than a four point setup because it will allow for movement in a specific axis with the rotation of a single point and removes potential support redundancies. In a four point set-up, a single point may be moved but the other three points restrict any rigid

plane from following the singular movement. This initial evaluation platform design was also important in the ongoing design of the larger scale test bridge to be used in analyzing the completed tilt sensor array. The adequacy of this initial platform was considered in the test bridge design.

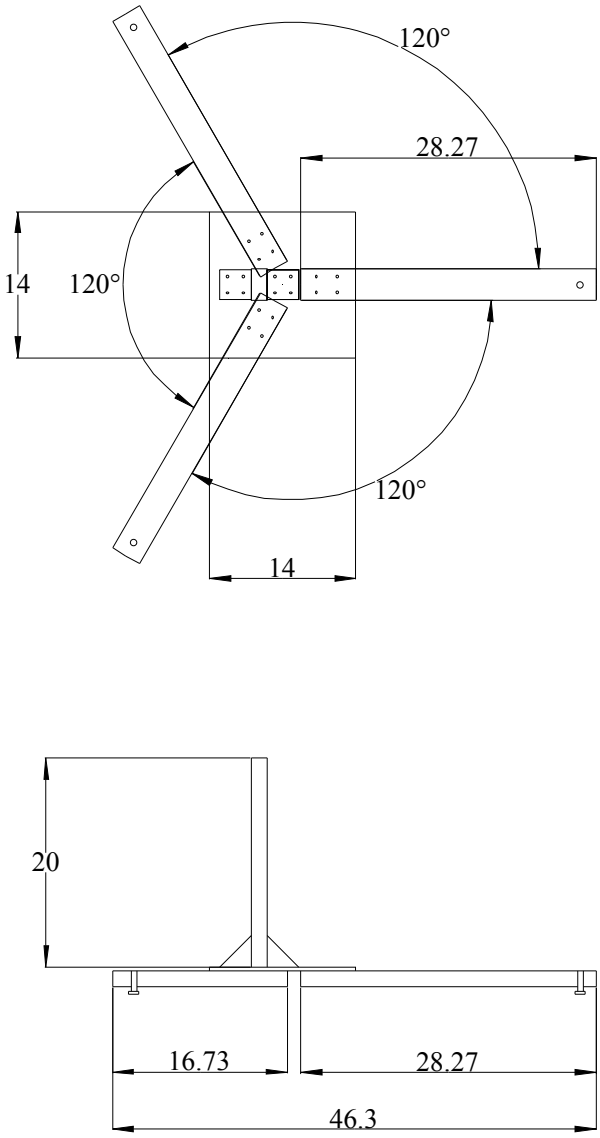

Figure 4-6: Drawing of an initial design for the evaluation platform with dimensions (inches).

The first design shown in and Figure 4-6 exhibited the desired characteristics of being a tripod style platform. It consisted of a central base with three legs protruding from this center. The central base would need to provide precise through-holes to attach the legs in an array that would place the adjustable points in an equilateral triangle formation. Considering the somewhat complicated machining and construction of this design, the extended legs that would not be as stable and rigid as desired, and the hardships that would be encountered when replicating it, other designs were considered.

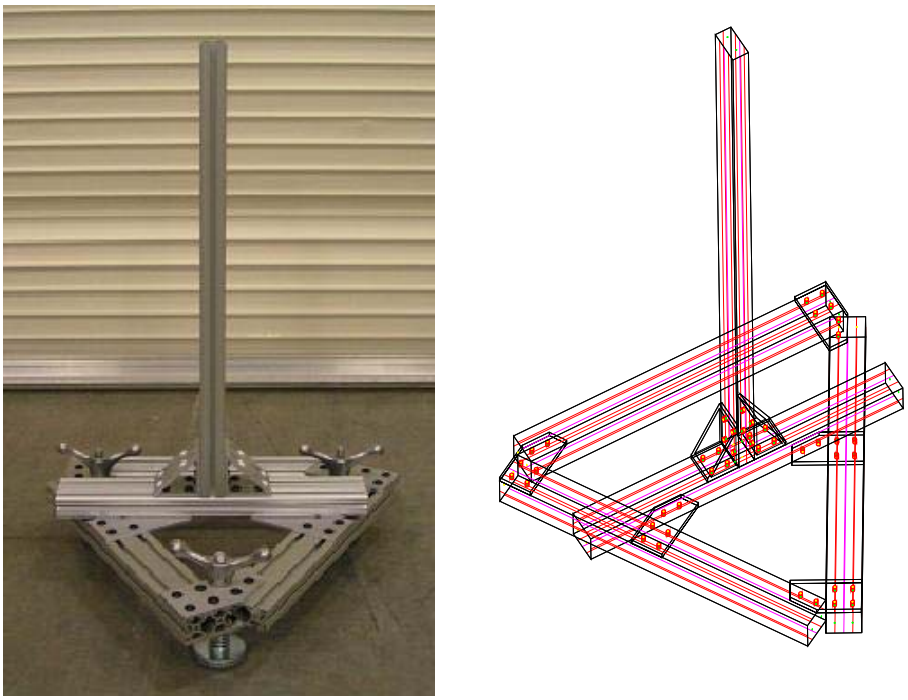

Figure 4-7: Picture and draft image of the final tilt sensor evaluation platform.

The final design of the sensor evaluation platform shown in Figure 4-7 was similar, however provided easier replication and ease of construction. It was built using 80/20™ extruded aluminum parts. These parts can be ordered at pre-cut lengths. The

associated fasteners and joining plates are designed specifically for the intended 80/20™ structural members. The equilateral positioning required of the three legs is achieved without precision machining. The joining plates are pre-machined with holes at 60° angles ensuring that members of equal length must fit in an equilateral configuration when fastened to them. The company also furnishes many other accessories for their material that can be utilized in a wide variety of applications and would be necessary in the future of the ongoing project.

The triangular platform has adjustable points in each of the three corners. These adjustable points use a screw-type jack in order to raise or lower the platform in that corner. The three adjustable points are arrayed in a near-perfect equilateral triangle. Adjustment of these points allows for the three-dimensional movement of the platform. Figure 4-8 shows a top view of the platform with the adjustable points arranged in an equilateral triangle.

Figure 4-9 shows the screw jacks from a side view. The springs keep the platform in contact with the handle by applying upward force. The thread count for the screw was 11 threads per inch. This allowed for 0.091 inches of movement per rotation of the knob. This travel distance of the screw jack was used for prediction of platform movements as described in the following section.

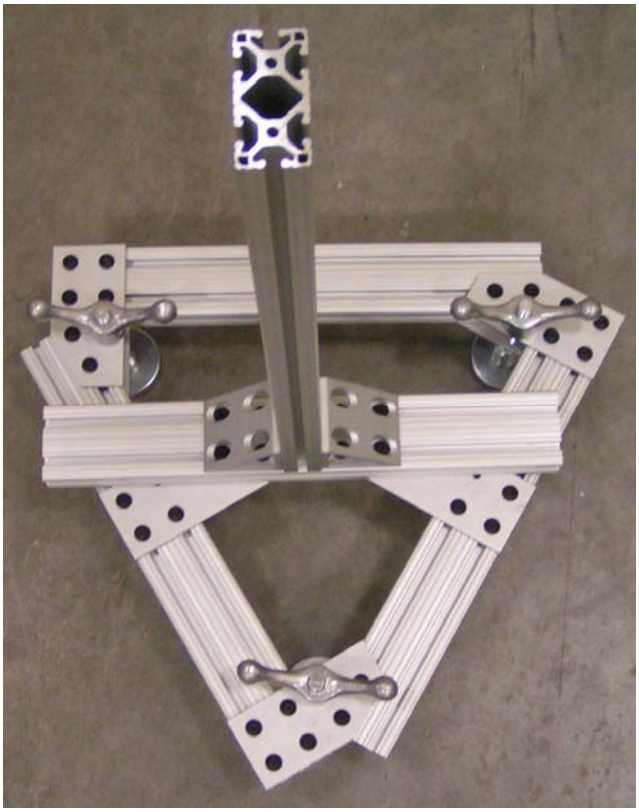

Figure 4-8: Photograph of a test platform showing the triangular base with adjustable points.

Figure 4-9: Photograph of adjustable screw jack at platform corner.

4.3.1.2 Testing of Evaluation Platform

This section describes the calculation of predetermined movements of the sensor platform and initial testing that was conducted to determine the effectiveness of the system.

Because the purpose of the platform was to evaluate the sensor behavior, the angle of tilt that the platform is experiencing must be predictable. To determine the angle of tilt that the platform is experiencing, the original coordinate positions of each adjustable point must be identified using one corner as a zero and the others to be in plane with the first. Because this is an equilateral triangle, the length of one side is measured, recorded and then used to find the three subsequent coordinates.

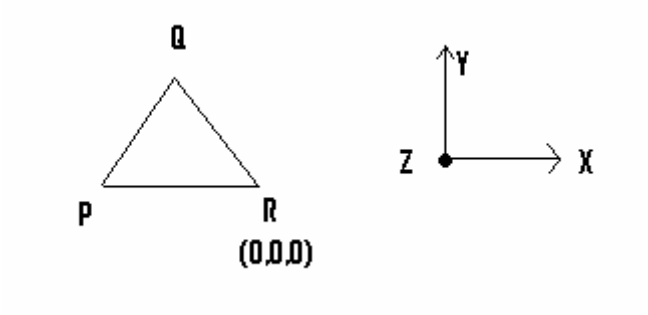

Figure 4-10: Example of coordinate system and zero point selection.

With this plane as an initial starting position, a normal unit vector is assumed as <0 0 1>. From this plane, any variation will create new coordinates for the adjustable points according to the corner tilted and the magnitude of that tilt. These new points are found geometrically by analyzing the distance and direction traveled by the adjustment relative to the original coordinates. Once the coordinates are found for the three new

points, two vectors can be created that correspond to these coordinates. Since these two vectors lie in the plane, their cross product is the normal vector for the plane. With the new normal vector, the angle difference from the initial position normal vector can be found. An example of this concept can be seen in Figure 4-11.

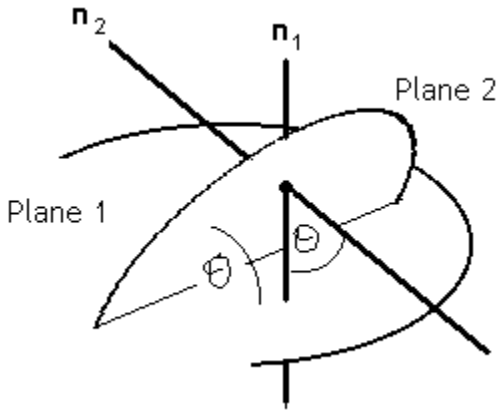

Figure 4-11: Example of angle difference between two normal vectors of two planes (http://members.tripod.com/vector_applications/angle_between_two_planes/).

The development of formulas to predict the angle of tilt experienced by the platform was completed to compare the measurements that the sensors output to the expected angle experienced by the platform. For this positioning technique, it is important to know the pitch of the threads that are on the screw jack. With this information, the distance traveled in the vertical direction per turn of the screw jack is known. Because the platform is rigid, the position of each screw is found using geometrical correlations between all three points. The new points create a new plane. Once the normal vector of this new plane is found, the angle between the original and the new vector is found using Equation 1.

$$\cos\theta = \frac{n1 \bullet n2}{|n1||n2|} \qquad \textbf{Equ. 1}$$

The expected angle determined by this method can be used to tilt the platform a specified amount for sensor testing. The ability to predict the sensor output allows for experiments to be conducted in a predictable manner.

This method was tested using the wireless tilt sensor assembled during early research for the project. The number of turns for the screw jack was planned and analyzed using the numerical method in order to develop a prediction of the platform behavior. The calculations were then compared to the sensor output in order to determine their accuracy.

This test required for one screw to be turned five times to get a tilt angle of approximately one degree. The output of the wireless system was given in degrees of pitch and roll. In order to find the resultant angle of tilt, the pitch and roll had to be combined into one resultant angle. This is done by taking the square root of the sum of the squares of pitch and roll for small angle changes. This was compared to the predicted angle from numerical analysis.

The results of this numerical method of predicting the platform behavior were satisfactory. The prediction showed good correlation to the sensors output. The results from one of the tests are seen in Table 4-3. This 0.83% error provides an acceptable level of accuracy for predictable tilting of the platform.

Table 4-3: Correlation between sensor and calculated angle.

Change in Angle		
	DEGREES	
P:	-0.9873	
R:	0.1162	
Resultant =	0.9941	**DEGREES**
Model Prediction =	1.0025	**DEGREES**
Percent Error =	0.83%	

Another method that was developed to better understand the tilt of the platform was a laser and target technique. For this method, a target was place on the ceiling (approximately twenty feet high) and a laser was fixed to the tilt platform directly below the target. It was assumed that under small angle tilting, the flat target, at a known distance, could have a predictable increment that correlated to the tilting of the platform. These increments could be shown in a bulls-eye style pattern on the target shown in Figure 4-12.

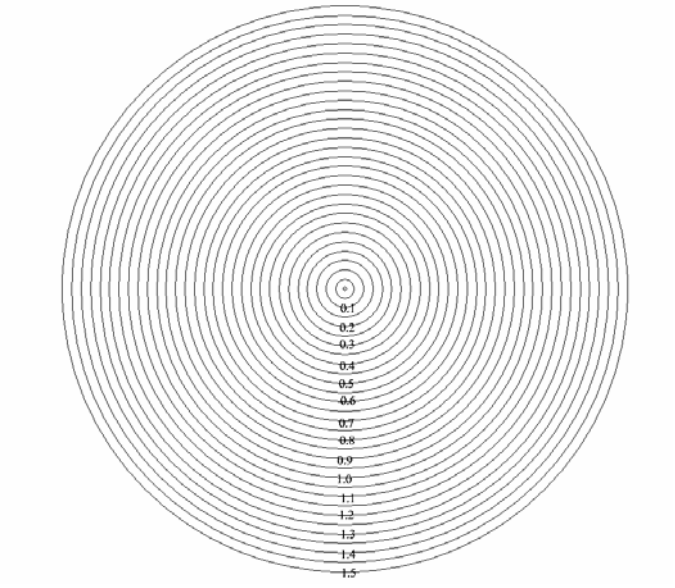

Figure 4-12: Example of the laser target used for determining tilt angle in degrees.

This method for determining the tilt experienced by the tilt platform was set-up and evaluated. It included a wireless sensor system and laser affixed to the tilt platform, and a target affixed to the ceiling. The experimental set-up can be seen in Figure 4-13.

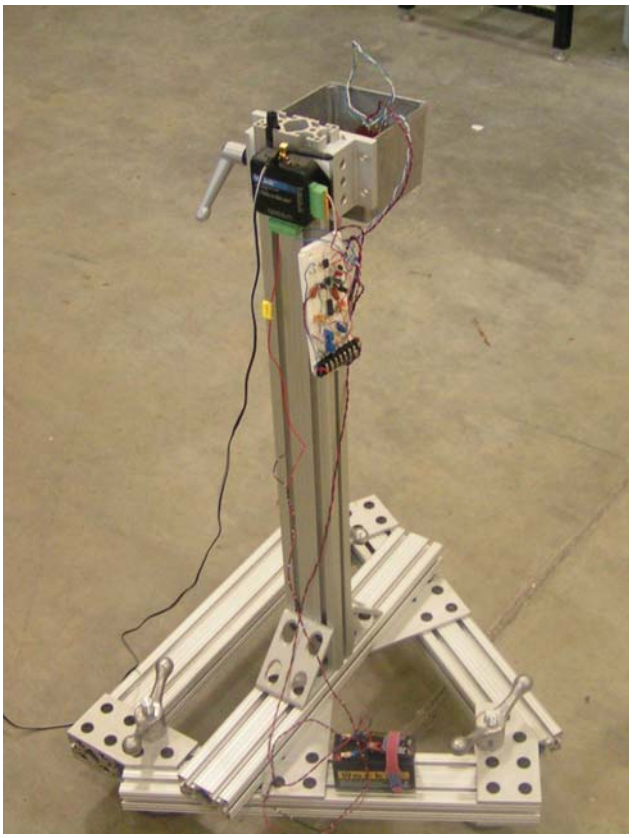

Figure 4-13: Photograph of the tilt platform with wireless tilt sensor system and laser affixed.

This method of determining the tilt angle experienced by the platform was found to be inconsistent and difficult to quantify. There were several reasons for this. One of the reasons for this was that, at a distance of twenty feet, the target and laser point were difficult to see. The optics that were used to enhance vision were not adequate. The laser was not as focused after the twenty feet of travel, and therefore showed an indistinct point on the target. This large point covered a range that was beyond the tolerance needed. The difficulty of creating a twenty foot high test set-up was not something that is

desirable to be repeated and so the method was deemed inadequate. Results from the laser target testing can be seen in Table 4-4. They show over 20% error in every movement. The numerical method was chosen as the preferred method for predicting tilt angles in the platform.

Table 4-4: Table showing the correlation of the laser target and the tilt sensor.

Test #1		
Laser Position	**Sensor Output (Degrees)**	**Percent Error (%)**
0.00	0.00	
0.90	0.74	21.79
1.30	1.02	27.83
Test #2		
Laser Position	**Sensor Output (Degrees)**	**Percent Error (%)**
0.00	0.00	
0.40	0.31	27.21
0.75	0.60	24.89

4.3.2 Test Bridge Design and Construction

Design of the test bridge for the project was based on the initial test platform. The initial platform proved to be easily repeatable, rigid, durable, and cost effective. The versatile parts from 80/20™ Inc. allowed for sensor placement on the structure that was convenient, fast and easily repeatable. Using AutoQuoterX™ software that could be obtained online from 80/20™ Inc. along with AutoCAD™, a three dimensional model of the bridge was created. This model not only showed the bridge, but also the cumulative cost of the associated parts and fasteners that would be used to construct it. An image of this model can be seen in Figure 4-14.

The test bridge consisted of the same triangular base that was seen in the initial test platform; however this triangular base had sides that were five feet in length. All extruded aluminum consisted 1.5 x 3 inch cross-section pieces. The three spring-loaded feet to hold the pier were similar to the test platform, but were higher strength to accommodate for the extra weight of the bridge. The modeled pier was made up of two five foot tall extruded aluminum sections that were fully braced and attach to a top pier cap. The girder spans were just over eight feet in length. They rested on wooden abutments on the ends and the adjustable pier in the center.

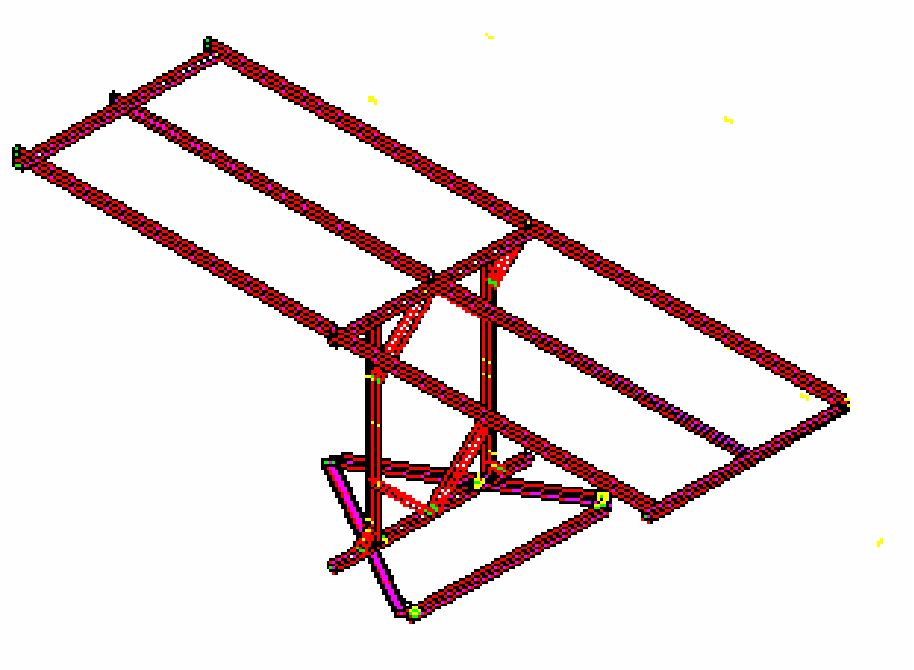

Figure 4-14: Isometric drawing of the test bridge without the abutments.

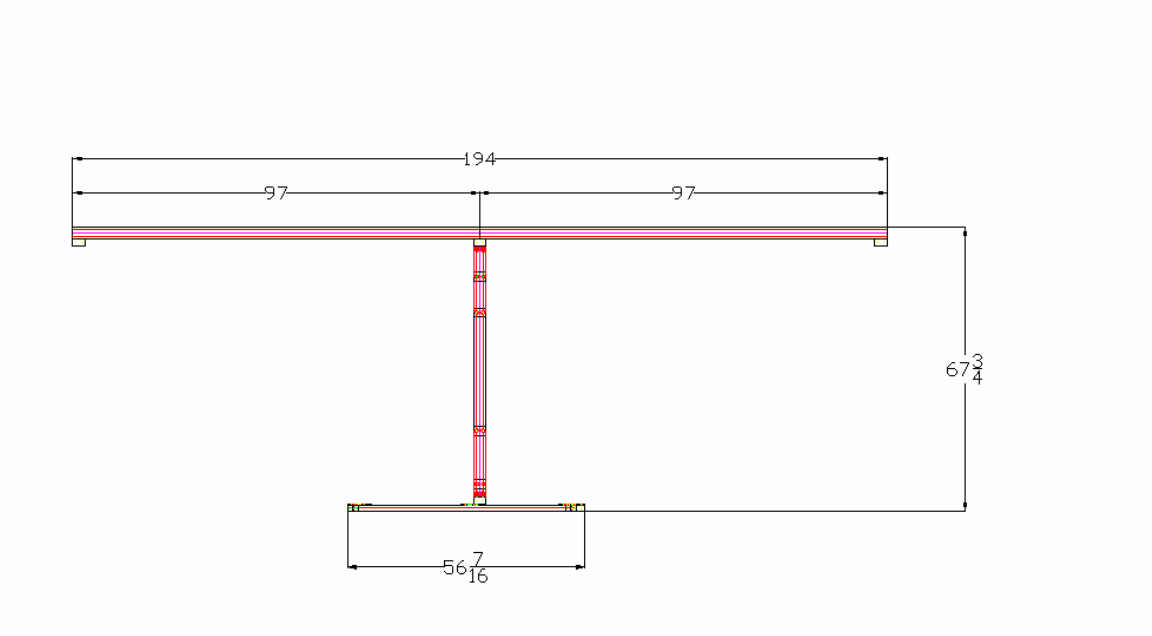

Figure 4-15: Drawing of the side view of the test bridge (inches).

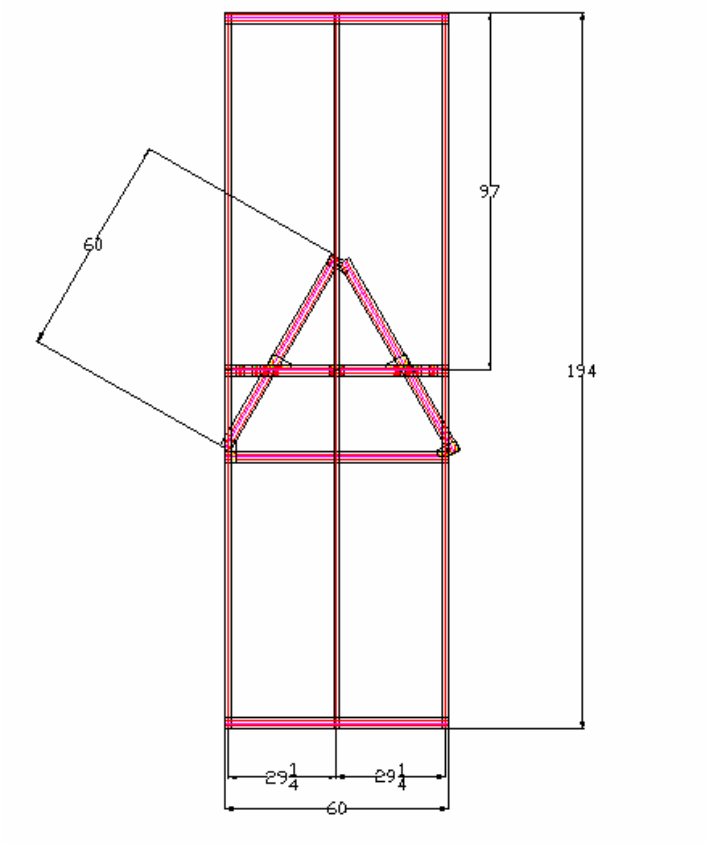

Figure 4-16: Drawing of the top view of the test bridge (inches).

The abutments for the bridge girders were not as critical to the overall tilt sensing and adjustable bridge. They simply needed to be strong rigid ends for the girders to rest on. For this reason, a simple wood construction was chosen for its simplicity, low cost, and speed of construction. The design of these abutments can be seen in Figure 4-17.

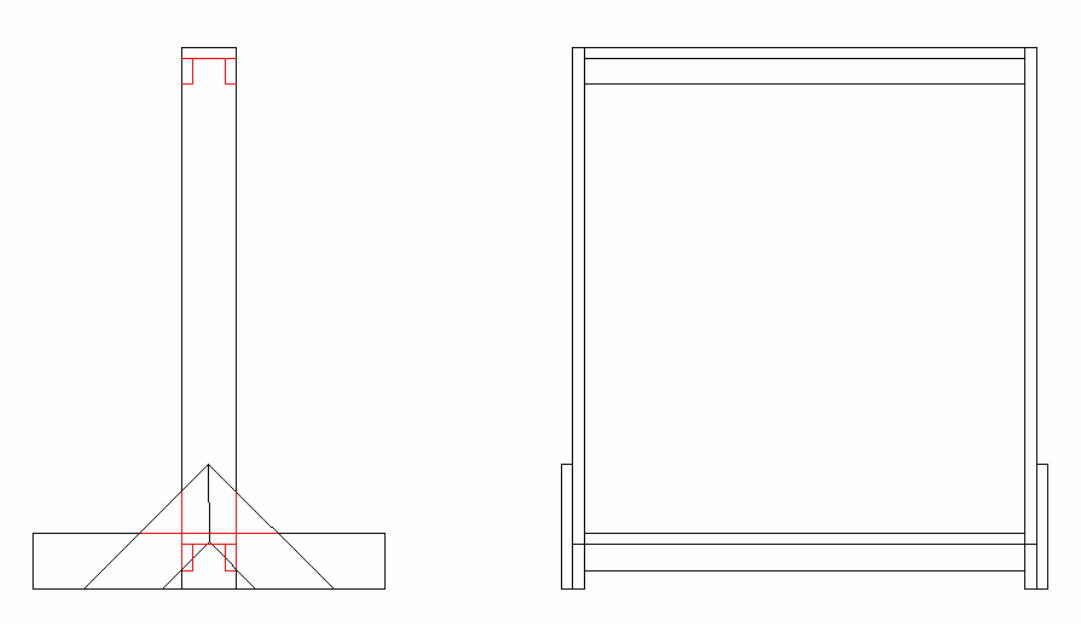

Figure 4-17: Side and front view drawing of abutments for the test bridge.

The construction of the test bridge began once the designs were deemed adequate. The software from the AutoQuoterX™ and AutoCAD™ created a materials list to be ordered. These materials were ordered from 80/20™ Inc. The material for the wooden abutments was chosen and purchased from a local hardware store. Once all the material was received, the construction ensued. Extra materials were necessary throughout the process, and were purchased accordingly. The construction process can be seen in the following photographs.

In Figure 4-18, the construction process of both the central pier and the abutments can be seen. Figure 4-19 shows the assembled abutments and central pier. Figure 4-20 shows the abutments after being painted. Weights can be seen placed on the abutments and will be discussed along with the other additions. Figure 4-21 shows the completed test bridge with all modifications.

(a) **(b)**

Figure 4-18: Photographs showing early construction of the (a) aluminum pier and (b) wooden abutments.

Figure 4-19: Photographs showing completed framework of the bridge pier and abutments.

Figure 4-20: Photographs of abutments after painting and addition of weights.

Figure 4-21: Photograph of the completed test bridge with girders and security chain.

Several additions were made to the test bridge after the original design plans. The wooden abutments were painted for presentability. Four fifty pound weights were placed on the abutments to contribute to the inertial properties of this stationary structure. Safety cords were strung through the aluminum girders to prevent the accidental collapse. This was prioritized after the hospitalization of a research assistant. One inch diameter steel rods were placed on top of the pier cap to act as roller bearings for the eight foot long extruded aluminum girders. Stiffer springs were added to the screw jacks due to the large weight of the structure. Extra support brackets were added perpendicular to the central pier structure in order to increase the rigidity of the pier structure. Nine sensor attachment platforms were fabricated. Six sensor platforms were to represent the pier sensor array (PSA) and three were to represent the super-structure sensor array (SSA). A security chain was placed around the test bridge to prevent interference from other individuals using the laboratory.

4.3.3 Calibration Stage Design and Construction

To effectively characterize the tilt sensors, platforms that allowed for known, precision angle movements were required. This section describes the construction of a precision calibration stage for use in defining the performance characteristics of the sensors.

Due to the small size, inconsistent soldering, fluid amounts, and differing sensor shapes, the manufacturing process of the sensor is not completely precise and repeatable. Taking this into consideration, it is conceivable that the different sensors would output

voltages proportional to the angle of tilt at different rates than the other sensors. This creates a need for calibration tests to be conducted to characterize each individual sensor. This test needs to be performed for each axis of each sensor. The linear range of the sensor was the focus of the calibration testing. Initial testing was conducted to illustrate the behavior of the sensor over the full range as shown previously in Figure 4-4. However, given the anticipated tilt angles for a bridge structure are small, the linear range of the sensor is the most relevant range to be characterized. Typical bridge tilt angles are on the order of 1 degree and the linear range of the sensors goes from -8 to +8 arcdegrees.

In order to calibrate the sensors, an appropriate tilt stage was needed to move the sensor in a consistent manner that allowed for movement through a known angle of tilt. With the EZ-Tilt 3000-008-op sensors, a stage that was capable of moving plus/minus twenty degrees was desired in order to cover the full measurement range of the sensor. Common tilt stages, found by searching manufacturer's online catalogs, were capable of accurate tilts with a maximum range of plus/minus eight arcdegrees maximum. For this reason, a rotary stage that covered a full 360 arcdegree range was chosen to fulfill the full range necessary for the EZ-Tilt 3000-008-op sensors. However, in order to use a stage of this type, the 360 arcdegree rotary stage would have to be mounted vertically, but still allow the sensor to be mounted horizontally. This was done using right angle brackets to achieve the appropriate positioning. The proposed design of this tilt calibration device is seen in Figure 4-22.

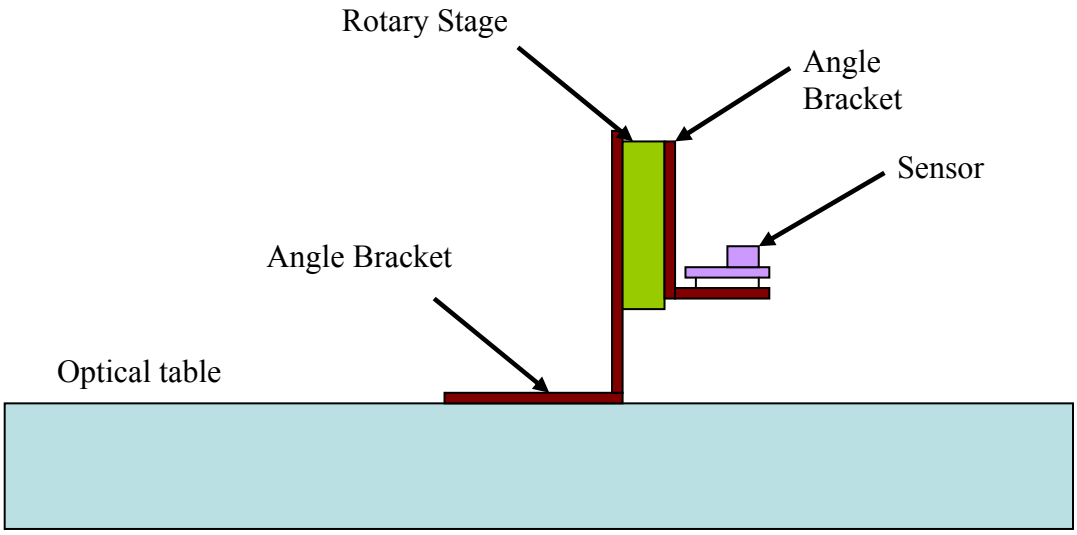

Figure 4-22: Drawing of the tilt calibration design

The rotary stage chosen was from Edmunds Optics. It was a 60 mm rotary stage that had 360 arcdegrees of coarse rotation and a fine rotation region that was approximately 10.5 arcdegrees. This stage can be seen in Figure 4-23 and Figure 4-24. The fine rotation region was capable of movement in increments as precise as 0.46 arcminutes per step. This was an attractive option because the fine rotation region could be used for an accurately stepped calibration region for the linear range of the sensors. The associated parts for the rotary stage mount, including two precision ninety degree angle brackets and fasteners, were also purchased from Edmunds Optics.

Figure 4-23: Front photograph of precision rotary stage mounted on angle bracket.

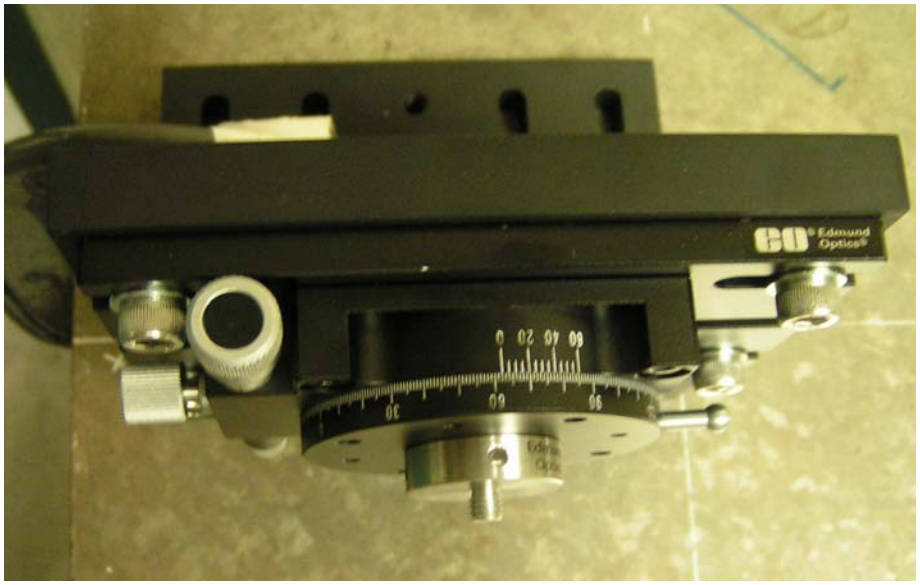

Figure 4-24: Top photograph of precision rotary stage mounted on angle bracket.

The rotary stage was somewhat complex with respect to the units and increments shown for both coarse rotation and fine rotation. The course rotation has 360 marks denoting the 360 arcdegrees covered by a full rotation of the stage. There is also a vernier scale to determine approximate arcminutes traveled. The fine rotation knob is divided in linear increments, unlike the angular increments of the coarse rotation. The incremental "tick" marks are spaced to relate one tick to five microns of linear movement. This, in turn, relates to 0.46 arcminutes. There are 50 ticks per full turn of the knob and this is equal to exactly 23 arcminutes. Table 4-5 shows the relationship between interval markers, linear movement, knob rotations and angular motion.

Table 4-5: Relationship between fine rotation and angular movement.

Ticks	Micron		Millimeters	Turns of Knob	Angular Distance (minutes)	(degrees)
0.2	1	=	0.001	0.004	0.092	0.0015
1	5	=	0.005	0.02	0.46	0.0077
50	250	=	0.25	1	23	0.3833
100	500	=	0.50	2	46	0.7667
150	750	=	0.75	3	69	1.1500
200	1000	=	1.00	4	92	1.5333

With the rotary stage prepared for the sensor calibration, a suitable mounting platform was necessary to place the sensor in position for tilt calibrations. A simple aluminum base plate that could be attached to the rotary stage via angle bracket was designed and machined. The plate had four bolts which secured it to the angle bracket, four stand-offs for sensor attachment, and a wiring strip for the power supply and data output. The wire mount also acts as a strain reliever. The finished base plate mounted on the rotary stage can be seen in Figure 4-25 and Figure 4-26.

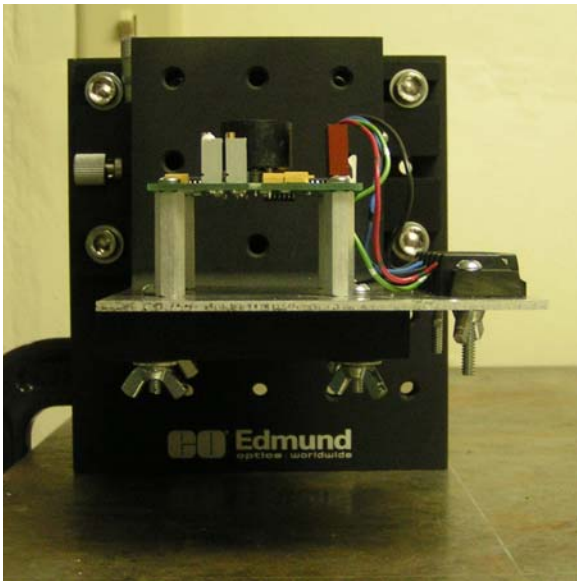

Figure 4-25: Front photograph of finished base plate with sensor attached.

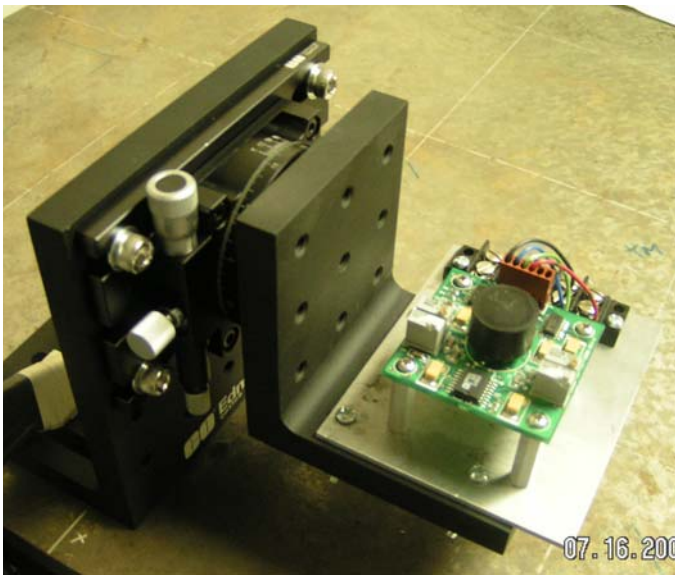

Figure 4-26: Isometric photograph of finished base plate with sensor attached.

Two electronic components that were necessary for rudimentary operation of the tilt sensors were a power supply and a digital multimeter. Both of these items were purchased from Fotranic Corporation. The Triple Output DC Power supply (Model

1760A), manufactured by B+K Precision is shown in Figure 4-27. The 6.5 Digit Precision Multimeter (Model 8845A), manufactured by Fluke Corporation, is shown in Figure 4-28.

Figure 4-27: Photograph of the Power Supply.

Figure 4-28: Photograph of the digital multimeter.

This data acquisition system was used for fundamental testing of the individual tilt sensors. With this system, the real time output from the sensor was displayed on the digital multimeter and could be captured utilizing the software provided with the system. This system, seen fully assembled in Figure 4-29, was very useful for troubleshooting problems with the sensor, initial sensor performance analysis, and confirmation of the datalogger system performance.

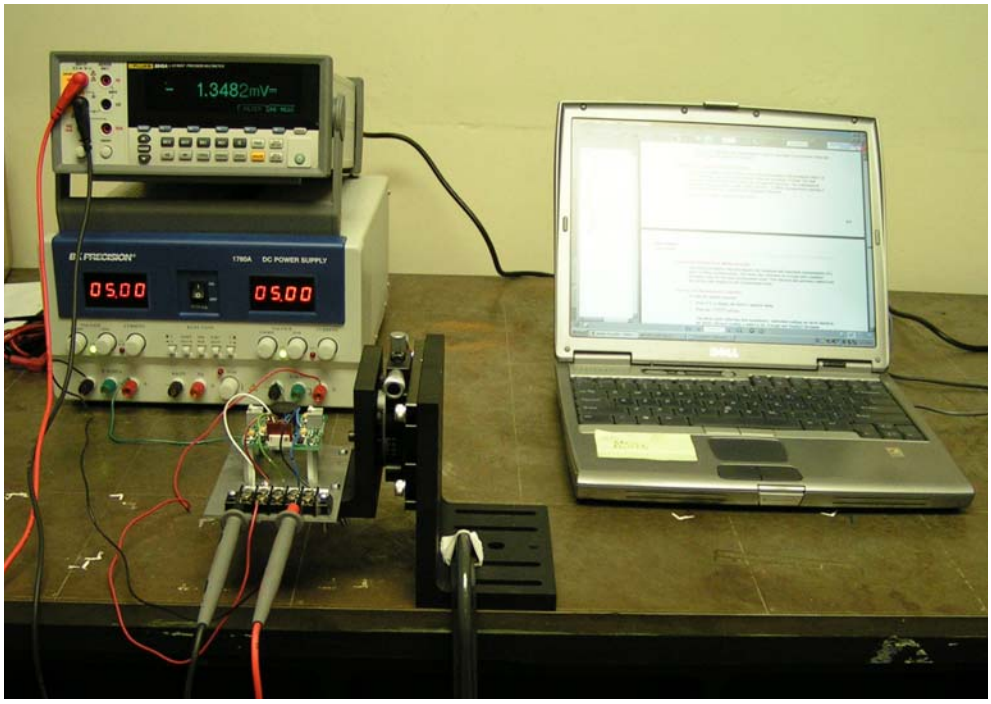

Figure 4-29: Photograph of sensor system with multimeter output.

4.4. Characterization Test Set-up

A series of tests were conducted to characterize different aspects sensor behavior. There were nine separate testing schemes employed. This section will provide a brief explanation of these tests and why they were performed. The results of these tests can be found in Chapter 5.

4.4.1 Sensor Testing with Multimeter

This part of the testing was necessary to validate the datalogger and multimeter systems that will be used throughout the sensor characterization. The multimeter was also be used for troubleshooting individual sensors. Sensors can be quickly connected and the real-time ouputs can be read from the multimeter. Results from the datalogger and multimeter were compared to compare performance of the systems.

4.4.2 Calibration of Sensors

Sensor calibration was the most important part of the characterization process. The tilt sensors output a voltage that must be correlated with angular tilt. The calibration process consisted of stepping the sensors through a known pattern of specific tilt angles in order to determine the correlation between voltage output and tilt angle for each axis (X and Y) of the sensors.

4.4.3 Stationary Testing on Iron Table

During calibration, it was discovered that the sensors experienced warm-up drift after the initial power-up. An understanding of this initial drift was required in order to determine the amount of time necessary before sensor calibrations could be performed. This testing consisted of placing the sensors in a stable location atop an iron table and analyzing their behavior in the stationary position.

4.4.4 Stationary Sensors with Varying Temperature

This was the first test performed with relation to a changing temperature. It was completed in order to find the change in stationary sensor output under temperature

changes. To do this, the sensors were placed in a stationary position within a temperature chamber. The temperature was changed and allowed to remain constant over 24 hour periods so that the sensors could reach equilibrium with their environment. Sensor behavior during these changes was analyzed.

4.4.5 Fixed Temperature with Varying Sensor Angles

This testing was done in order to find the temperature coefficient that is needed to adjust the slope of the calibration plot. As the temperature changes, it is expected that the slope of this plot will change. The test was performed by placing the calibration stage in a temperature chamber, and developing calibration plots for the sensors under different thermal conditions.

4.4.6 Analysis of the Test Bridge

Testing was conducted on the test bridge so that sensor behavior under the conditions that will exist during long-term analysis can be evaluated. Behavior of the bridge using the wireless system was checked. This testing also included testing of the sensor array on the test bridge. The sensors were mounted on the preassembled brackets and bridge movements were analyzed to check that there was agreement in the sensor outputs. The sensors were left in the stationary position during another test for long-term drift analysis of the sensors on the test bridge.

4.4.7 Long-Term Stationary Testing at Controlled Temperature

This test was conducted in order to see the long-term drift behaviors of the sensors at a controlled temperature. The tests were conducted with the sensors placed in a temperature chamber such that a constant temperature could be maintained.

4.4.8 Slowly Varying Angle Changes

These tests were conducted to see how well small angular changes could be distinguished from sensor drifting and system noise. These tests were conducted within the temperature chamber in order to maintain constant conditions.

4.4.9 Resolution Testing

The resolution of the system was tested to see the smallest change the sensor system could detect. This was done by analyzing the analog to digital converter and by finding the smallest changes in tilt that could be seen using the rotary stage.

5: Results

5.1. Introduction

This section provides the results of the sensor characterization. These tests include sensor testing with the multimeter, calibration of the sensors, stationary testing on an iron table, stationary sensor analysis with varying temperature, fixed temperature with varying sensor angle testing, analysis of the test bridge, long-term stationary testing at controlled temperature, slowly varying angle change analysis, and resolution testing. Application of these results to algorithms that will process collected data will also be discussed.

It should be noted how sensors will be referred to throughout testing. Each sensor has two axis that will be referred to as the X and Y axis. The system being used has a total of ten sensors, so, for example, sensor output will be referred to as Sensor 1X or 1Y depending on the axis and the sensor. Sensors #1 and #4 have been replaced during part of the testing due to behavior that was uncharacteristic to the overall sensor group. Sensor #1 had adjusted gain settings and Sensor #4 was determined to be malfunctioning due to a bent pin within the sensor.

5.2. Sensor Testing with Multimeter

The first step in the characterization process was to verify that the multimeter, which would be used largely for troubleshooting, had consistent results to the datalogger created by FCI. This was done by stepping the sensors from 0 arcdegrees through 161 arcminutes in 23 arcminute steps (one full rotation of the fine rotation knob), then repeating with the other data acquisition (DAQ) system . A precision block, typically used for caliper calibrations, was used to space the sensor as close to parallel with the angle bracket as possible. This was done to prevent bleedover into the other axis of the sensor and will be discussed in Section 5.2. As seen in Table 5-1, the data closely relates and assures that both systems offer suitable data outputs. The multimeter showed 2.117 mV/arcminute and the datalogger showed 2.102 mV/arcminute. This is less than one percent difference, with a standard deviation of 0.0074. These mV/arcminute correlations are not consistent with the majority of the sensor correlation data, because gain settings were modified during the course of testing for this sensor, but are suitable for this analysis. The differences between the two readings can be attributed to sensor noise and inconsistencies in the fine rotation of the rotary stage.

Table 5-1: Correlation between the multimeter output and the datalogger from FCI.

Measurements from Multimeter

Minute Change	Output (mV)	Change (mV)
0	0.00	
23	-47.90	-47.90
46	-96.10	-48.20
69	-144.20	-48.10
92	-192.70	-48.50
115	-242.50	-49.80
138	-290.00	-47.50
161	-340.80	-50.80
	Average Change (millivolts) =	-48.686
	millivolts/arcminute =	-2.117

Meaurements from DAQ

Minute Change	Output (mV)	Change (mV)
0	-3.40	
23	-51.75	-48.35
46	-100.10	-48.35
69	-148.45	-48.35
92	-196.12	-47.67
115	-245.15	-49.03
138	-292.82	-47.67
161	-341.85	-49.03
	Average Change (millivolts) =	-48.349
	millivolts/arcminute =	-2.102

Another test was executed to compare the multimeter and the datalogger system. This test stepped the Y-axis of sensor one plus/minus approximately five arcdegrees (299 minutes). The data was plotted as millivolts vs. arcminutes and can be seen in Figure 5-1 and Figure 5-2.

Comparison of the slope of the two systems during the second type test shows excellent correlation between the results. The graphs can be seen in Figure 5-1 and Figure 5-2. The multimeter slope was -2.12 millivolts/arcminute and the datalogger slope

was -2.15 millivolts/arcminute. This is a 1.4% difference, with a standard deviation of 0.015. Once again, this slope is distinct for this particular sensor due to an adjustment of the gain on the module. The Coefficient of Determination (R^2) value is equal or approximately equal to one for both tests, showing the sensors are within their linear range. Coefficient of determination values are used to determine the amount of variation in a data set. The equation used to find this value can be seen in Equation 2.

$$r = \frac{\sum (x - \bar{y})(y - \bar{y})}{\sqrt{\sum (x - \bar{x})^2 \sum (y - \bar{y})^2}} \qquad \textbf{Equ. 2}$$

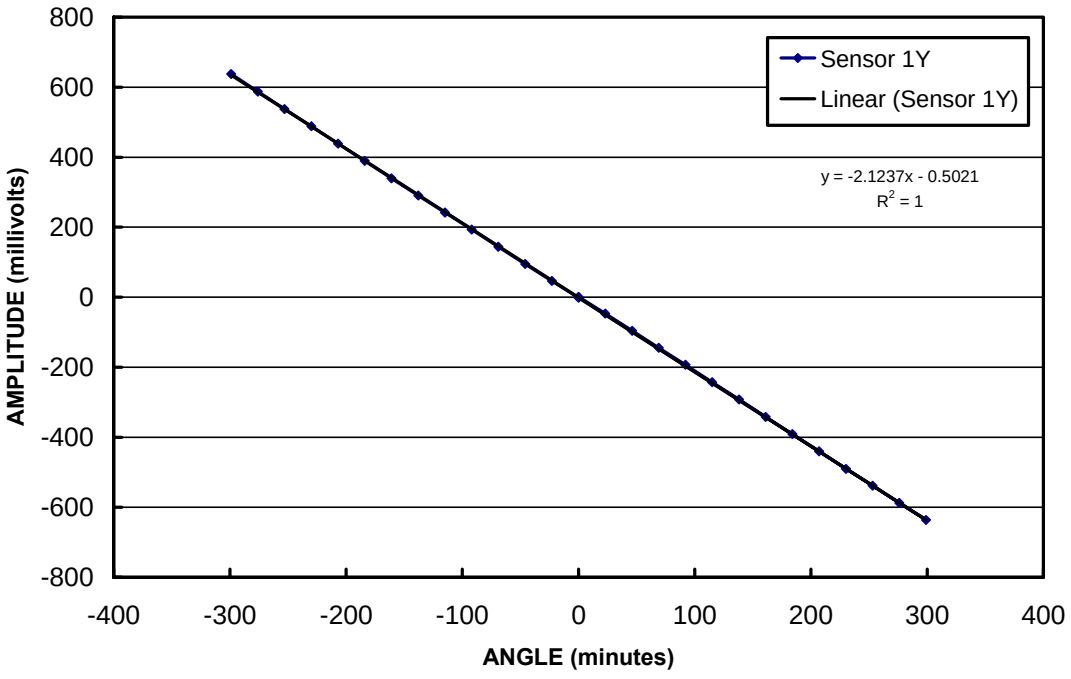

Figure 5-1: Graph showing multimeter results from Sensor #1, Y-Axis.

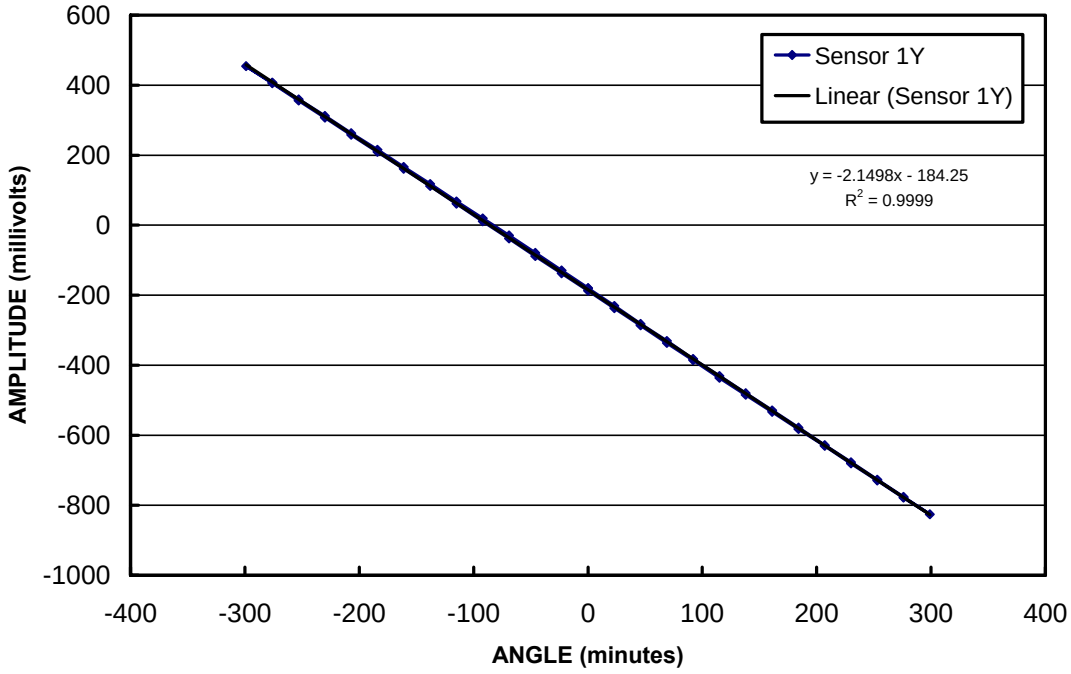

Figure 5-2: Graph showing datalogger results from Sensor #1, Y-Axis.

Results from these tests assure that each DAQ system is capable of correctly processing the output signals from the sensor. This validated each system so that further testing using both the multimeter and datalogger could proceed. The datalogger was used for the majority of calibration and long-term testing, however, the multimeter system functioned well for quick, real-time troubleshooting of the sensors.

5.3. Calibration of Sensors

Developing a calibration process that could be used in a repeatable manner and understood easily was of importance to this step in characterization. Because of the relatively small angles that were to be measured with the completed tiltmeter system, the calibrations were performed within the plus/minus eight arcdegree maximum linear range

of the sensor. A procedure was developed that would allow for simple data processing. This procedure required movement of the fine rotation knob of the rotary stage to move the sensor plus/minus 5 arcdegrees in 23 arcminute steps every 30 seconds of time for a total of twenty-seven minutes of time exactly. The reason for this was that the steps were timed to take place every thirty seconds of time in order to analyze them with a computer program according to their timestamps. Once the calibration process started, the fine rotation knob was moved one full rotation, or 23 arcminutes, every thirty seconds of time. This stepped the sensor from a relative zero angle, to positive 299 arcminutes, reversed back to zero, then to negative 299 arcminutes, and finally back to zero. It is important to note that the starting position is a relative zero angle, and that there will be an initial offset voltage associated with this. This will not affect the calibration number because the sensor will still be operating in the linear range.

A Matlab™ program was developed so that a quick analysis of the data could be completed. The program took outputs from the datalogger, analyzed readings from a five second time period during each step and averaged the five seconds of readings to get a single averaged reading for each step. This created a resulting file that graphed the voltage outputs versus known tilt angle for that data step. An example of this data table created by Matlab™ processing of the calibration data can be seen in Table 5-2. The table shows the averages for each step, the maximum and minimum values during that step, and the standard deviation of the data at that step. This data can be plotted to get a better visual representation of the calibration data.

Table 5-2: Data sheet created by MatLab processing of calibration data. The first column is in arcminutes and the other four columns are in millivolts.

Minutes	Averages	Maximums	Minimums	STD	Linear Fit	
0	-9.49425	-9.193053	-9.533537	0.110934	1.567786	-8.570155
23	24.81601	25.53626	24.51481	0.324114		
46	61.28702	61.28702	61.28702	7.25E-15		
69	97.8628	98.05923	97.37827	0.275315		
92	133.8755	134.491	133.4695	0.319696		
115	170.1238	170.2417	169.9012	0.165199		
138	206.4639	207.0139	205.9925	0.36131		
161	242.1754	242.4242	241.7433	0.227021		
184	278.3845	278.856	277.8345	0.273706		
207	314.5281	314.9472	314.2662	0.199887		
230	350.9206	351.0385	350.698	0.165199		
253	387.6012	388.1512	387.1297	0.290156		
276	423.8888	424.2424	423.5614	0.203863		
299	461.3027	461.6956	461.0146	0.229777		
276	426.2198	426.2853	425.9448	0.136853		
253	390.469	390.875	390.194	0.193078		
230	354.2992	354.7838	354.1028	0.196739		
207	318.4568	318.6925	318.0115	0.210323		
184	282.3132	282.6013	281.9203	0.20862		
161	246.51	246.51	246.51	1.74E-13		
138	210.72	211.0997	210.4188	0.222253		
115	174.3406	174.668	174.3275	0.066778		
92	138.7863	138.9173	138.5768	0.168935		
69	101.2022	101.4641	100.7831	0.199887		
46	65.37283	65.37283	65.37283	1.45E-14		
23	28.60061	28.60061	28.60061	7.25E-15		
0	-7.490636	-7.490636	-7.490636	3.62E-15		
-23	-43.58188	-43.58188	-43.58188	1.45E-14		
-46	-80.24933	-80.01361	-80.3541	0.160261		
-69	-116.0525	-115.7644	-116.7858	0.267082		
-92	-152.5366	-152.5366	-152.5366	5.8E-14		
-115	-189.3088	-189.3088	-189.3088	8.7E-14		
-138	-224.9548	-224.7191	-225.7405	0.268431		
-161	-261.4258	-260.8103	-261.4913	0.167344		
-184	-296.7444	-296.2206	-296.9016	0.240399		
-207	-331.5261	-331.2904	-331.9714	0.268442		
-230	-366.3602	-366.0197	-366.7007	0.096308		
-253	-402.0586	-401.7705	-402.4514	0.208597		
-276	-437.0236	-436.4998	-437.1808	0.220265		
-299	-471.6875	-471.5696	-472.2505	0.19121		
-276	-438.6344	-437.8617	-439.5641	0.436649		
-253	-404.1146	-403.8134	-404.4944	0.22228		
-230	-369.1103	-368.7436	-369.4246	0.164658		
-207	-334.6298	-334.3548	-335.0357	0.215742		
-184	-299.4814	-298.9445	-299.6254	0.219002		
-161	-264.2151	-264.2151	-264.2151	1.16E-13		
-138	-228.7918	-228.4644	-228.8049	0.066778		
-115	-192.3863	-192.0327	-192.7136	0.225432		
-92	-157.0546	-156.6224	-157.6438	0.227033		
-69	-121.1335	-120.8716	-121.2121	0.146302		
-46	-84.4399	-84.4399	-84.4399	1.45E-14		
-23	-48.12603	-47.66768	-48.68913	0.332801		
0	-12.12645	-11.91692	-12.2574	0.168925		

The slope of the graphed line created by the Matlab™ program was the calibration number needed to relate the tilt angle to the change in the voltage throughout the linear range. This is a scale factor that relates the voltage for determining the tilt angle. The equation can be seen in Equation 3, where V is voltage, θ is the angle and S is the scale factor.

$$\Delta V = \Delta\theta * S \qquad \textbf{Equ. 3}$$

In order to determine the repeatability of the test, the calibration process was completed on Sensor #2, Y-Axis two times. The results were compared to determine if the process was repeatable. It can be seen from Figure 5-3 and Figure 5-4 that the slope of each test is approximately equal.

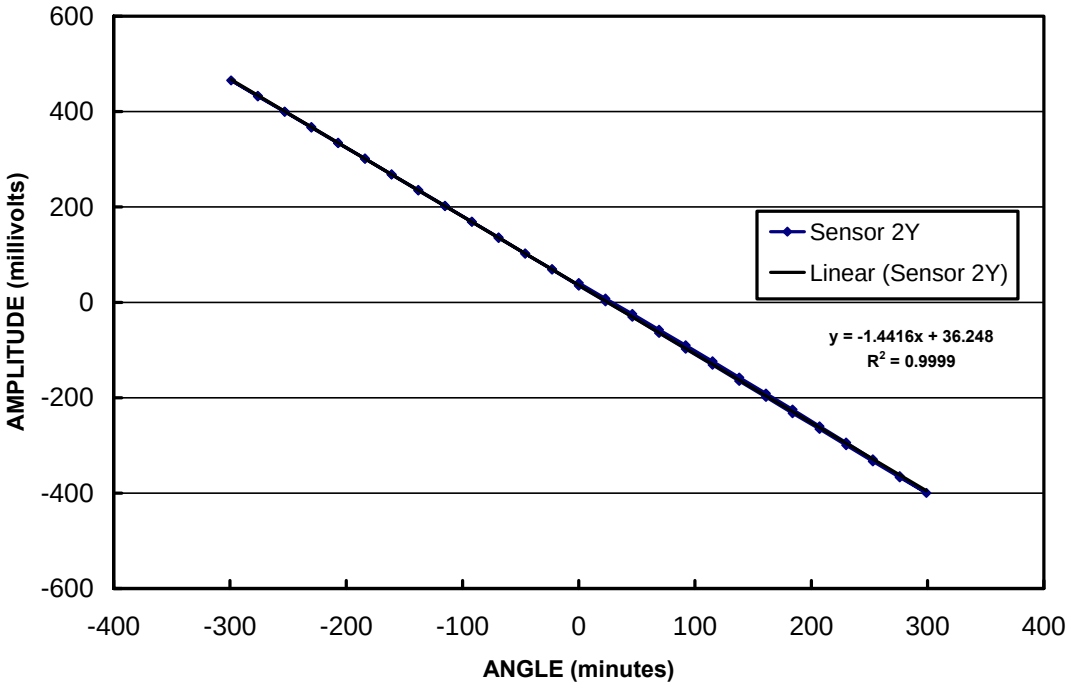

Figure 5-3: Graph showing the first calibration of Sensor #2, Y-Axis.

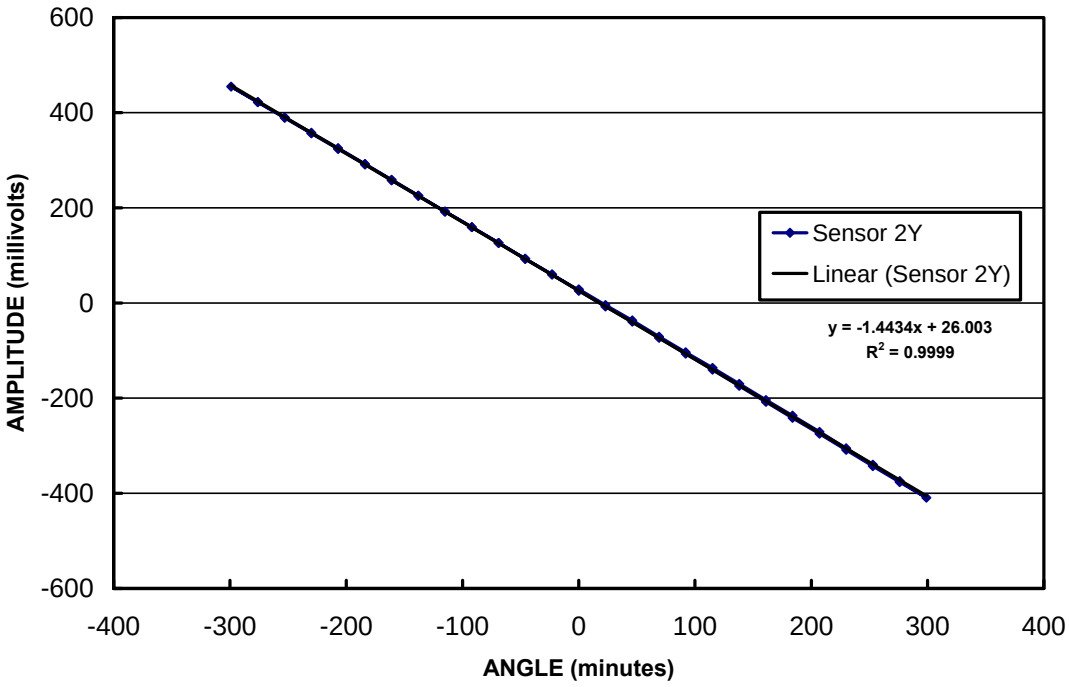

Figure 5-4: Graph showing the second calibration of Sensor #2, Y-Axis.

The first test showed a slope of -1.442 (mV/arcminute) and the second test showed a slope of -1.443 (mV/arcminute). The Coefficient of Determination (R^2) value is approximately equal to one, which shows linearity of the sensor output for both sensors. From these relationships, it was determined that the calibration process was repeatable. The near equal values also show that the calibration process is of high enough precision to be used for the entire sensor array.

A problem that occurred during sensor calibration was a short circuiting of the module's board. The aluminum standoffs used to mount the modules onto the calibration platform were just wide enough to cause a short-circuit near the mounting holes. This would cause the sensors to immediately output a constant voltage despite the tilt angle

experienced. This problem was resolved by installing small insulating washers placed between the module board and the aluminum standoffs.

Another problem during calibration was isolating each of the two axes for calibration. In order to do this, the sensor must be tilted in the one axis without bleeding over to the other. The resulting bleed over could create an inaccurate tilt angle correlation. The biggest obstacle in creating an ideal one axis tilt was that each sensor was soldered together differently, so that no sensor was mounted precisely perpendicular to the module board. This being known, the solution to the problem would have to be to minimize the amount of voltage overflow that each of the sensors would experience into the axis not being calibrated.

In order to minimize the bleed over, a precision spacer was used to distance the module board from the angle bracket. This spacer was placed between the board and bracket, and the sensor was tightened into place. Resulting measurements showed that this method kept the bleedover to a minimum, but was still going to be a small source of error that would affect the sensor calibration measurements.

The calibration procedure was completed for all of the sensors. The scale factor, which relates the voltage output to the angle experienced by the sensor, will be applied to the sensor output for a more complete sensor characterization. A table of the scale factors as well as the calibration graphs for each axis of each sensor can be found in Appendix A.

5.4. Stationary Testing on Iron Table

It was found that drift created a significant problem during calibration. Drift is the gradual change of outputs over time. This is a known characteristic of supporting electronics that is not just characteristic of this specific system. It is typically caused by warm-up of the equipment due to thermal effects on circuits as well as long time drift of that circuit. Drift is an error that cannot be fully eliminated but can be mitigated in order to obtain better data. In order for the calibration process to better reflect actual sensor behavior, the effects of drift needed to be minimized. In order to do this, an overnight test was run on the sensors to determine the drift magnitudes after the initial power-up of the sensors. A graph of the data can be seen in Figure 5-5.

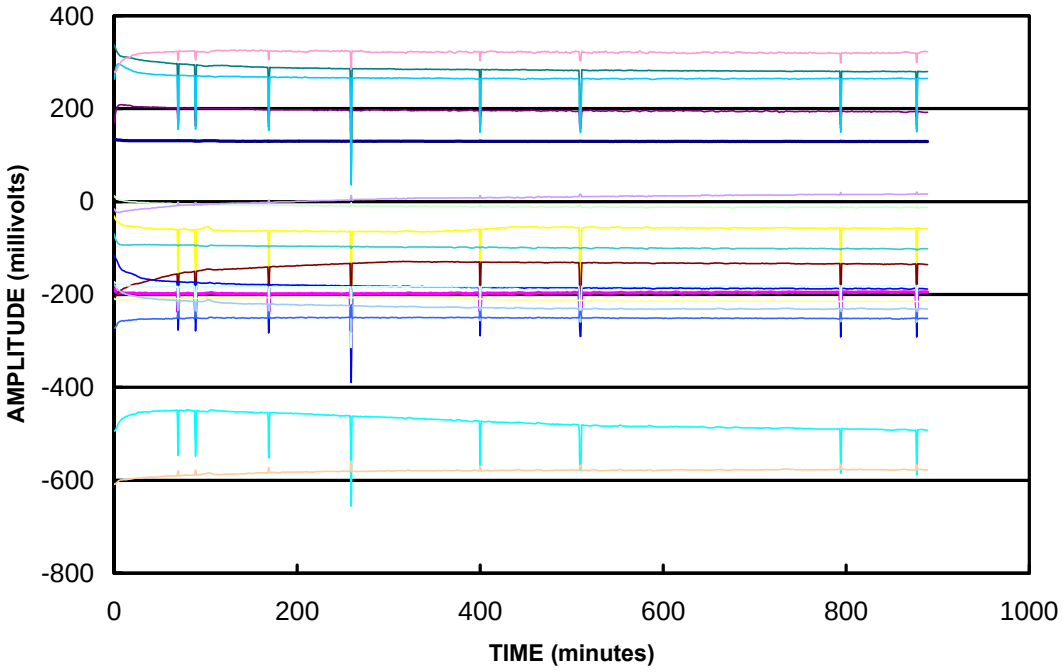

Figure 5-5: Graph of the Sensors #1-3 and 5-10, X and Y-Axis, voltage output exhibiting drift after initial power-up.

It was found from this data that the most significant drift occurs in the first hour after sensor power-up. Drift averages can be seen in Table 5-3. The average drift in the sensors was approximately 24 millivolts in the first hour, but was approximately 3 millivolts in the second hour. The drift became less than one millivolt per hour after the first six hours of warm-up. For this reason, during the calibration process, the sensors were allowed to warm-up for an hour prior to calibration. This resolved nearly all drift problems during the calibration process. However, a long term drift issue was found and can be seen in Figure 5-5. The occurrence of long term drift needed further observation and stationary tests were designed in order to understand this problem. There are several errant points seen on the graph that can be eliminated using basic filter algorithms.

Table 5-3: Averaged data from X and Y axis of all sensors showing the drift in the first six hours.

Time Period (minutes)	Average Change (mV)
0-60	24.058
60-120	2.912
120-180	2.105
180-240	1.409
240-300	1.416
300-360	0.913

Stationary tests also were conducted for several days to better understand the drift problems. This test set-up can be seen in Figure 5-7. A closer view of the sensors can be seen in Figure 5-6. In this case, the sensors were attached to a custom machined mounting plate that accommodated standoffs, strain relief and plate mounting on the rotary stage. These plates provided locations for up to five sensors apiece. Utilizing datalogger, several 24 hour periods of data were collected in order to determine the drift.

For the sake of comparing drift information, the drifting has been calculated as a drift per day. The results shown in Table 5-4 and Table 5-5 consist of two 1-day periods in the stationary position. These two days were at the end of the testing so that a true drift without warm-up periods could be analyzed. The first ½ hour and last ½ hour of each day has been averaged into one tilt value for each axis. The standard deviation of the drift during the period is calculated along with the average drift over the period. The difference between the last and first ½ hour average is considered the drift per day. Because calibration numbers are sensor dependent, the drift data presented here will be presented in millivolts rather than arcdegrees. To limit the effect of temperature compensation, which was not done on the data, the temperature during the tests was kept relatively constant. For the stationary tests, it was recorded that the temperature over the course of the test changed less than 0.25°C, so the effects of slight temperature differences was not considered.

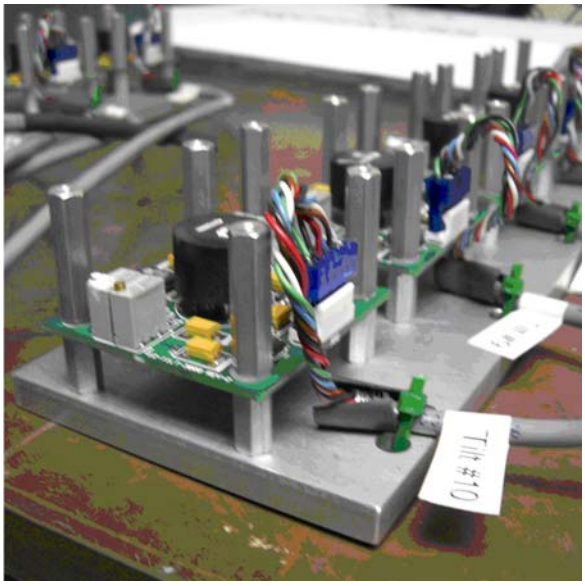

Figure 5-6: Close-up photograph of sensors on aluminum plate.

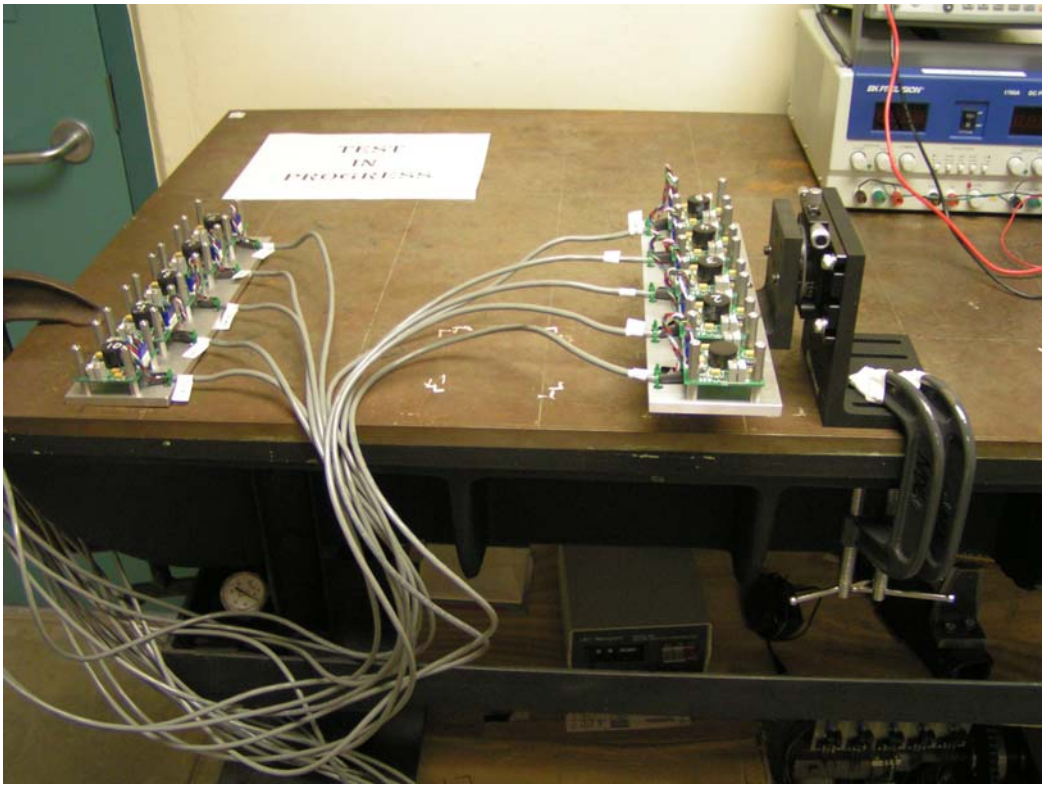

Figure 5-7: Photograph of stationary test set-up.

Table 5-4: Drift data from stationary testing for X-Axis.

Sensors Stationary X-axis										
Drift per Day in mV - average of 1/2 hour (excluding errant points)										
		Sensor 2	Sensor 3	Sensor 4	Sensor 5	Sensor 6	Sensor 7	Sensor 8	Sensor 9	Sensor 10
22-Sep	Difference	8.258427	-0.39125	34.47195	6.935633	3.7212	-16.3083	0.898267	-5.8407	5.4709833
23-Sep		5.180738	-1.62525	-3.8231	4.2782	1.63744	-18.6355	-1.5872	-9.0926	-2.210583

Maximum		8.258427	-0.39125	34.47195	6.935633	3.7212	-16.3083	0.898267	-5.8407	5.4709833
Minimum		5.180738	-1.62525	-3.8231	4.2782	1.63744	-18.6355	-1.5872	-9.0926	-2.210583
STD		2.176254	0.87257	27.07869	1.879089	1.473441	1.645591	1.75749	2.299441	5.4316879
Average		**6.719583**	**-1.00825**	**15.32442**	**5.606917**	**2.67932**	**-17.4719**	**-0.34447**	**-7.46665**	**1.6302**

Table 5-5: Drift data from stationary testing for Y-Axis.

Sensors Stationary Y-axis										
Drift per Day in mV - average of 1/2 hour (excluding errant points)										
		Sensor 2	Sensor 3	Sensor 4	Sensor 5	Sensor 6	Sensor 7	Sensor 8	Sensor 9	Sensor 10
22-Sep	Difference	5.791342	1.6695	-54.8978	-13.3585	-1.27113	15.7377	-0.04228	5.583367	-0.110938
23-Sep		2.712238	0.330267	-4.69981	-9.981	0.007983	18.18237	1.636567	5.027517	-1.020883
Maximum		5.791342	1.6695	-4.69981	-9.981	0.007983	18.18237	1.636567	5.583367	-0.110938
Minimum		2.712238	0.330267	-54.8978	-13.3585	-1.27113	15.7377	-0.04228	5.027517	-1.020883
STD		2.177255	0.946981	35.49537	2.388253	0.904472	1.72864	1.187126	0.393045	0.6434283
Average		**4.25179**	**0.999883**	**-29.7988**	**-11.6698**	**-0.63157**	**16.96003**	**0.797142**	**5.305442**	**-0.565911**

For the stationary tests a new sensor was used as Sensor #4. Because Sensor #1 was replaced shortly after the stationary tests, it was not included in this analysis.

The stationary sensors drift from one day to another. Based on the data collected from these stationary tests, the sensors with the most drift are Sensors 2, 4, 5, 7, and 9. These sensors have a drift larger than 5 mV per day. Sensors 4 and 7 have an average drift larger than 10 mV per day for both axis. Sensor 4 was later found to be defective and had to be replaced.

The stationary testing shows that all sensors, with the exception of the new Sensors 1 and 4, have an average drift of less than 18 mV per day, with four of eight sensors having a drift of less than 5 mV per day for both axis.

5.5. Stationary Sensors with Varying Temperature

Testing was conducted to evaluate the effects of varying temperatures on sensors at a constant tilt angle. Data from the sensors has all been collected under relatively stable temperature conditions in previous tests. However, when the sensors are placed in a harsher environment, such as on an actual bridge pier, they will be susceptible to significant changes in the data output due to the more extreme temperature changes. This

is caused by sensor enclosure expansion and contraction and, more importantly, volumetric changes in the electrolytic fluid. For this reason, testing was necessary to better understand the effects of temperature changes on the sensor's output.

The temperature control was accomplished using a temperature chamber that could be regulated within +/- 0.1 °C. Sensors were initially placed inside the chamber in a relatively level position. They were mounted on the two aluminum plates that accommodate five sensors apiece which were also used in the initial stationary tests.

For this test, the sensors were left in the stationary position while the chamber temperature was increased. Temperature was changed from 20°C to 30°C to 40°C with 24 hours between each increase. A graph showing typical sensor behavior during this test can be seen in Figure 5-8.

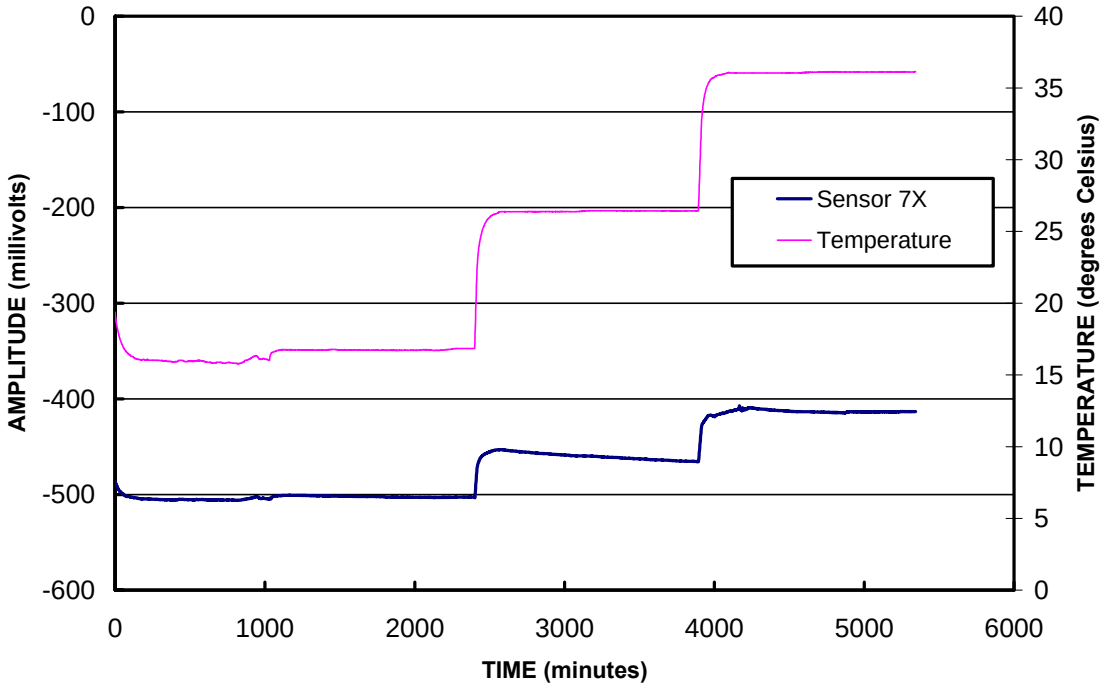

Figure 5-8: Graph of Sensor #7, X-Axis output during stationary test with temperature change.

This graph shows the sensor output from Sensor #7, X-Axis. The voltage output increases with the temperature without sensor movement occurring. An analysis of this data from all the sensors can be seen in Appendix B. The average, minimum, maximum, standard deviation and variance of the sensors voltage output at the different temperatures can be seen. Many of the sensors showed no observable trend with temperature change. This test gave data showing changes in voltage offsets, however, it was not the data needed for the temperature correction factor that will adjust the calibration slope. This data will is useful for understanding the stationary sensor behavior during temperature fluctuations. Variation may be the result of thermal effects on the stage, temperature chamber or sensor boards.

5.6. Fixed Temperature with Varying Sensor Angles

The behavior of the sensors is known to change with respect to the temperature. For this reason, a temperature correction factor must be used to adjust the equation for the tilt angle with respect to the temperature of the sensor. Manufacturer specifications suggest a 0.08% change in the calibration slope per degree Celsius. In order to verify this specification, the sensors were tilted through precise increments, similar to the calibration process, at different temperatures. The mV/angle slope of these tests was then compared to the expected change of slope in order to verify the manufacturer's specification.

For this test, the sensors were mounted on the rotary stage within the temperature chamber. This allowed the sensors to be tilted in precise increments while operating in an environment of a specified temperature. Sensors #1-5 were tilted in 69 arcminute

increments every hour at 20°C, 30°C and 40°C temperatures. These increments covered approximately (-) 5 arcdegrees to (+) 5 arcdegrees. The test set-up can be seen in Figure 5-9.

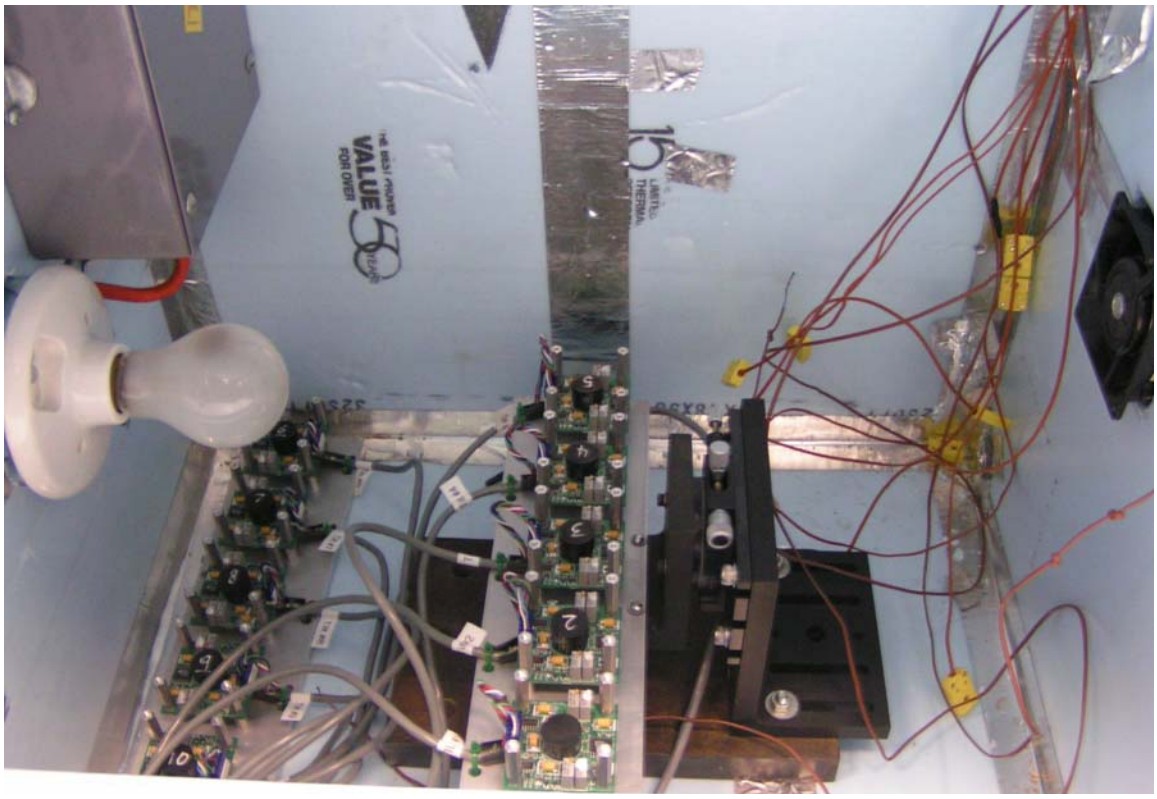

Figure 5-9: Photograph of the test set-up for the temperature effects on tilt.

Results from this test provided the needed data showing the sensor behavior at different temperatures while tilting through specific increments. A half hour average of the sensor output at each increment was analyzed. Graphs of this data can be seen in Figure 5-10, Figure 5-11, and Figure 5-12. This data is also found tabled in Appendix C.

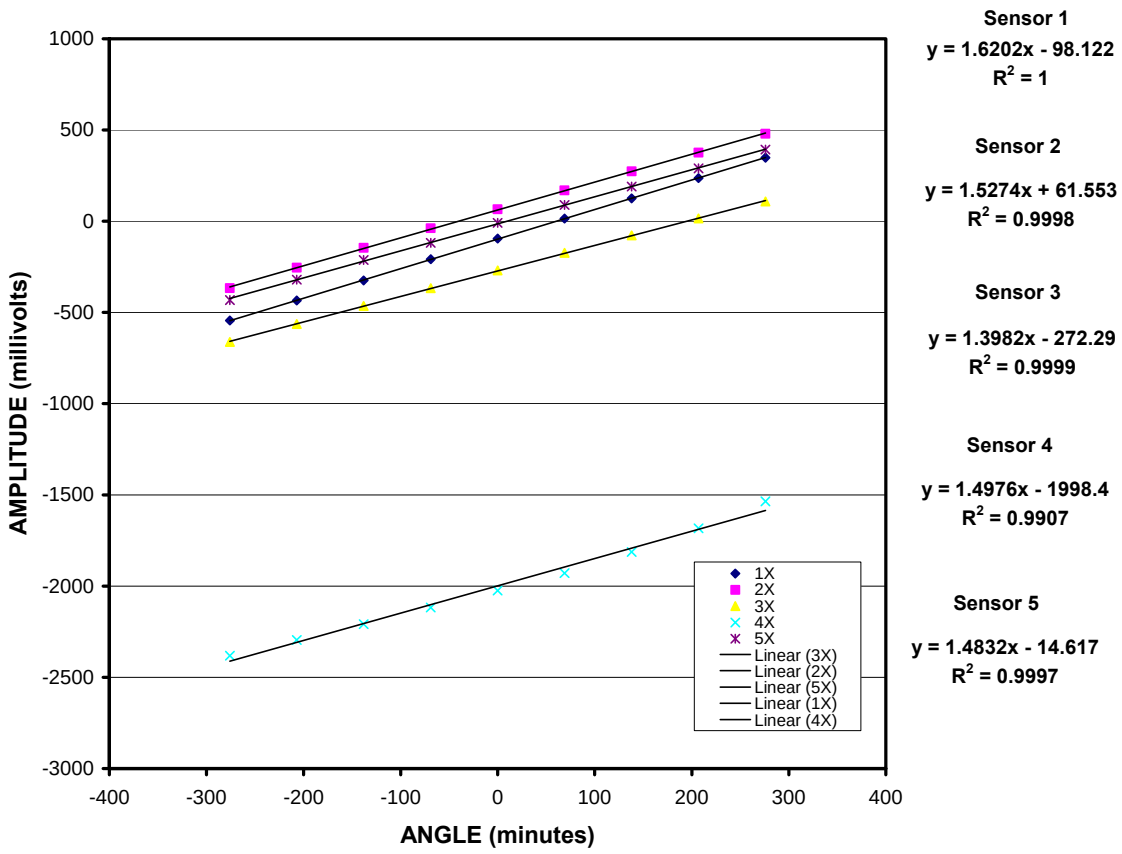

Figure 5-10: Graph showing Sensors #1-5, X-Axis at 20°C stepped in increments covering approximately 10 arcdegrees.

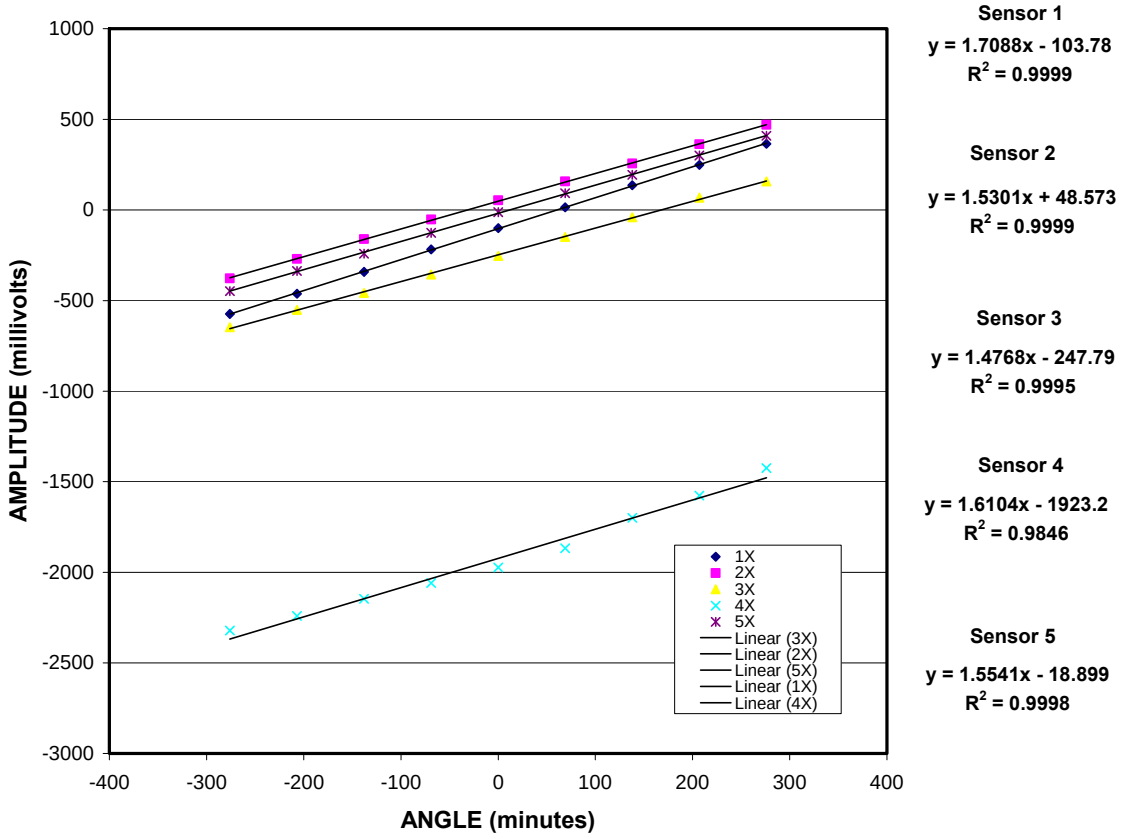

Figure 5-11: Graph showing Sensors #1-5, X-Axis at 30°C stepped in increments covering approximately 10 arcdegrees.

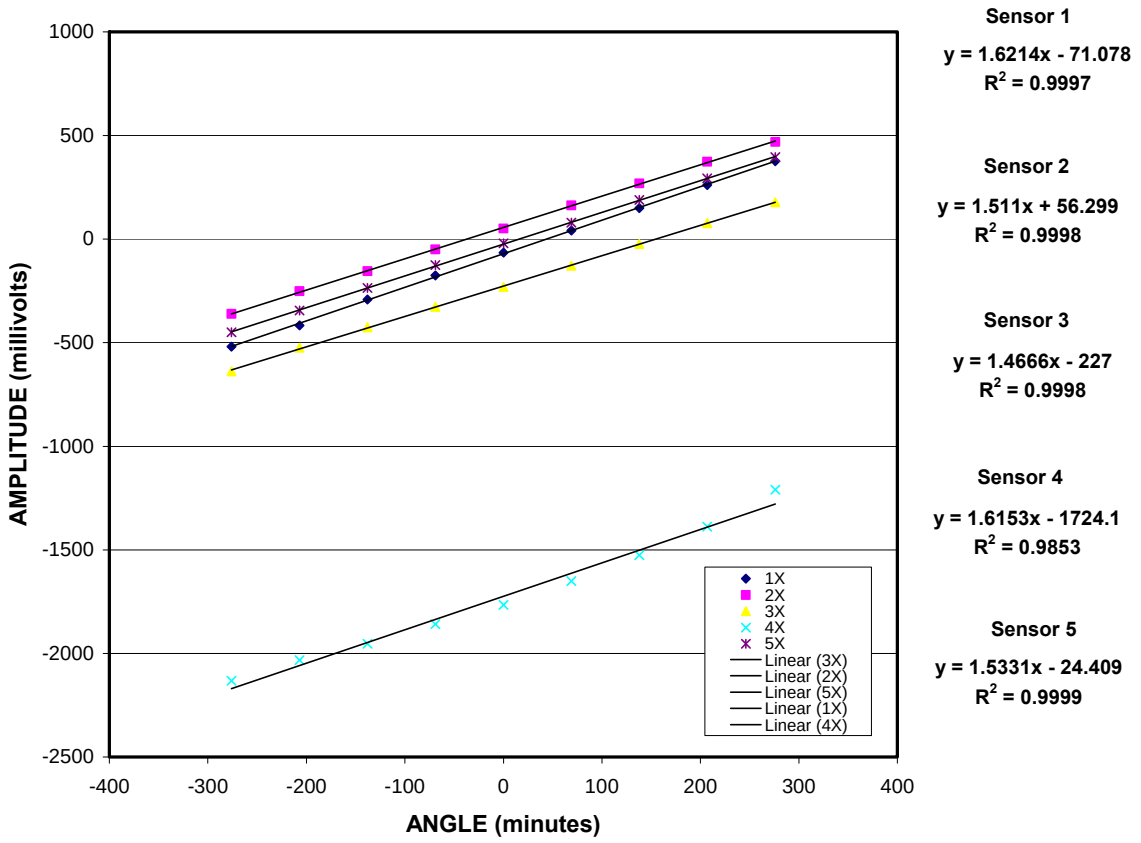

Figure 5-12: Graph showing Sensors #1-5, X-Axis at 40°C stepped in increments covering approximately 10 arcdegrees.

From the graphs, it can be seen that Sensor #4 behaves in an inconsistent manner. For this reason, this sensor, along with Sensor #1, was replaced after this test was completed.

Using this data, calibration numbers can be found for each sensor at the three different temperature levels. These calibration numbers can also be compared to the original calibration numbers. These numbers can be seen in Table 5-6.

Table 5-6: Calibration numbers from incremental tests at specified temperature.

Calibration Numbers (mV/min)				
	Initial Calibration	20°C Test	30°C Test	40°C Test
Sensor 1	---	1.6202	1.7088	1.6214
Sensor 2	1.5884	1.5274	1.5301	1.5110
Sensor 3	1.5245	1.3982	1.4768	1.4666
Sensor 4	1.5610	1.4976	1.6104	1.6153
Sensor 5	1.6317	1.4832	1.5541	1.5331

The temperatures that the sensors were experiencing during these tests can be seen in Table 5-7. The calibration process does not record individual sensor temperature, so an external temperature was recorded and used. Because the accuracy of the sensor temperature is only +/- 3°C, this was acceptable.

Table 5-7: Temperature readings from sensors.

Sensor Temperatures during Tests				
	Initial Calibration	20°C Test	30°C Test	40°C Test
Sensor 1	---	---	---	---
Sensor 2	18.8*	17.63	31.72	46.05
Sensor 3	17.7*	16.08	30.23	44.57
Sensor 4	17.8*	16.64	30.86	45.27
Sensor 5	17.8*"	16.87	30.71	44.81

* - Temperature was determined from the ext_temp using relationship from previous tests
" - Initial ext_temp was assumed based on other tests

From the initial calibration numbers, the 0.08% change in the calibration slope per degree Celsius, specified by the manufacturer, was applied. This gives an idea of what the expected calibration numbers would be after a temperature change. This can be seen in Table 5-8.

Table 5-8: Expected Calibration numbers with applied 0.08% slope change.

Expected Calibration Numbers (mV/min)				
	Initial Calibration	20°C Test	30°C Test	40°C Test
Sensor 1	---	---	---	---
Sensor 2	1.5884	1.5899	1.5720	1.5538
Sensor 3	1.5245	1.5265	1.5093	1.4918
Sensor 4	1.5610	1.5624	1.5446	1.5267
Sensor 5	1.6317	1.6330	1.6149	1.5965

By comparing the values from Table 5-8 with those from Table 5-6, an error can be determined. This resulting error can be seen in Table 5-9.

Table 5-9: Data showing the percent error in the experimental calibration numbers.

Percent Error in experimental calibration numbers				
	Initial Calibration	20°C Test	30°C Test	40°C Test
Sensor 1	---	---	---	---
Sensor 2	n/a	3.93%	2.67%	2.75%
Sensor 3	n/a	8.41%	2.15%	1.69%
Sensor 4	n/a	4.15%	4.26%	5.81%
Sensor 5	n/a	9.17%	3.76%	3.97%

The maximum percent error from the comparison of the experimental and expected calibration numbers is less than ten percent. Seventy five percent of the comparisons show less than five percent error. This relatively small percent error is acceptable due to the limitations of the test setup. Based on these results, the value of 0.08% can be used in future processing.

5.7. Analysis of Test Bridge

In order to prepare for the evaluation of the sensor array, it was necessary to analyze the test bridge with the wireless tilt monitoring system. A test was run in which the test bridge was tilted a known amount along one axis. The bridge was tilted in only one axis by only adjusting a single screw jack. This was done to simplify the test so that any problems that might be found during the test could be isolated more effectively.

Because the bridge axes do not coordinate with the sensor axes, some manipulation was required in order to ensure that the sensor's tilt output corresponded correctly with the predicted tilt. To analyze the repeatability of the test, the sensor was later moved to the opposite side of the test bridge where the analysis was redone.

Figure 5-13: Photographs of the wireless tilt monitoring system on test bridge pier.

In the beginning of the test, the tilt output for the starting position was recorded. Then, the screw was tightened by turning it five complete turns, placing the bridge corner in a lower position. Once the movement was complete, the sensor was allowed to settle for 30 seconds. Once 30 seconds elapsed, the tilt output was recorded. The bridge was then tilted back to its starting position by turning the screw back five times. With the bridge back in its original position, the sensor was allowed to settle and data was recorded. This process of screwing and unscrewing was repeated for a total of ten times. Once the test was completed with the box on the left side of the bridge pier, the box was removed and placed on the right side. The entire test was then repeated with the box on the right side of the bridge.

The goal was to determine if the data correlated correctly with the predicted tilt of the bridge. Knowing that the bridge was tilted along one axis by turning the screw five times, the actual tilt could be determined using the numerical angle prediction method. It was predicted that the test bridge tilted 0.529 degrees. The average angle that the sensor measured was 0.554 degrees. The difference is 0.025 degrees. This is less than five percent error and can be considered suitable for the evaluation platform.

Overall, the test was successful for determining the correlation between sensor output and actual tilt of the test bridge. The results allow further testing of the sensors using the test bridge to continue.

Initial analysis of the test bridge to evaluate the long-term performance of the sensor system under simulated conditions was completed. For this testing, the sensors were mounted on the machined angle brackets, which were attached to the test bridge. The sensor configuration consisted of three sensors on each side of the adjustable pier, making up the PSA, and three sensors on three separate girders, making up the SSA. This setup can be seen in Figure 5-14, Figure 5-15, Figure 5-16 and Figure 5-17. Because of problems with the sensors, Sensor #1 and #4 were removed for some of the testing. Figure 5-14 and Figure 5-15 show the overall array placement on the test bridge. Figure 5-16 and Figure 5-17 show a close-up picture of the SSA and PSA.

Figure 5-14: Photograph showing sensor placement on test bridge.

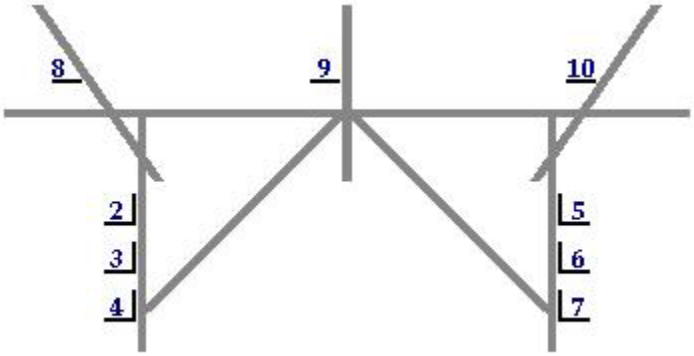

Figure 5-15: Diagram showing sensor locations.

Figure 5-16: Photograph of sensors mounted on pier of test bridge.

Figure 5-17: Photograph of sensors mounted on the girders of the test bridge

In order to test the sensor array on the test bridge during bridge movement, a series of tests were run to determine if the sensors showed similar outputs. This was done by adjusting the screw jack at one corner and observing the change of angle that the sensors exhibited. For this test, Sensors #2-7 made up the PSA and will be the only sensors analyzed. The calibration factors were applied to the voltage output of each of the sensors used during the test in order to get an angular change. The output of the sensors was analyzed by converting the X and Y axis of tilt into a vector. The initial and final vectors were analyzed to find the change of angle between them. Sensor #4 showed bad results and was replaced.

These tests show that there was good correlation between the sensors. Tabulated data from one test with a five screw turn movement can be seen in Appendix D. This data shows the sensor outputs and the statistical analysis of the outputs. The sensors showed an average of 0.53 arcdegrees with a standard deviation of 0.03 arcdegrees. This deviation is acceptable for the sensor array.

To determine the long-term drift behavior of the sensors while mounted on the test bridge, the datalogger was programmed to obtain readings every five minutes of time. This testing lasted three weeks. The room temperature was kept at approximately 22°C during this testing. Although there were some disturbances during this analysis, the bridge was left stationary for the majority of the testing.

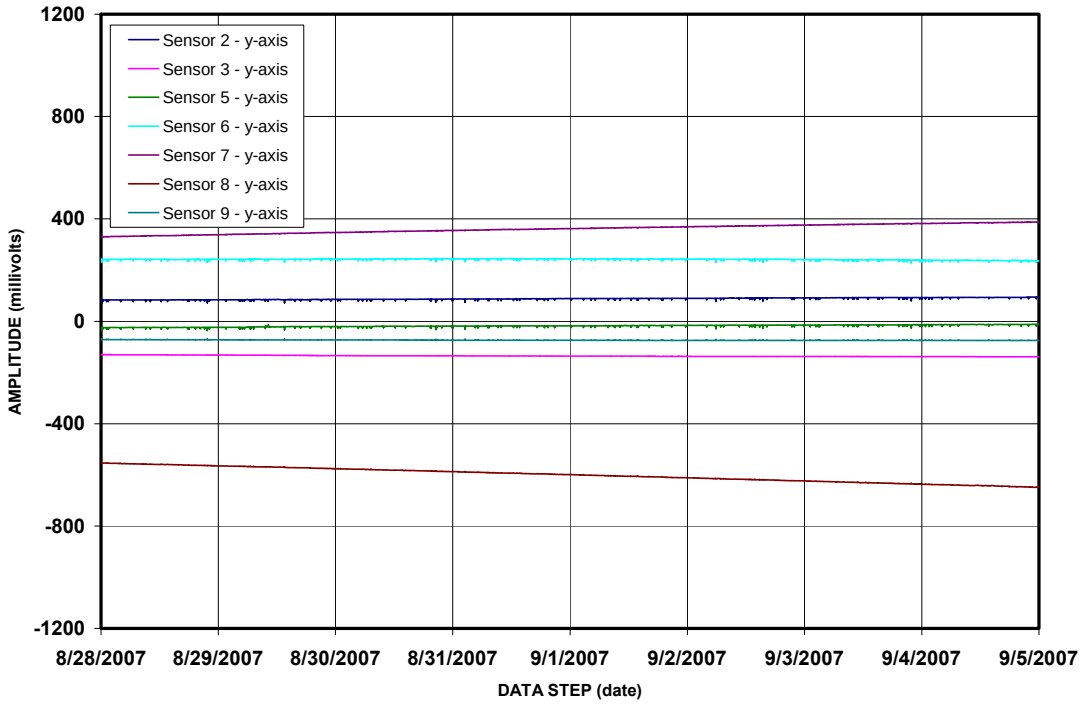

Figure 5-18: Graph showing the drift in sensor output over an eight day period for the X-axis.

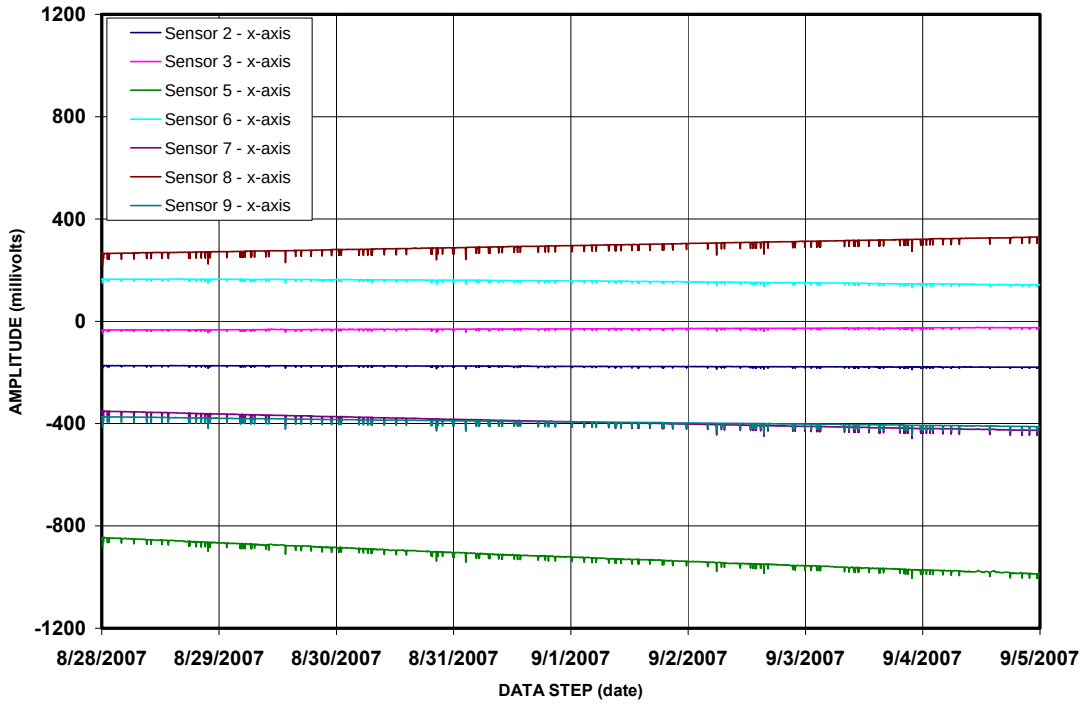

Figure 5-19: Graph showing the drift in sensor output over an eight day period for the Y-axis.

The data from the sensor outputs showed obvious drift in some of the sensors. A graph of this behavior can be seen in Figure 5-18 and Figure 5-19. It is important that some of the sensors exhibited only slight variations when other sensors showed drift over the duration of the testing. This more stable characteristic shown by some sensors will allow for sensor groups to work together in determining the true behavior that is being experienced at their location. An analysis of the daily drift in the sensors can be found in Appendix D. This shows the daily initial and final half hour voltage outputs for Sensors #2,3 and 5-9, X and Y-Axis. The difference in voltage throughout each day is shown along with the maximum, minimum, standard deviation and average drift in voltage for the entire test. The drift in the sensors ranged from 19.75 mV/day to 0.06 mV/day.

5.8. Long-Term Stationary Testing at Controlled Temperature

Because the issue of drift has caused a significant problem in testing, another long-term test was completed. This test was to analyze sensor behavior in an environment that is as stable as could be simulated for approximately two weeks. For this reason the sensors were placed in a stationary position within the temperature chamber. This environment was set at 20°C. Change in the sensors' behavior was analyzed to see the drift characteristics.

It was discovered during this testing that, in general, the sensors will continue to drift for up to five days before reaching a steady output. This may to be caused by a settling time that is associated with electrolytic tilt sensors. During this period a thin layer of fluid will drain from the walls of the sensor and settle down to the base (Vitro 2000). After this settling period is over, many of the sensors show stable output. An example of this can be seen in Figure 5-20.

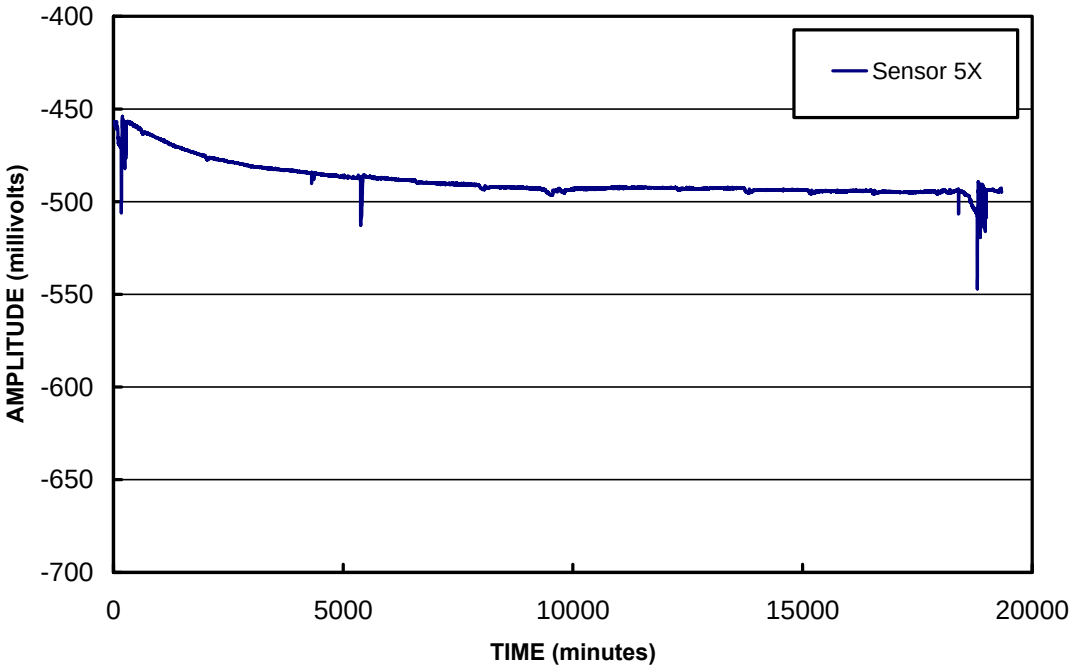

Figure 5-20: Graph showing the behavior of Sensor #5, X-Axis during long-term testing at controlled temperature.

Also, it is expected that some of the drift characteristics of the sensors may be sinusoidal. This type of behavior would allow for data processing to cancel out drift errors by averaging the output over a period of time. An example of sinusoidal behavior exhibited by one sensor can be seen in Figure 5-21. Sinusoidal behavior was not seen in all sensors.

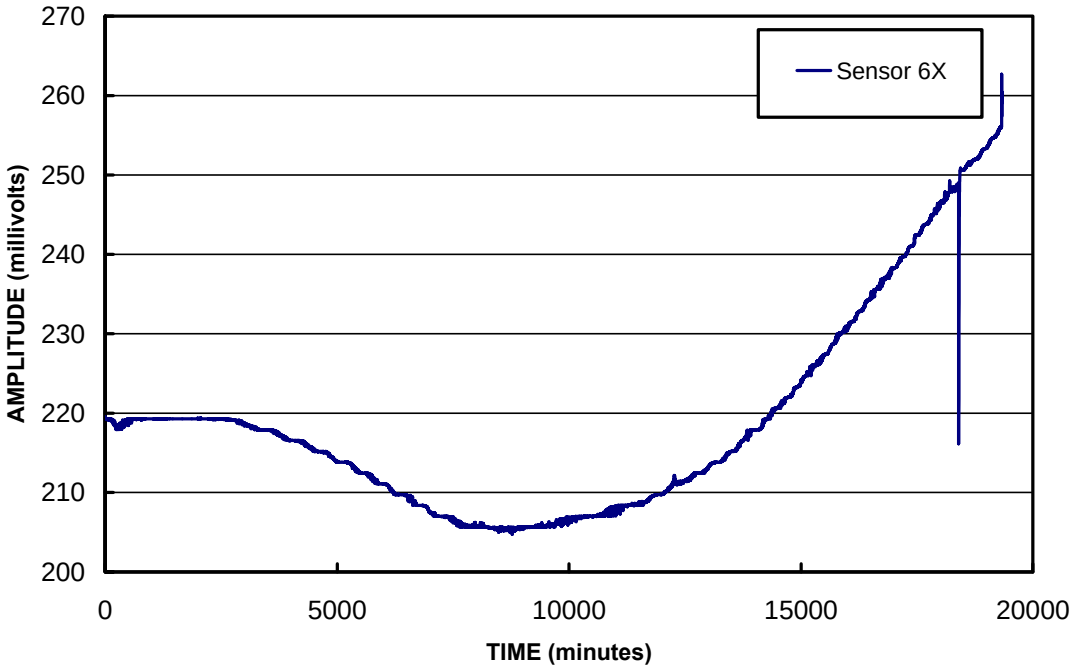

Figure 5-21: Graph showing the behavior of Sensor #6, X-Axis during long-term testing at controlled temperature.

Further analysis of the data can be found in Appendix E. This shows the daily initial and final half hour voltage outputs for Sensors #1-10, X and Y-Axis. The results of this test show that, given a period of approximately five days, the typical sensor shows greater stability. It can also be hypothesized that the drift in some of the sensors shows sinusoidal behavior that can be averaged in order to obtain a more accurate sensor output. This is being further investigated so that processing algorithms can compensate for this behavior.

5.9. Slowly Varying Angle Changes

This test was performed while keeping the sensors in the temperature chamber at a constant temperature (22°C). The sensors were placed on two aluminum plates, one

stationary with Sensors #6-10, the other tilting with Sensors #2-5. Sensor #1 was removed because of a defective module. Sensor #4 had a new 008-OP sensor to replace the defective one. This sensor may have required adequate break-in time that was not allowed before the testing began. For this reason, the sensor shows poor results. Sensors #2-5 were tilted 2.3 arcminutes (5 tick marks of the precision knob on the rotary stage) approximately every hour, excluding overnight. The rotary stage was tilted in 2.3 arcminute steps up to 23 arcminutes then reversed back to the starting position. It should be noted that the starting position was approximately 5 arcdegrees from level and the stage was tilted towards level position during the test. Testing began on 11-1-07 at 12:30 PM and ended on 11-3-07 at 3:30 PM.

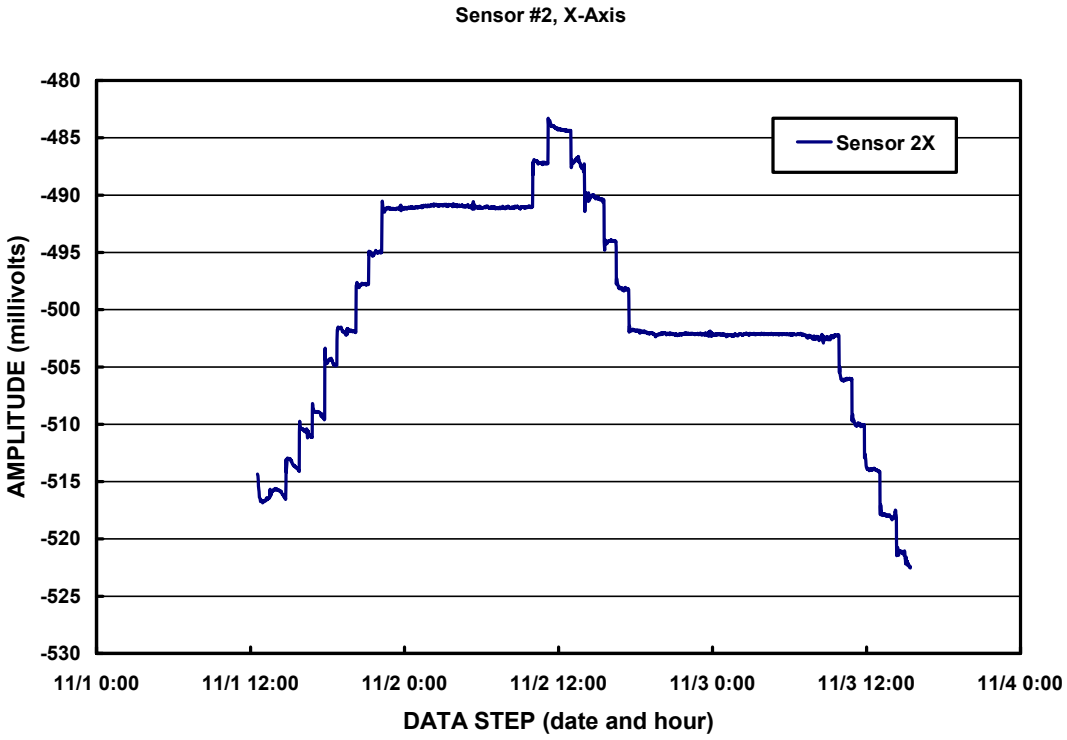

Figure 5-22: Graph showing Sensor #2, X-Axis behavior during 2.3 arcminute steps.

Data from one of the sensors can be seen in Figure 5-22. Data taken during the overnight periods shows little change. This testing showed that small angular changes could be detected with the sensors. The 2.3 arcminute steps are clearly visible and can be distinguished from the drift and noise of the system.

In order to determine the difference between drift and movement in post-processing, data statistics were used. The average, maximum, minimum, standard deviation and variance has been computed for each sensor's output. This was done over several different time periods including the entire test, 48 hours, 2 – 24 hours, 4 – 12 hours, and 8 – 6 hour periods. Tables of this data can be found in Appendix F.

Table 5-10 shows a statistical analysis of two different sensor groups. The stationary sensors are not on the rotary stage and do not move throughout this test. The other sensor group is being tilted on the rotary stage during this test; however, there are overnight periods when the sensors are not moved. Analysis of these sensors during time periods when they are not moving and time periods when they are moving is shown.

Table 5-10: Statistical Analysis of sensors during slowly varying angle changes.

Statistics for Standard Deviation from 8 - 6 hour periods					
	Average (mV)	Maximum (mV)	Minimum (mV)	STD (mV)	Variance (mV^2)
Stationary Sensors	0.504	1.077	0.056	0.272	0.074
Sensors NOT Moved	0.133	0.289	0.048	0.081	0.007
Sensors Moved	4.315	7.564	2.835	1.247	1.555

Using the standard deviation of the sensor groups, an obvious difference in the sensors' behavior can be seen during the period of movement. Based on this test, a movement resulted in an average standard deviation of 4.3 mV per 6 hour period, whereas drift alone resulted in an average of less than 0.5 mV per 6 hour period. This verifies that small sensor movements can be distinguished from the sensor drift

objectively. Results from this test can be used during the development of future algorithms that will rely on some statistical analysis of data processing.

5.10. Resolution Testing

There is more than one method of determining the resolution of the system. First of all, the resolution of the analog to digital (A/D) converter is considered. The A/D converter is capable of resolving 0.67 millivolts over a ten volt range. This is with a 13 bit conversion plus a differential measurement scheme, as reported by the manufacturer.

In the measurements from calibration, the data was collected over a ten arcdegree range, which covers nearly 1 volt and corresponds to approximately 1.5 millivolts/arcminute. If the A/D converter can resolve 0.67 millivolts and the calibration factor is 1.5 millivolts/arcminute, then there are 1.5 / 0.67 = 2.239 intervals per arcminute. This is equal to 26.8 arcseconds per interval as the max resolution of the A/D converter.

To determine the resolution of the sensors from observing collected data, it was necessary to find the smallest change that the sensor could detect in the quantity that was being measured. The initial resolution test was conducted with five sensors mounted on a machined plate that could be mounted on the rotary stage. The test was completed by changing the tilt every thirty seconds of time. Starting at a zeroed position, the tilt stage was tilted one tick mark of the rotary stage's precision knob. One tick is equivalent to 0.46 arcminutes. After five movements were made, the number of ticks traveled during the interval was increased to two ticks. Two tick marks are equivalent to .92 arcminutes. After five movements of two ticks were completed the number of ticks traveled during

the interval was increased to five ticks for five movements. Five ticks is equivalent 2.3 arcminutes. After this, the movements were reversed in the same fashion to return to zero. There are 50 ticks per full turn of the knob. One full knob turn is equivalent to 23 arcminutes.

Sensor #1 was replaced with one of the new sensors during this test and it shows bad results. Sensor #2 shows sensible results. A graph of the X-Axis of Sensor #2 shows visible steps and can be seen in Figure 5-23. Drifting is probably still an issue, and is most likely caused by lack of sensor warm-up time in this case. It should be noted, that no post-processing algorithms have been applied to the data.

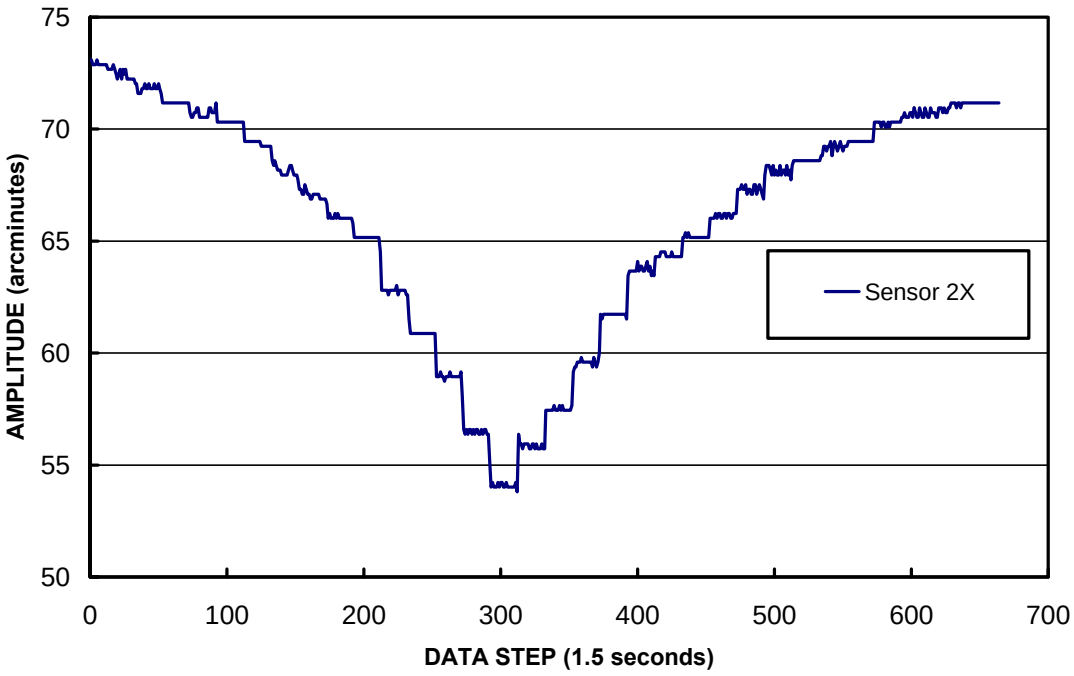

Figure 5-23: Graph showing stepped data for resolution test with Sensor #2, X-Axis.

It can be seen from Figure 5-23 that the 0.46 arcminute steps are visible. Because the rotary stage that is being used can only step in calibrated increments as small as 0.46

arcminutes, this is the highest resolution that can be observed with the lab tests being conducted. For this test, it can be said that the resolution of the sensors was at least 0.46 arcminutes.

In order to relate this resolution to the behavior of a bridge pier, a tilt angle with the lowest observable magnitude can be analyzed. Assuming a rigid structure, if a one hundred foot bridge pier is tilted 0.46 arcminutes, the displacement at the tip is only 0.16 inches from the original position. This is a very small displacement for a pier of this height.

The typical resolution that Advanced Orientation Systems, Inc specified as the maximum the sensors are capable of reaching is <3 arcseconds. A significant amount of this maximum resolution is lost due to the specific gain settings used, the A/D conversion and system noise. However, company specifications of their products are typically of higher quality than what is possible.

The purpose of another resolution test was to show two characteristics of the sensors. The first characteristic was to show that there would be less noise in the resolution data when the sensor was started at an initial tilt. The second characteristic was to verify the resolution of the sensor at the smallest increment possible with the rotary stage.

This test was conducted using the TiltFast program that collected data at 1.5 second intervals. The sensors were mounted on the aluminum plates that held five sensors at a time. The sensors were started at a five degree position, where they had been placed the day before. The data was cleared and the first movement began one minute afterwards. The sensors were moved one tick mark of the fine rotation knob every

minute of time for ten minutes of time. After ten movements, the datalogger was allowed to run for another two minutes of time, and then the data was collected.

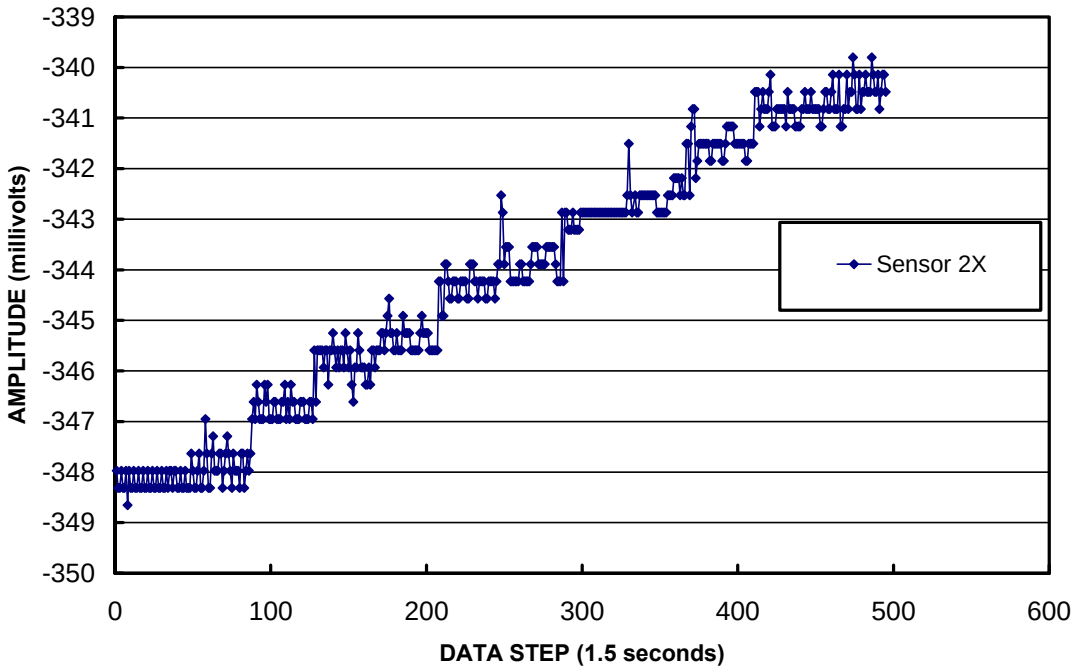

Figure 5-24: Graph showing the movements of Sensor #2, X-Axis.

One of the things to note about the data in Figure 5-24 is that the data shows clear steps of 0.340 millivolts between data points. This could be considered the resolution of data acquisition system for this test. This system uses a differential measurement scheme, as stated earlier, and apparently exhibit resolution that is different than specified by the manufacturer.

This data shows clear steps from the test of 0.46 arcminute increments. If the average standard deviation of the noise at each step is evaluated for this resolution test and the first resolution test, it can be seen that the noise was reduced by inducing an initial tilt. The average standard deviation for the first resolution test was 0.374 and it was 0.294 for the second test. It was hypothesized that the reason for this is that, at a

relatively level position, the electrolytic fluid amount on the conductive pins is less stable than when tilted.

This test also verified the resolution of the system that was found in the first resolution test. Clear steps from the rotary stage are easily seen when the data is analyzed. A graph displaying the average values at each step can be seen in Figure 5-25.

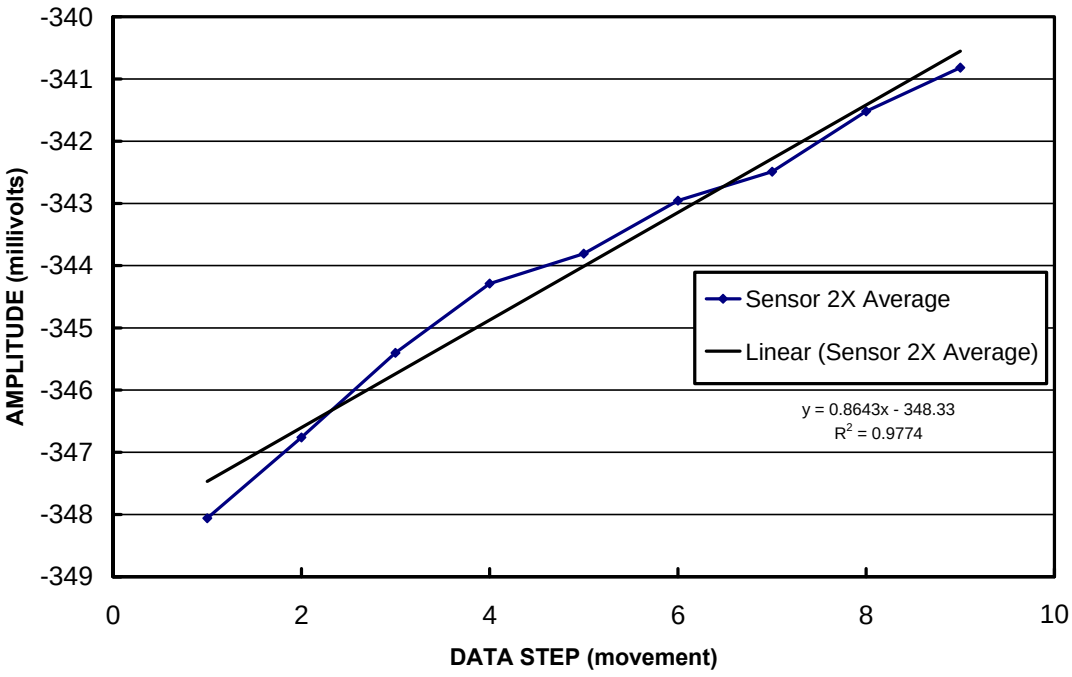

Figure 5-25: Graph showing averaged data at each 0.46 arcminute step from Sensor 2, X-Axis.

5.11. Algorithms

Algorithm development for processing the collected data will be a crucial part of this project. The function of these algorithms has been discussed in the task descriptions. It should be noted that calibration numbers, temperature coefficients and drift effects have been investigated and will be incorporated into the processing of the data.

Statistical methods of reducing sensor errors will also be considered during algorithm development.

6: Conclusion

6.1. Conclusion

Initial design of the long-term remote sensing system for bridge piers, utilizing tilt sensors as the primary instrumentation, has been completed. Design and construction of the sensor array and laboratory test fixtures has been completed. The system is currently being analyzed to better understand the long-term behavior under simulated conditions on the test bridge. Once a full characterization of the system's behavior can be completed, the system will move towards field analysis on a real bridge. Characterization of the system has yielded the following results:

- The multimeter and datalogger systems both perform adequately. Testing showed less than one percent difference between the two systems.
- A sensor calibration procedure was developed and performed on the sensor array. This provided a voltage/arcdegree correlation for each sensor. These values range from 0.074 Volts/arcdegree to 0.098 Volts/arcdegree.
- Short-term drift analysis was conducted that confirmed a significant warm-up period after initial power-up. This warm-up averaged 24 mV in the first hour compared to 3 mV in the second hour. Therefore, a warm-up period is required before sensor calibrations.

- Temperature analysis of stationary sensors showed a change in sensors' output voltage that correlated to change in the temperature. This voltage change must be considered when analyzing sensor output during diurnal temperature changes.
- The changing slope of the calibration curve due to temperature changes shows close relationship to the expected 0.08% change of slope per degree that was specified by the manufacturer.
- Analysis of the test bridge using the sensor array showed that the sensors had similar outputs after bridge movement. Stationary analysis of the test bridge shows similar behavior to other stationary analysis in regard to drift. Effective sensor mounting and performance was shown during this test. The results ensure that future testing on the test bridge can proceed.
- Stationary testing with controlled temperature typically exhibited a five day settling time for most sensors. This may be attributed to a thin viscous layer of electrolytic fluid slowly draining from the sensor walls. Some sensors exhibited a drift behavior that could be evident of sinusoidal drift.
- Slowly varying angle changes proved that small angular changes over a three day period were observable and could be distinguished from drift objectively. Stationary sensor output compared to the moving sensors showed statistical differences in voltage change during small angular changes.
- Testing showed the resolution of the system being used. The steps that could be resolved were at least 0.46 arcminutes, however this was the

smallest calibrated step the tilt stage was capable of performing. The sensor system is expected to resolve tilt steps of at least 0.46 arcminutes.

These portions of the overall sensor characterization will be applied to the algorithms that are to be developed for post-processing of the sensor output. The processing will provide more reliable data that will model the overall behavior structural behavior of bridge piers.

6.2. Future Work

Further characterization of the sensor array will be conducted in order to clarify their behavior under a variety of conditions. More long-term testing on the Test Bridge will be conducted to model the behavior of a real bridge. Development of algorithms for improving the robustness, redundancy and overall reliability of the system will proceed.

Appendix A. Calibration Numbers and Graphs

Table A-1: Scale factors from the calibration of Sensors #1-10, X and Y-Axis.

	mV/min			V/deg	
Sensor #	**X**	**Y**		**X**	**Y**
1	1.568	-1.516		0.094	-0.091
2	1.588	-1.443		0.095	-0.087
3	1.525	-1.576		0.091	-0.095
4	1.561	-1.448		0.094	-0.087
5	1.632	-1.626		0.098	-0.098
6	1.533	-1.496		0.092	-0.090
7	1.519	-1.533		0.091	-0.092
8	1.233	-1.615		0.074	-0.097
9	1.638	-1.535		0.098	-0.092
10	1.510	-1.503		0.091	-0.090

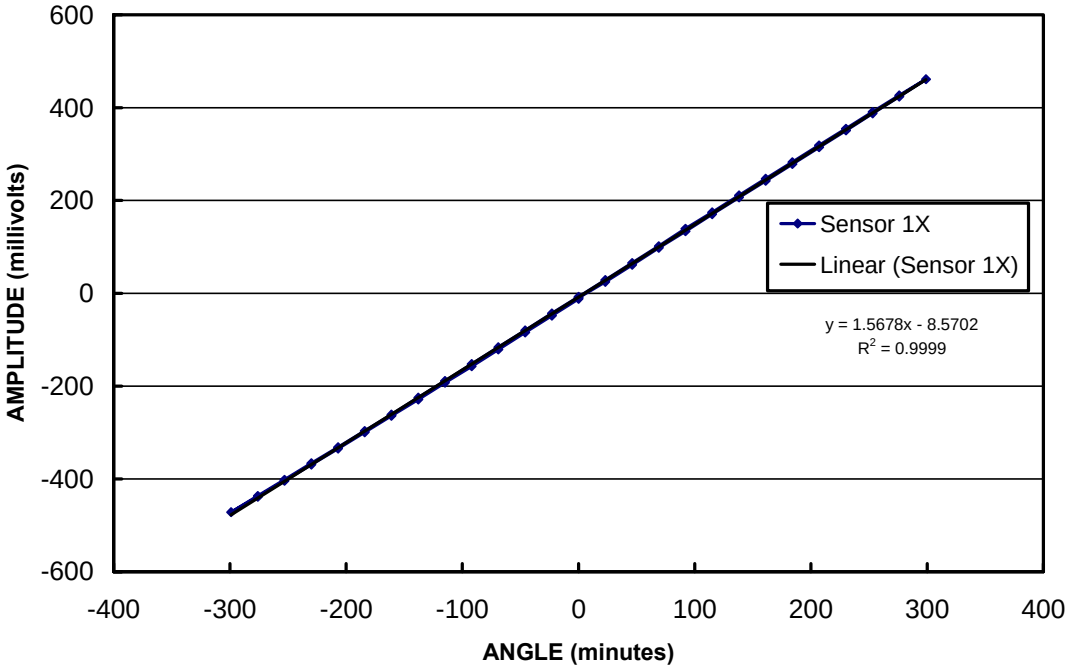

Figure A-1: Graph showing the calibration points for Sensor #1, X-Axis.

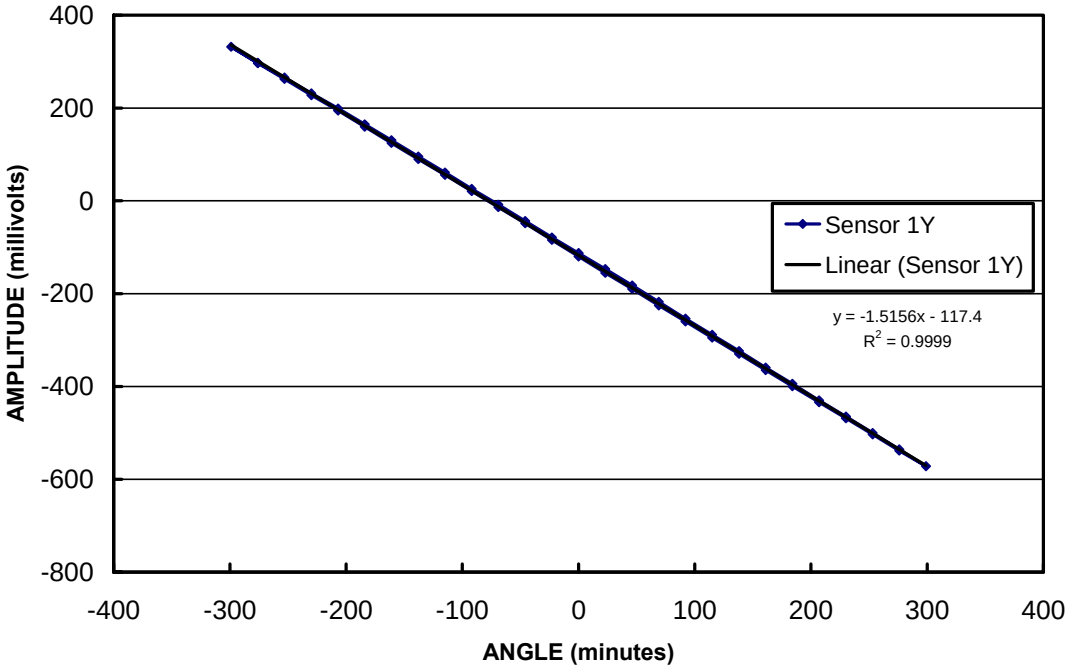

Figure A-2: Graph showing the calibration points for Sensor #1, Y-Axis.

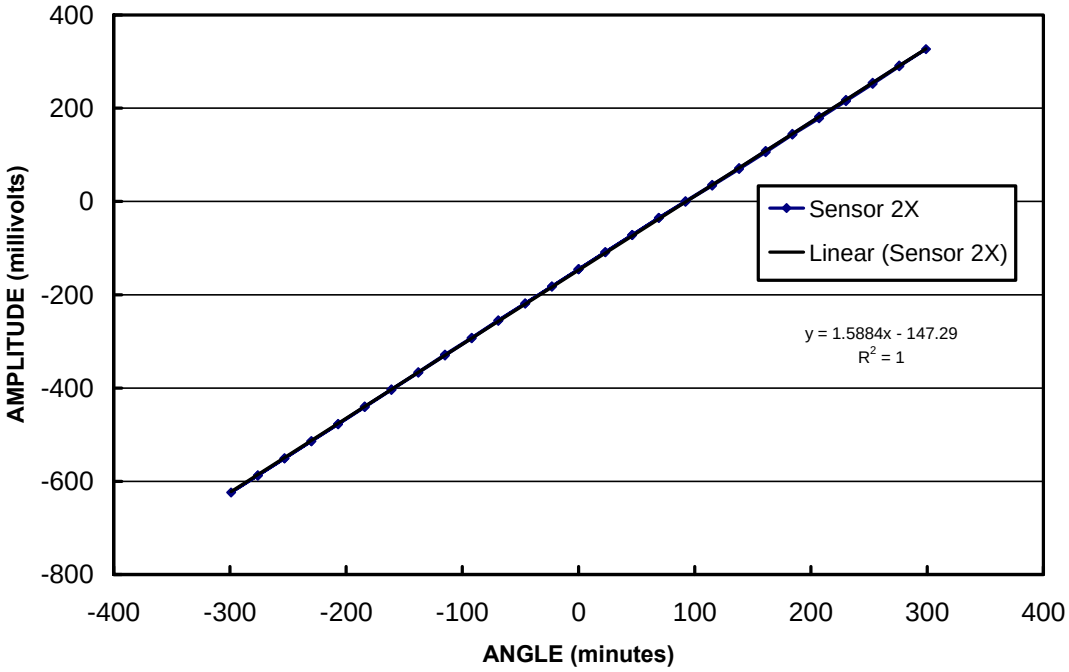

Figure A-3: Graph showing the calibration points for Sensor #2, X-Axis.

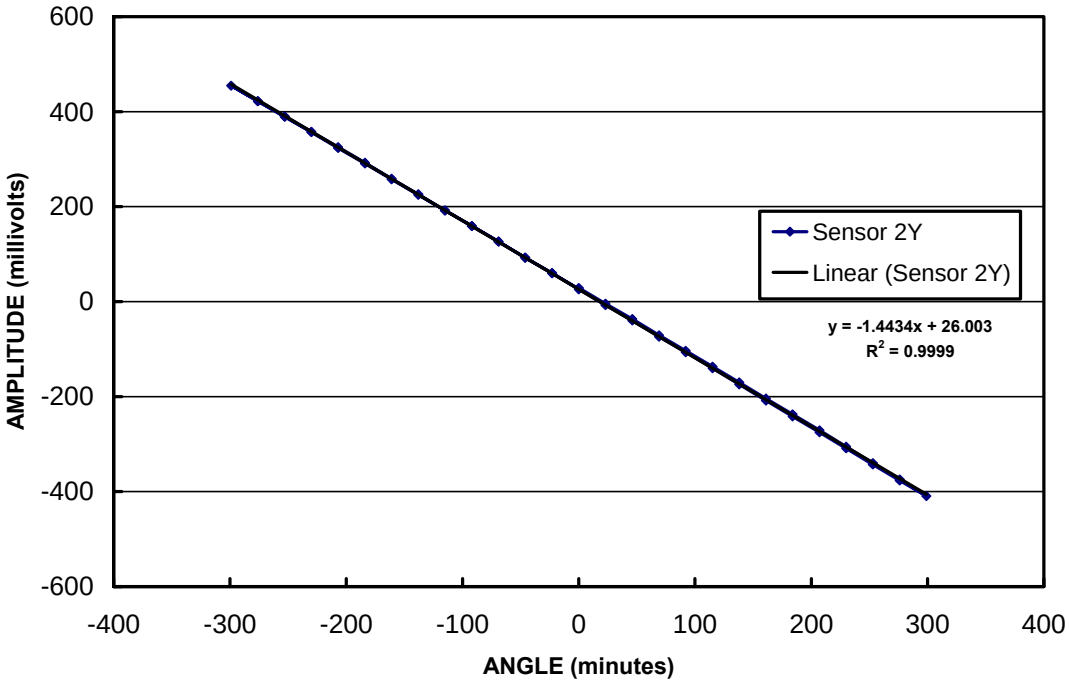

Figure A-4: Graph showing the calibration points for Sensor #2, Y-Axis.

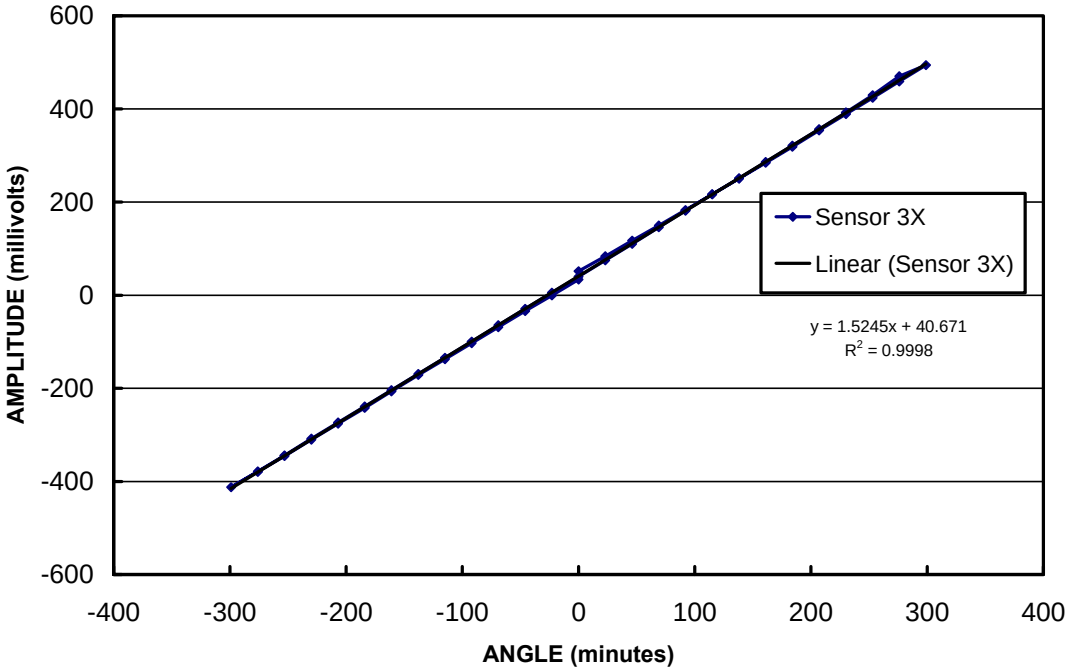

Figure A-5: Graph showing the calibration points for Sensor #3, X-Axis.

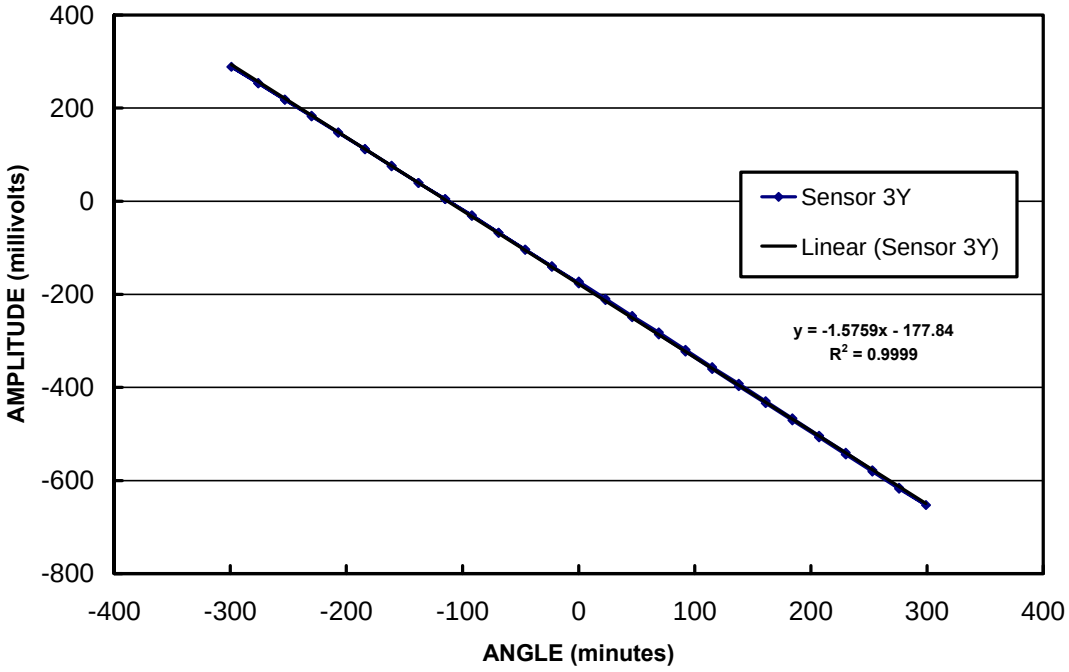

Figure A-6: Graph showing the calibration points for Sensor #3, Y-Axis.

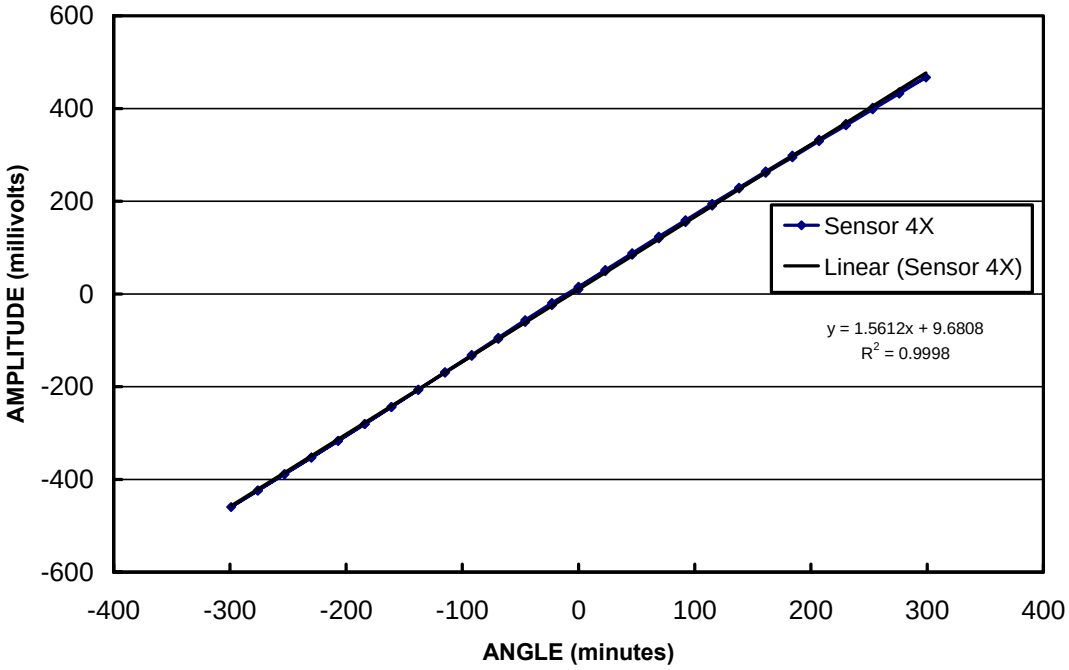

Figure A-7: Graph showing the calibration points for Sensor #4, X-Axis.

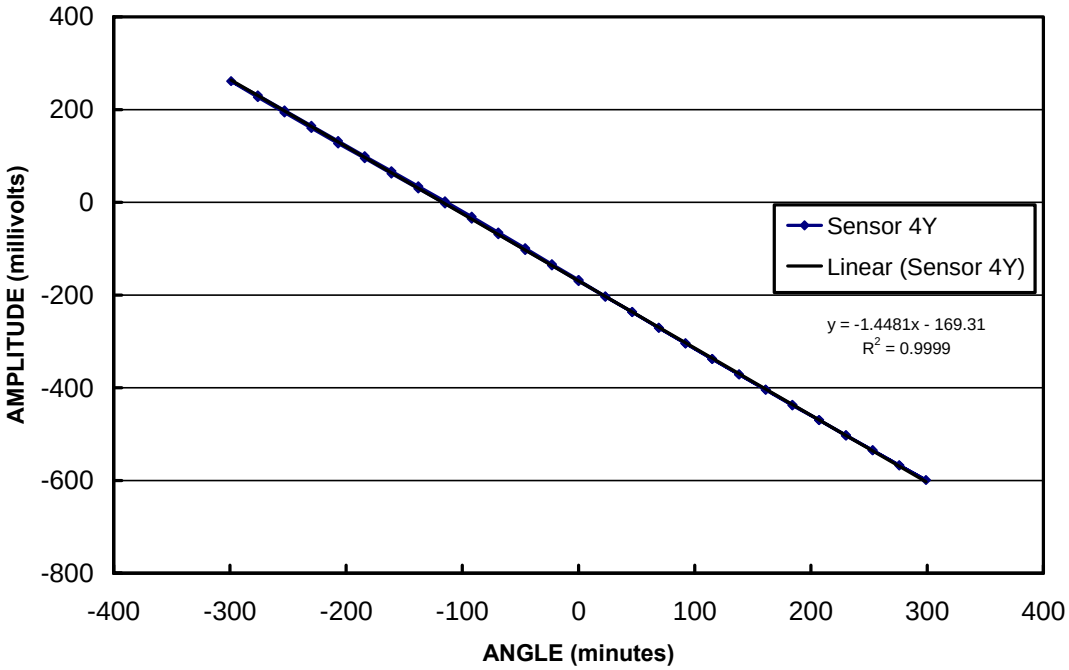

Figure A-8: Graph showing the calibration points for Sensor #4, Y-Axis.

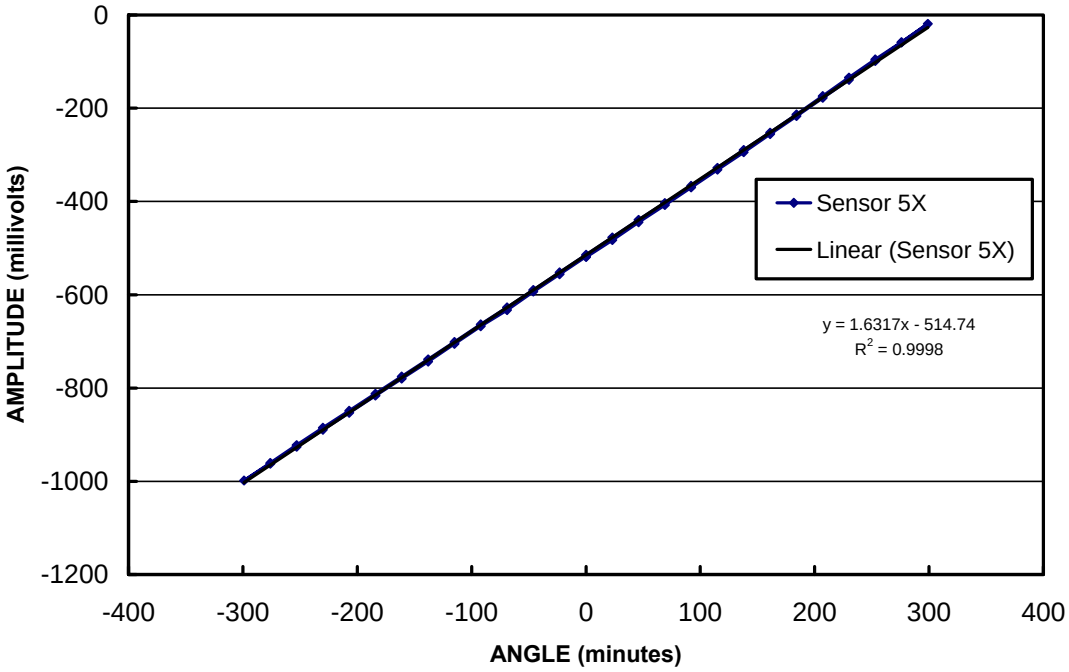

Figure A-9: Graph showing the calibration points for Sensor #5, X-Axis.

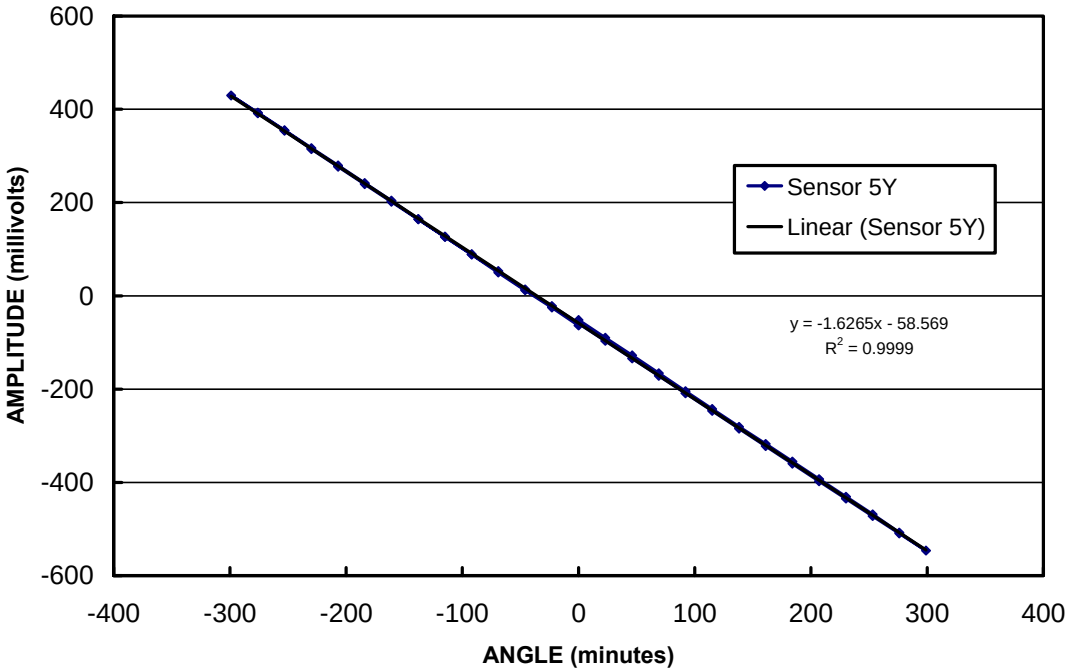

Figure A-10: Graph showing the calibration points for Sensor #5, Y-Axis.

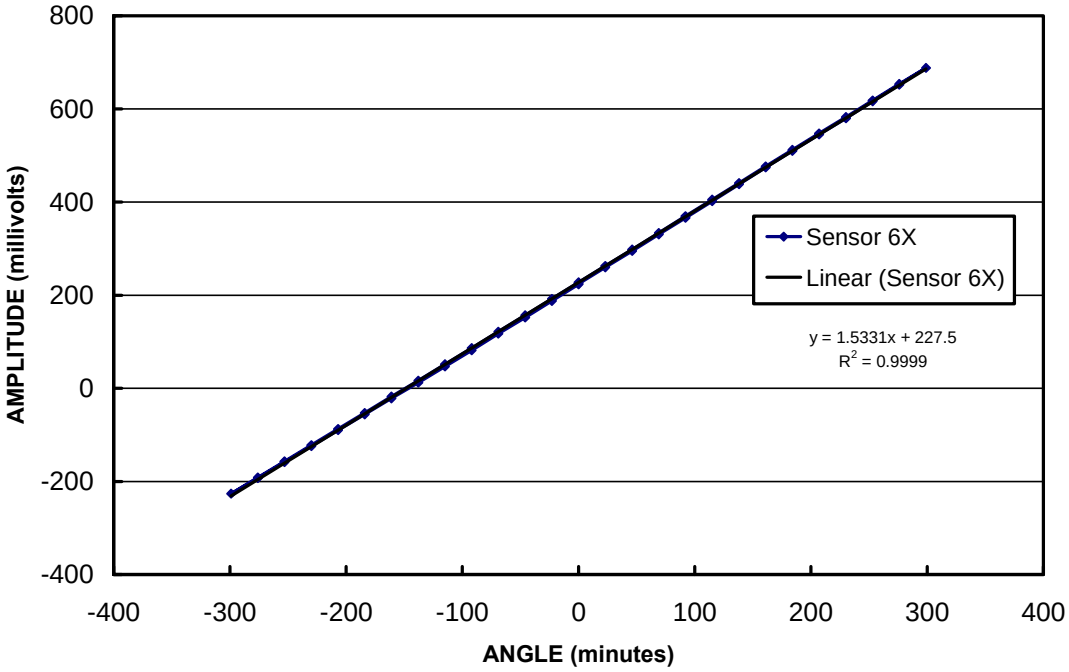

Figure A-11: Graph showing the calibration points for Sensor #6, X-Axis.

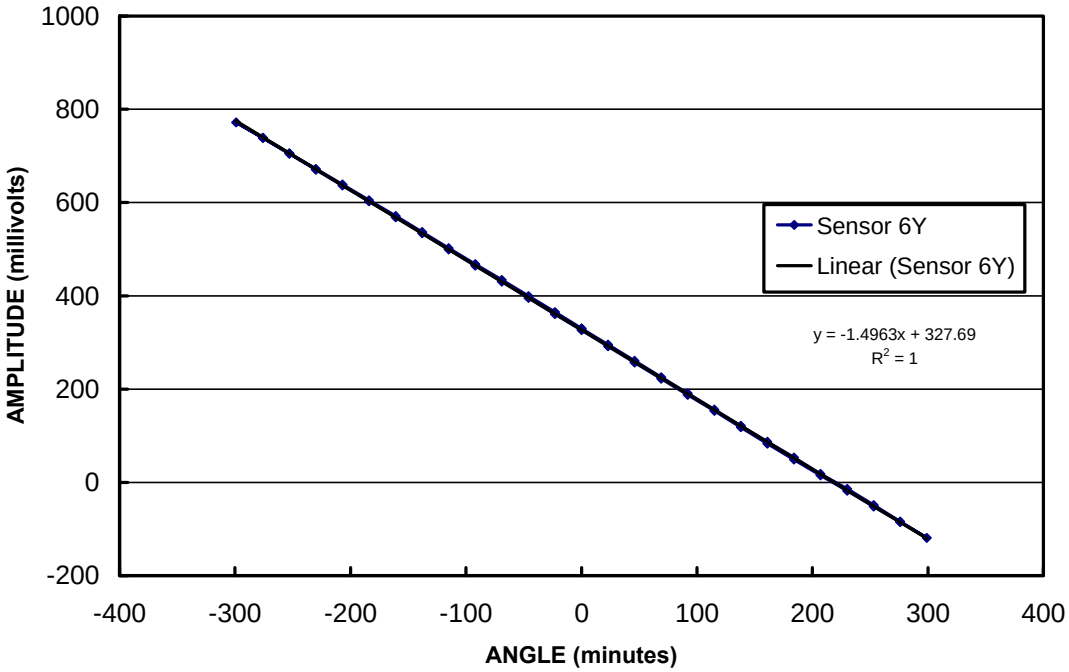

Figure A-12: Graph showing the calibration points for Sensor #6, Y-Axis.

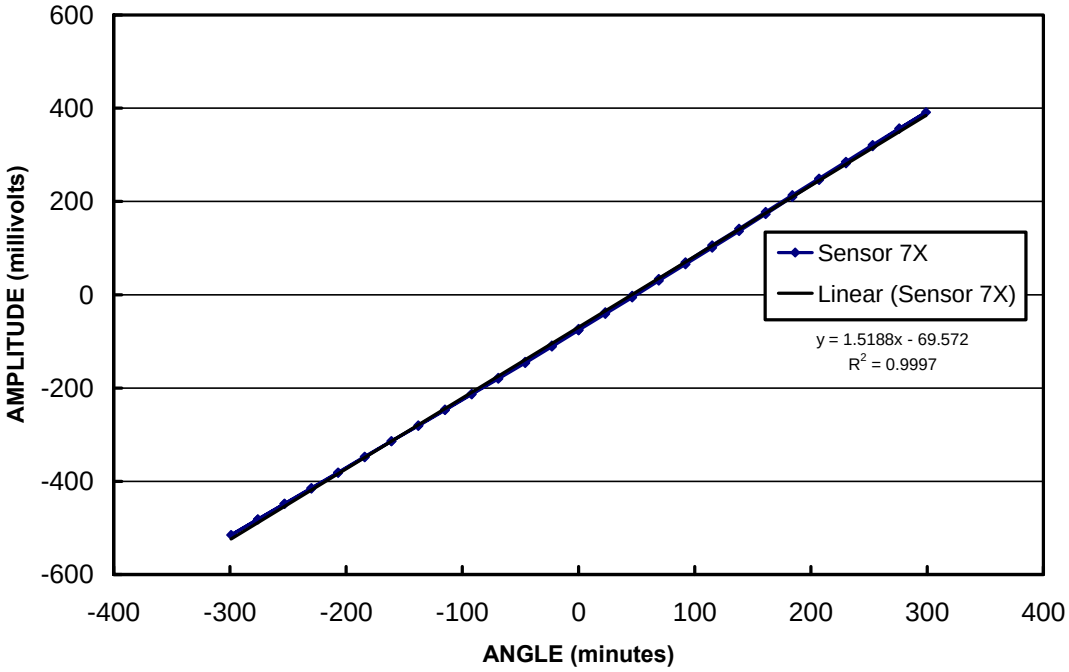

Figure A-13: Graph showing the calibration points for Sensor #7, X-Axis.

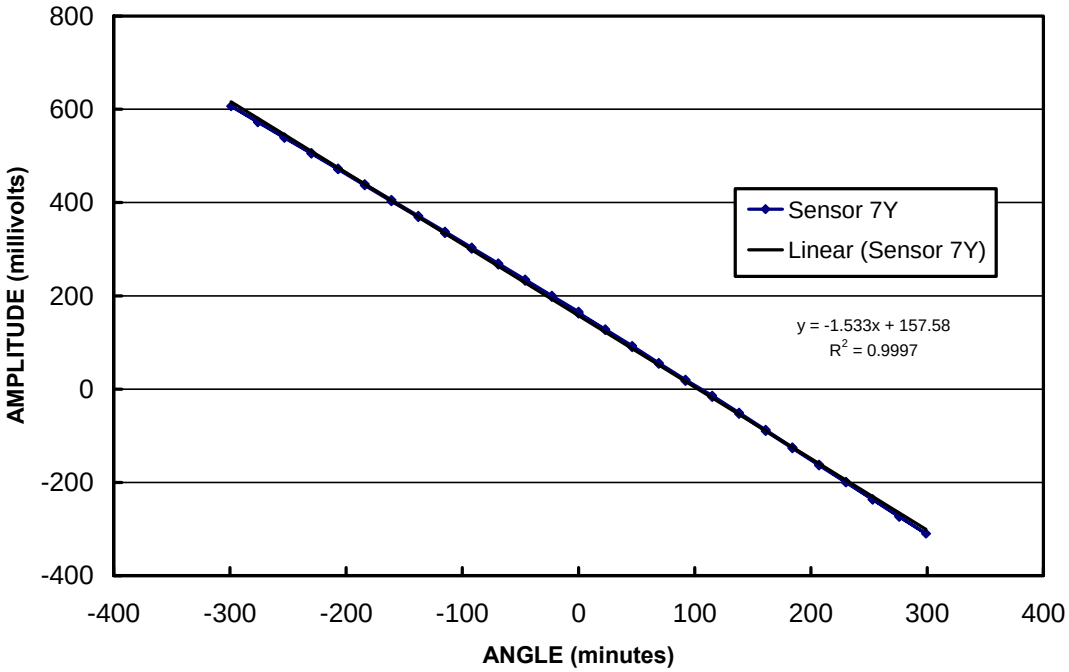

Figure A-14: Graph showing the calibration points for Sensor #7, Y-Axis.

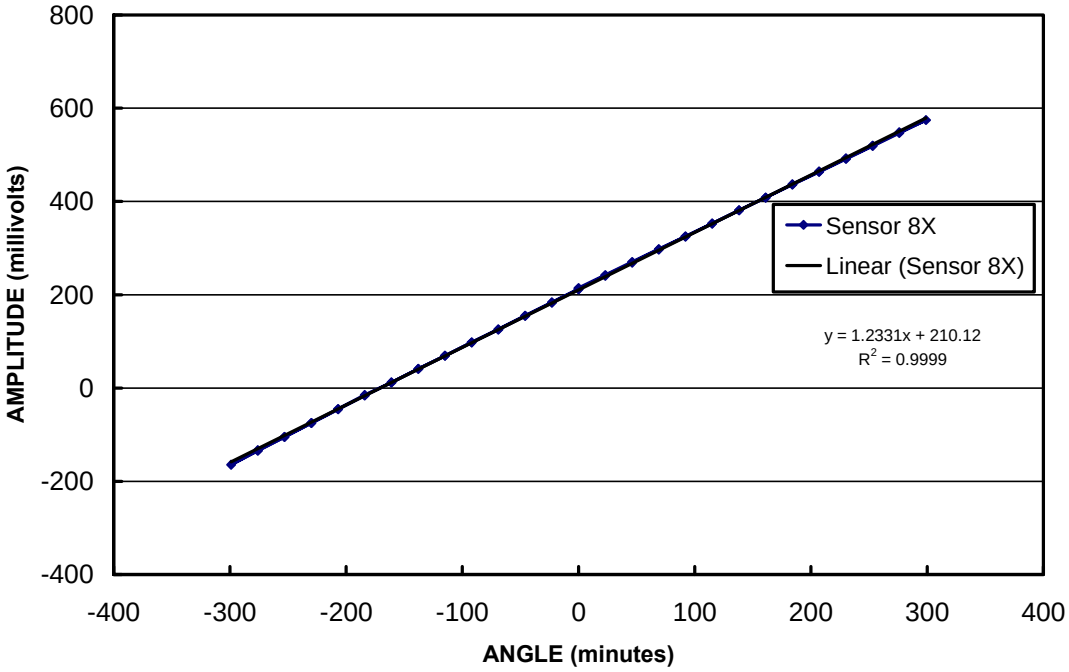

Figure A-15: Graph showing the calibration points for Sensor #8, X-Axis.

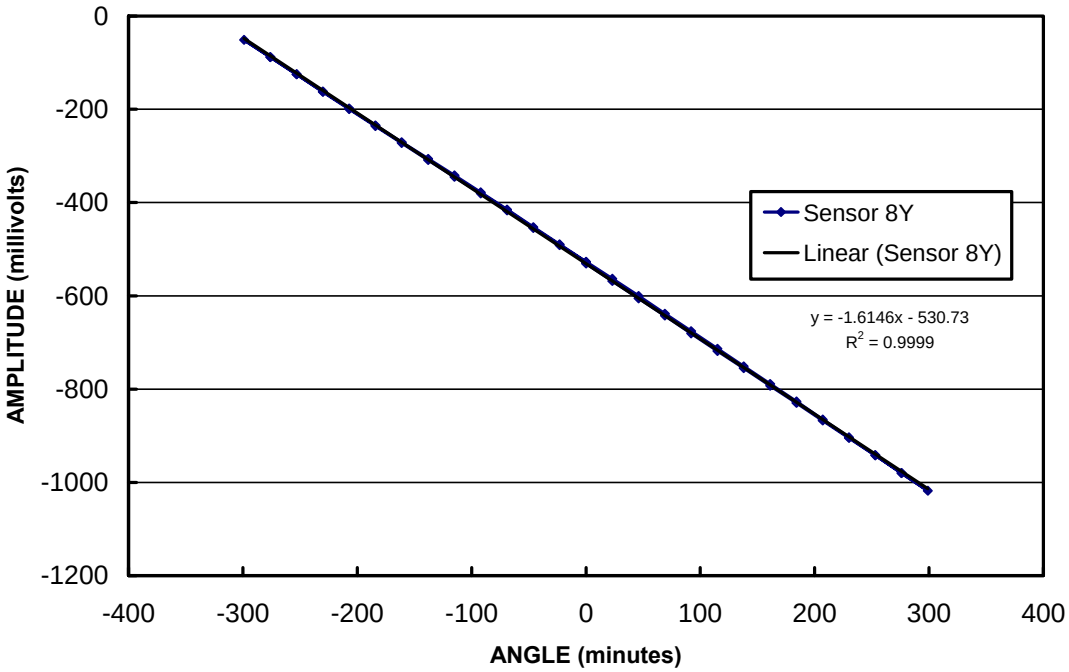

Figure A-16: Graph showing the calibration points for Sensor #8, Y-Axis.

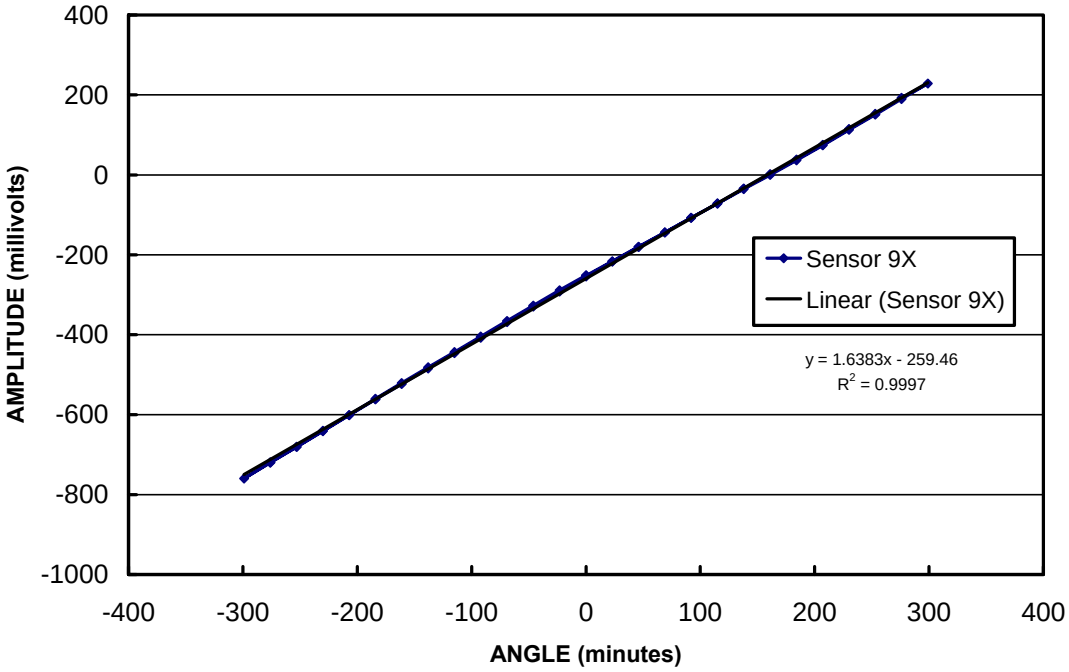

Figure A-17: Graph showing the calibration points for Sensor #9, X-Axis.

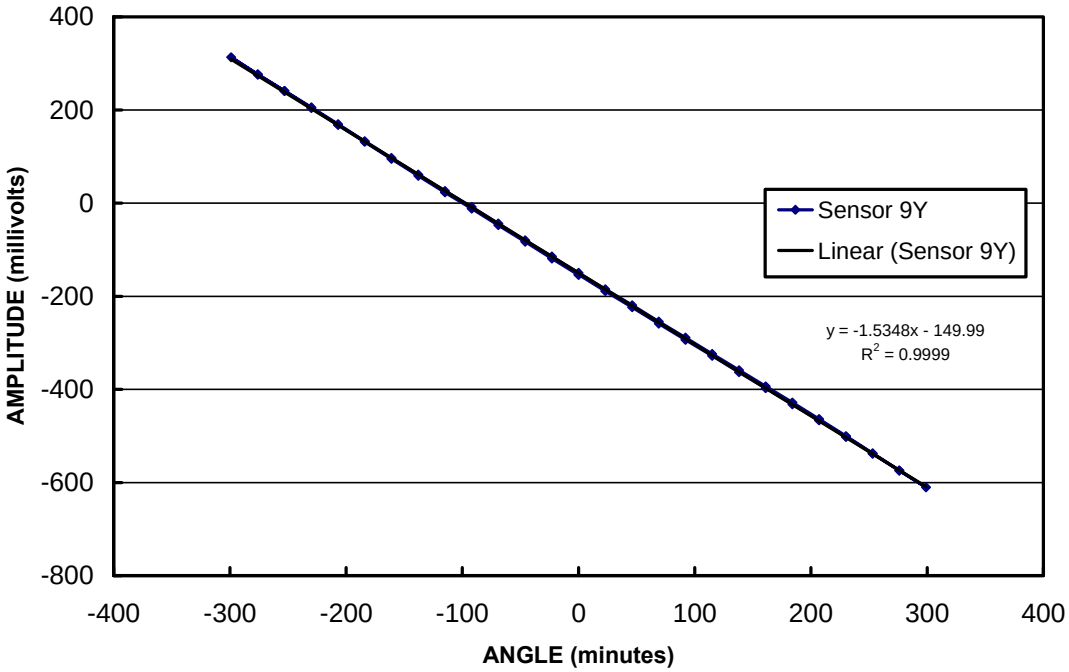

Figure A-18: Graph showing the calibration points for Sensor #9, Y-Axis.

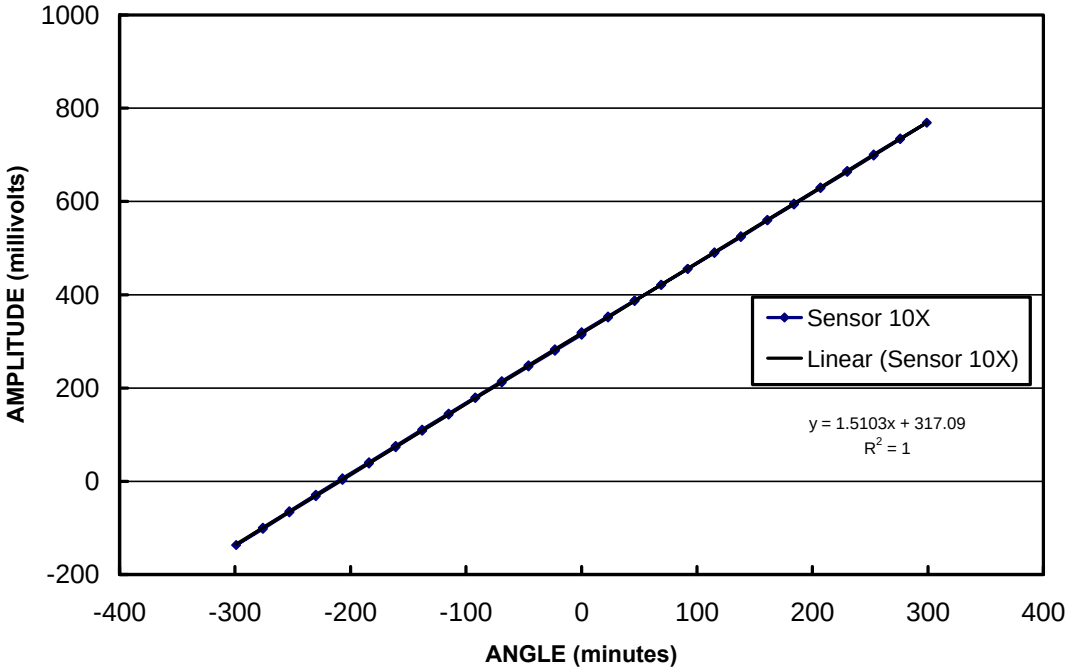

Figure A-19: Graph showing the calibration points for Sensor #10, X-Axis.

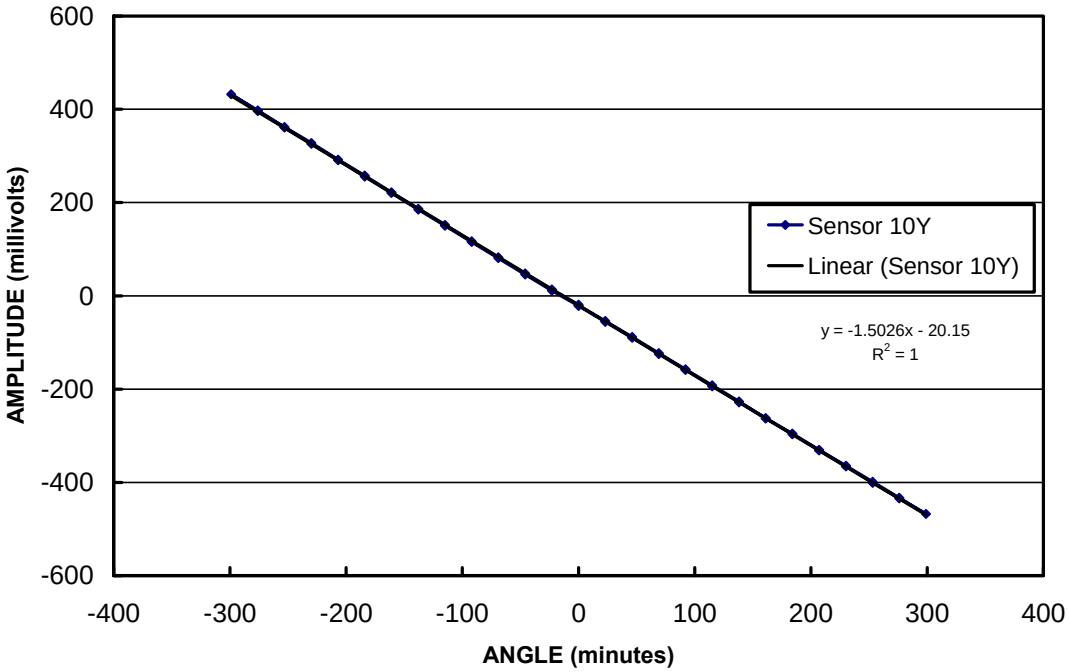

Figure A-20: Graph showing the calibration points for Sensor #10, Y-Axis.

Appendix B. Stationary Sensors with Varying Temperature

Table B-1: Statistical data showing the sensor output (millivolts) during stationary testing with varying temperature. X-Axis of Sensors #1-10 is shown.

		1X	2X	3X	4X	5X	6X	7X	8X	9X	10X
20°C	average	-37.438	122.589	-209.432	-1883.158	101.791	130.848	-503.307	388.085	-482.390	457.527
	max	-32.125	125.043	-204.673	-1874.310	107.252	134.832	-500.689	390.398	-477.962	473.212
	min	-38.815	72.915	-210.640	-1948.706	-20.301	17.748	-598.706	270.804	-579.247	325.323
	std	0.701	5.218	0.588	7.370	12.028	11.896	10.038	12.406	10.135	16.818
	variance	0.491	27.224	0.346	54.312	144.664	141.516	100.768	153.907	102.718	282.843
30°C	average	-29.408	117.214	-194.690	-1818.741	99.667	139.169	-461.091	359.653	-474.327	437.915
	max	-24.030	120.140	-184.925	-1777.102	106.188	144.391	-453.098	365.415	-468.735	440.747
	min	-31.222	69.203	-197.668	-1908.350	-9.074	27.026	-559.602	241.556	-571.527	321.408
	std	0.768	5.007	2.473	21.768	11.564	11.606	10.541	12.303	10.112	12.215
	variance	0.590	25.070	6.117	473.864	133.718	134.704	111.105	151.373	102.249	149.212
40°C	average	-12.998	117.850	-183.799	-1756.296	82.391	153.685	-413.911	320.803	-449.390	440.296
	max	4.401	120.055	-164.649	-1709.065	97.225	159.448	-407.201	332.627	-446.127	448.613
	min	-23.102	25.468	-194.263	-1874.080	-130.907	-59.423	-599.413	100.758	-632.005	216.675
	std	6.851	4.897	4.591	25.398	12.948	11.395	9.640	14.097	9.544	14.054
	variance	46.933	23.980	21.073	645.039	167.663	129.837	92.928	198.726	91.097	197.510

Table B-2: Statistical data showing the sensor output (millivolts) during stationary testing with varying temperature. Y-Axis of Sensors #1-10 is shown.

		1Y	2Y	3Y	4Y	5Y	6Y	7Y	8Y	9Y	10Y
20°C	average	-41.759	2.813	-151.421	-17.403	1148.560	253.355	520.962	-807.111	-291.551	-76.021
	max	-40.824	4.767	-144.016	-12.462	1162.904	256.180	522.463	-798.970	-273.834	-65.245
	min	-109.985	-1.055	-152.341	-25.826	1071.382	246.978	510.129	-808.265	-292.935	-94.646
	std	7.213	1.503	0.890	2.584	8.413	1.738	1.312	0.884	1.911	7.469
	variance	52.025	2.258	0.792	6.675	70.777	3.020	1.720	0.781	3.651	55.787
30°C	average	-41.260	-4.573	-168.079	-16.997	1047.638	255.533	478.994	-765.692	-294.953	-69.405
	max	-36.925	-3.882	-154.307	-14.913	1067.041	264.368	484.508	-752.417	-277.409	-66.301
	min	-110.070	-6.214	-171.825	-23.221	957.916	239.922	464.845	-767.518	-298.017	-82.057
	std	7.189	0.387	2.201	1.191	10.906	6.151	3.509	1.940	1.895	2.081
	variance	51.684	0.150	4.843	1.419	118.948	37.837	12.311	3.762	3.590	4.332
40°C	average	-32.566	-8.764	-160.217	-40.157	941.870	266.829	435.551	-698.645	-296.852	-62.662
	max	-27.281	-7.772	-145.948	-33.282	952.715	274.728	440.177	-672.463	-265.790	-35.742
	min	-163.441	-10.938	-170.259	-47.617	815.901	249.294	421.987	-722.957	-299.889	-80.397
	std	7.518	0.828	2.312	2.394	7.922	6.436	1.565	13.562	2.239	4.650
	variance	56.518	0.685	5.345	5.733	62.759	41.419	2.448	183.925	5.012	21.626

Appendix C. Fixed Temperature with Varying Sensor Angles

Table C-1: Data showing sensor output with fixed temperature and varying sensor angles at 20 degrees Celsius.

20 Degrees Celsius					
X - Axis					
	Tilt (mV)				
Tilt (minutes)	Sensor 1	Sensor 2	Sensor 3	Sensor 4	Sensor 5
276	348.5819	478.8255	108.9947	-1535.592	392.9102
207	236.4221	376.1857	16.04386	-1683.169	289.7554
138	125.2979	272.4909	-77.40494	-1812.258	189.233
69	14.27675	168.8798	-172.7752	-1928.747	88.42525
0	-95.62676	65.70224	-269.3406	-2024.008	-8.695947
-69	-208.5762	-39.2847	-366.9016	-2117.325	-118.1733
-138	-324.4311	-146.7424	-464.5601	-2208.104	-212.5712
-207	-434.4665	-255.5294	-562.9026	-2295.339	-320.4139
-276	-544.576	-366.5475	-661.7761	-2381.459	-432.0238
Note: Average middle 30 minutes of 1 hr period					
Y - Axis					
	Tilt (mV)				
Tilt (minutes)	Sensor 1	Sensor 2	Sensor 3	Sensor 4	Sensor 5
276	78.99216	89.17744	-65.2877	202.0154	1182.45
207	76.5648	93.97343	-56.64907	181.8202	1188.362
138	74.93246	99.40244	-49.44671	149.8712	1186.354
69	73.54669	105.0099	-42.7162	129.4989	1176.911
0	69.9387	111.6508	-36.54976	119.4507	1167.127
-69	65.4883	118.5569	-29.47962	107.4157	1163.589
-138	61.56054	126.268	-22.12263	94.916	1151.896
-207	61.55033	133.7652	-12.47077	83.47831	1150.412
-276	61.28702	141.2598	-4.271648	75.68521	1150.967
Note: Average middle 30 minutes of 1 hr period					

Table C-2: Data showing sensor output with fixed temperature and varying sensor angles at 30 degrees Celsius.

30 Degrees Celsius					
X - Axis					
	Tilt (mV)				
Tilt (minutes)	Sensor 1	Sensor 2	Sensor 3	Sensor 4	Sensor 5
-276	-574.3371	-377.5343	-646.2898	-2321.652	-448.0214
-207	-461.971	-270.7144	-551.6388	-2240.778	-337.5184
-138	-341.8218	-161.1494	-457.4843	-2146.359	-241.121
-69	-217.8722	-52.90488	-356.649	-2059.444	-126.9475
0	-100.7167	53.27175	-253.5092	-1972.852	-12.71337
69	13.73368	156.9138	-149.1403	-1867.023	91.93819
138	135.49	257.0457	-40.54874	-1699.287	194.3664
207	248.8693	362.6302	68.13272	-1576.596	300.2079
276	364.5919	469.5979	157.0156	-1424.631	409.7176
Note: Average middle 30 minutes of 1 hr period					
Y - Axis					
	Tilt (mV)				
Tilt (minutes)	Sensor 1	Sensor 2	Sensor 3	Sensor 4	Sensor 5
276	62.21569	126.6156	-11.16587	50.47696	1050.859
207	68.98365	121.7819	-20.35637	59.76364	1058.469
138	68.64089	114.567	-21.00215	69.32952	1052.708
69	77.16915	108.5535	-30.26784	80.10355	1062.251
0	77.8226	100.6642	-40.82879	92.63959	1069.018
-69	81.23396	95.18668	-52.68527	106.4113	1071.932
-138	82.78713	86.71007	-58.1262	129.3675	1042.828
-207	78.69707	82.27045	-74.14509	156.1474	1058.238
-276	86.28844	80.07546	-75.27607	179.3173	1074.404
Note: Average middle 30 minutes of 1 hr period					

Table C-3: Data showing sensor output with fixed temperature and varying sensor angles at 40 degrees Celsius.

40 Degrees Celsius					
X - Axis					
	Tilt (mV)				
Tilt (minutes)	Sensor 1	Sensor 2	Sensor 3	Sensor 4	Sensor 5
276	375.7428	469.0057	177.5281	-1209.809	395.684
207	260.8844	373.27	77.07439	-1388.152	292.7272
138	150.0042	268.8812	-22.77494	-1525.679	188.6999
69	41.49841	161.8749	-128.2967	-1650.627	79.15871
0	-64.92934	51.18771	-231.3117	-1765.786	-20.34531
-69	-175.166	-49.24724	-327.2128	-1858.201	-125.4452
-138	-292.0207	-155.0811	-425.5467	-1953.496	-236.2297
-207	-416.4677	-251.9634	-524.0205	-2032.713	-343.9223
-276	-519.2517	-361.2339	-638.4255	-2132.415	-450.0062
Note: Average middle 30 minutes of 1 hr period					
Y - Axis					
	Tilt (mV)				
Tilt (minutes)	Sensor 1	Sensor 2	Sensor 3	Sensor 4	Sensor 5
276	80.53483	70.32629	-67.80274	126.539	888.4966
207	83.30722	74.84819	-56.66978	119.363	887.4661
138	89.85046	78.45618	-53.90392	96.67205	884.0627
69	86.5892	82.74088	-48.17358	69.73924	875.9862
0	85.43155	87.25995	-34.06792	50.64408	871.9591
-69	81.78185	92.97553	-25.53541	43.27091	863.2305
-138	74.67227	101.476	-21.03024	33.58444	851.8226
-207	66.49131	107.1603	-12.49801	26.46862	835.6159
-276	78.84036	114.9285	-7.734365	16.44932	831.3314
Note: Average middle 30 minutes of 1 hr period					

Appendix D. Analysis of the Test Bridge

Table D-1: Data showing the X and Y Axis output of Sensors #2-7 for bridge movement of five screw turns.

Y-Axis Movement							
	mV				degrees		
	Sensor 5	**Sensor 6**	**Sensor 7**		**Sensor 5**	**Sensor 6**	**Sensor 7**
initial	48.40653	264.3655	447.0582		0.496032	2.944575	4.860461
final	76.22914	287.0063	479.0982		0.781136	3.196753	5.208803
difference	27.82261	22.64075	32.04007		**0.285104**	**0.252179**	**0.348343**
Average						**0.29520862**	
	mV				degrees		
	Sensor 2	**Sensor 3**	**Sensor 4**		**Sensor 2**	**Sensor 3**	**Sensor 4**
initial	57.15554	-187.9304	-3181.46		0.659955	-1.987514	-31.94698
final	31.06656	-215.7403	-3184.529		0.358715	-2.281626	-31.9778
difference	-26.08898	-27.80985	-3.069333		**-0.30124**	**-0.294111**	**n/a**
Average						**-0.297675828**	

X-axis

X-Axis Movement							
	mV				degrees		
	Sensor 5	**Sensor 6**	**Sensor 7**		**Sensor 5**	**Sensor 6**	**Sensor 7**
initial	-1090.24	96.74865	-459.3936		-11.13573	1.051794	-5.041285
final	-1050.008	136.2286	-418.0288		-10.72481	1.480997	-4.587357
difference	40.23167	39.47993	41.36478		**0.410927**	**0.429202**	**0.453928**
Average						**0.431352527**	
	mV				degrees		
	Sensor 2	**Sensor 3**	**Sensor 4**		**Sensor 2**	**Sensor 3**	**Sensor 4**
initial	-170.3521	-7.416013	-1335.088		-1.787424	-0.081074	-14.255
final	-213.829	-48.21444	-1346.152		-2.243606	-0.527096	-14.37313
difference	-43.4769	-40.79843	-11.064		**-0.456182**	**-0.446021**	**n/a**
Average						**-0.451101895**	

Table D-2: Data analysis of the change in angle experienced by sensors during bridge movement of five screw turns.

Sensor #	Δ Tilt Angle Θ (degrees)	Unit Direction X	Unit Direction Y
5	0.498	0.821	0.571
6	0.497	0.862	0.506
7	0.564	0.784	0.620
Average	**0.520**	**0.823**	**0.566**

Sensor #	Tilt Angle Θ (degrees)	Unit Direction X	Unit Direction Y
2	0.547	-0.834	-0.551
3	0.534	-0.835	-0.550
Average	**0.540**	**-0.835**	**-0.551**

Totals	Tilt Angle Θ (degrees)	Unit Direction X	Unit Direction Y
Average	**0.530**	**0.829**	**0.558**
Standard Deviation	**0.030**	**0.908**	**0.613**

Table D-3: Data and statistics for Sensors #2, 3 and 5-9, X-Axis on the test bridge.

X-axis

Sensors on Bridge X-axis								
Drift per Day in mV - average of 1/2 hour (excluding errant points)								
		Sensor 2	Sensor 3	Sensor 5	Sensor 6	Sensor 7	Sensor 8	Sensor 9
29-Aug	initial	-173.7331	-33.31801	-866.3508	164.4481	-362.2559	272.1646	-379.2154
	final	-174.3008	-31.63574	-884.0156	163.0626	-372.8319	280.6702	-383.8482
	difference	-0.56775	1.682272	-17.66487	-1.385467	-10.57597	8.50555	-4.6328
30-Aug	initial	-174.216	-31.74157	-884.6563	163.1055	-373.0947	281.1735	-383.9646
	final	-175.3344	-31.2002	-904.4064	160.857	-383.4855	287.4957	-388.9141
	difference	-1.11836	0.541366	-19.75017	-2.248507	-10.39083	6.322203	-4.949557
2-Sep	initial	-176.9737	-28.40143	-939.1927	154.8499	-401.7971	304.2231	-397.4563
	final	-177.9622	-27.01396	-954.7136	151.0347	-410.1065	312.4879	-401.5199
	difference	-0.988513	1.387469	-15.52089	-3.815147	-8.309367	8.2648	-4.06361
3-Sep	initial	-178.0107	-27.17597	-955.7561	150.591	-410.7964	312.7235	-401.951
	final	-178.954	-26.29043	-971.8136	146.1553	-418.8324	320.8093	-406.6945
	difference	-0.943357	0.885542	-16.05757	-4.435757	-8.036037	8.085747	-4.74359

Sensors on Bridge X-axis								
Drift per Day in mV - average of 1/2 hour (excluding errant points)								
		Sensor 2	Sensor 3	Sensor 5	Sensor 6	Sensor 7	Sensor 8	Sensor 9
29-Aug	Difference	-0.56775	1.682272	-17.66487	-1.385467	-10.57597	8.50555	-4.6328
30-Aug		-1.11836	0.541366	-19.75017	-2.248507	-10.39083	6.322203	-4.949557
2-Sep		-0.988513	1.387469	-15.52089	-3.815147	-8.309367	8.2648	-4.06361
3-Sep		-0.943357	0.885542	-16.05757	-4.435757	-8.036037	8.085747	-4.74359

Maximum		-0.56775	1.682272	-15.52089	-1.385467	-8.036037	8.50555	-4.06361
Minimum		-1.11836	0.541366	-19.75017	-4.435757	-10.57597	6.322203	-4.949557
STD		0.236435	0.509054	1.900407	1.401667	1.340872	0.996537	0.379285
Average		**-0.904495**	**1.124162**	**-17.24838**	**-2.971219**	**-9.32805**	**7.794575**	**-4.597389**

Table D-4: Data and statistics for Sensors #2, 3 and 5-9, Y-Axis on the test bridge.

Y-axis

Sensors on Bridge Y-axis								
Drift per Day in mV - average of 1/2 hour (excluding errant points)								
		Sensor 2	Sensor 3	Sensor 5	Sensor 6	Sensor 7	Sensor 8	Sensor 9
29-Aug	initial	84.4399	-131.8931	-23.29332	241.7804	338.4857	-564.8879	-72.63902
	final	85.4988	-133.9817	-20.53399	242.9804	346.7608	-576.0055	-73.30921
	difference	1.0589	-2.088583	2.759333	1.199933	8.275167	-11.11762	-0.670185
30-Aug	initial	85.37764	-134.0449	-20.57088	243.0476	346.9489	-576.2109	-73.2692
	final	86.98875	-135.034	-18.65543	243.8076	354.8685	-587.639	-73.683
	difference	1.611105	-0.989087	1.915447	0.760033	7.9196	-11.42806	-0.413805
2-Sep	initial	89.88763	-136.9183	-16.03308	242.6637	369.2591	-611.7509	-74.33661
	final	91.24956	-137.3187	-14.98774	240.8069	375.6656	-623.5631	-74.50527
	difference	1.36193	-0.400363	1.045344	-1.85678	6.406483	-11.81225	-0.168655
3-Sep	initial	91.26119	-137.315	-14.86409	241.2924	375.9173	-624.1209	-74.47707
	final	92.66836	-137.8955	-13.66156	239.302	381.9788	-636.3421	-74.5383
	difference	1.407165	-0.580477	1.20253	-1.990423	6.061553	-12.2212	-0.061229

Sensors on Bridge Y-axis								
Drift per Day in mV - average of 1/2 hour (excluding errant points)								
		Sensor 2	Sensor 3	Sensor 5	Sensor 6	Sensor 7	Sensor 8	Sensor 9
29-Aug	Difference	1.0589	-2.088583	2.759333	1.199933	8.275167	-11.11762	-0.670185
30-Aug		1.611105	-0.989087	1.915447	0.760033	7.9196	-11.42806	-0.413805
2-Sep		1.36193	-0.400363	1.045344	-1.85678	6.406483	-11.81225	-0.168655
3-Sep		1.407165	-0.580477	1.20253	-1.990423	6.061553	-12.2212	-0.061229

Maximum		1.611105	-0.400363	2.759333	1.199933	8.275167	-11.11762	-0.061229
Minimum		1.0589	-2.088583	1.045344	-1.990423	6.061553	-12.2212	-0.670185
STD		0.227993	0.757153	0.783346	1.68686	1.094658	0.477904	0.271422
Average		**1.359775**	**-1.014628**	**1.730664**	**-0.471809**	**7.165701**	**-11.64478**	**-0.328469**

Appendix E. Long-Term Stationary Testing at Controlled Temperature

Table E-1: Data showing the drift per day in Sensors #1-10, X-Axis. Daily initial and final half hour averages are shown with the difference throughout the day.

X-axis

Sensors in Temperature Chamber											
Drift per Day in mV - average of 1/2 hour											
		Sensor 1	Sensor 2	Sensor 3	Sensor 4	Sensor 5	Sensor 6	Sensor 7	Sensor 8	Sensor 9	Sensor 10
19-Oct	initial	-537.963	-341.6474	-663.8776	-2356.485	-461.991	215.5867	-498.2555	435.2037	-509.9706	465.3986
	final	-542.482	-349.6753	-670.8492	-2335.365	-470.9273	219.2713	-485.0862	440.1497	-516.868	485.7278
	difference	-4.518993	-8.027921	-6.971619	21.11972	-8.936331	3.684619	13.16936	4.945977	-6.897369	20.32924
20-Oct	initial	-542.5054	-349.7657	-670.8065	-2334.047	-471.3765	219.2713	-484.7691	440.3041	-516.9492	485.7784
	final	-544.2	-354.9358	-670.4172	-2328.327	-480.3482	218.9159	-481.3723	448.1939	-522.4178	488.2823
	difference	-1.694524	-5.170047	0.389272	5.719978	-8.971626	-0.355421	3.396819	7.889792	-5.468669	2.503854
21-Oct	initial	-544.2265	-354.9581	-670.4369	-2329.098	-480.4795	218.9023	-481.3115	448.5397	-522.4955	488.334
	final	-545.2654	-356.5821	-669.998	-2329.849	-484.6353	215.9751	-480.3165	459.9746	-527.447	490.7658
	difference	-1.038912	-1.624042	0.438842	-0.750785	-4.155828	-2.92719	0.995048	11.43495	-4.951559	2.431819
22-Oct	initial	-544.1153	-358.8723	-669.8476	-2332.08	-491.0592	208.556	-486.5613	452.4844	-533.8097	483.0573
	final	-545.6294	-356.8029	-670.1674	-2325.928	-487.2685	211.67	-480.6933	472.8205	-533.0741	490.091
	difference	-1.514065	2.069407	-0.319783	6.152628	3.79074	3.114045	5.86791	20.33617	0.735568	7.033672
23-Oct	initial	-545.5997	-356.8451	-670.1343	-2325.226	-487.3639	211.5484	-480.7384	473.2711	-533.0757	490.2761
	final	-547.0844	-358.6221	-671.4157	-2330.395	-490.442	207.0121	-481.7075	485.2529	-537.54	491.538
	difference	-1.484647	-1.777062	-1.281428	-5.169803	-3.07816	-4.536265	-0.969024	11.98176	-4.46427	1.261938
24-Oct	initial	-546.9982	-358.6713	-671.4962	-2332.054	-490.5348	207.0068	-481.7033	485.4734	-537.7172	491.4903
	final	-547.7214	-360.4367	-671.846	-2340.606	-495.6423	201.5163	-486.3313	492.6299	-545.0142	488.6498
	difference	-0.723174	-1.765353	-0.349808	-8.551899	-5.107577	-5.490467	-4.627971	7.156546	-7.296955	-2.840529
25-Oct	initial	-547.7626	-360.3784	-671.9097	-2339.312	-495.4402	201.7831	-486.1744	493.1688	-544.9965	488.6621
	final	-548.2822	-361.5089	-671.4909	-2350.929	-496.4507	202.8468	-488.3601	503.484	-548.847	491.0696
	difference	-0.519619	-1.130489	0.418843	-11.61776	-1.010476	1.063705	-2.18572	10.31519	-3.850489	2.40748
26-Oct	initial	-548.8077	-360.2562	-671.5786	-2349.771	-493.0252	206.7643	-485.1049	507.9343	-545.6689	495.2167
	final	-548.9336	-358.8073	-670.3558	-2353.573	-492.4116	208.4578	-485.3859	516.8163	-548.1549	495.227
	difference	-0.125882	1.448872	1.222752	-3.801792	0.613674	1.693447	-0.280972	8.882017	-2.485939	0.010307
27-Oct	initial	-548.9842	-358.8503	-670.4413	-2352.9	-492.3091	208.5467	-485.4336	516.8385	-548.1558	495.3976
	final	-549.3143	-358.7037	-670.716	-2343.33	-492.7858	212.9762	-488.0152	526.3631	-552.1652	498.4725
	difference	-0.330017	0.146631	-0.274689	9.570009	-0.476655	4.429542	-2.581636	9.524562	-4.009422	3.07481
28-Oct	initial	-549.2753	-358.6864	-670.7208	-2344.008	-492.7301	213.2376	-488.0295	526.4934	-552.2093	498.4667
	final	-549.9797	-360.7601	-670.3376	-2361.881	-497.0747	216.5534	-492.6452	530.4368	-559.2285	493.8378
	difference	-0.704383	-2.073708	0.383161	-17.87373	-4.344626	3.31571	-4.615721	3.943417	-7.019235	-4.628899
29-Oct	initial	-550.6048	-359.4237	-670.2889	-2359.733	-493.7658	220.5987	-489.3675	534.5903	-556.1229	497.9353
	final	-551.4928	-359.387	-670.0165	-2360.782	-494.3444	230.0717	-490.8535	541.8192	-559.2088	499.1537
	difference	-0.887931	0.036647	0.272349	-1.04878	-0.578599	9.47303	-1.486045	7.228919	-3.085973	1.218374
30-Oct	initial	-551.436	-359.3753	-670.1406	-2361.751	-494.4844	230.166	-490.8074	542.6032	-559.2545	499.0378
	final	-552.3466	-359.3316	-670.2276	-2344.16	-494.9816	240.3945	-493.1785	548.9676	-562.0102	501.2556
	difference	-0.910628	0.043777	-0.08697	17.59105	-0.497261	10.22852	-2.371094	6.364421	-2.755716	2.217826
31-Oct	initial	-551.1861	-361.5995	-670.0187	-2348.172	-501.224	233.4643	-499.3151	541.3437	-568.0966	493.4467
	final	-552.636	-359.9767	-669.6006	-2346.797	-505.5903	247.7648	-498.7058	545.0623	-565.3308	500.2738
	difference	-1.44991	1.622741	0.418086	1.37519	-4.366279	14.30053	0.609315	3.718651	2.765842	6.827091

Table E-2: Summarized drift per day for Sensors #1-10, X-Axis.

Sensors in Temperature Chamber											
Drift per Day in mV - average of 1/2 hour											
		Sensor 1	Sensor 2	Sensor 3	Sensor 4	Sensor 5	Sensor 6	Sensor 7	Sensor 8	Sensor 9	Sensor 10
19-Oct	Difference	-4.518993	-8.027921	-6.971619	21.11972	-8.936331	3.684619	13.16936	4.945977	-6.897369	20.32924
20-Oct		-1.694524	-5.170047	0.389272	5.719978	-8.971626	-0.355421	3.396819	7.889792	-5.468669	2.503854
21-Oct		-1.038912	-1.624042	0.438842	-0.750785	-4.155828	-2.92719	0.995048	11.43495	-4.951559	2.431819
22-Oct		-1.514065	2.069407	-0.319783	6.152628	3.79074	3.114045	5.86791	20.33617	0.735568	7.033672
23-Oct		-1.484647	-1.777062	-1.281428	-5.169803	-3.07816	-4.536265	-0.969024	11.98176	-4.46427	1.261938
24-Oct		-0.723174	-1.765353	-0.349808	-8.551899	-5.107577	-5.490467	-4.627971	7.156546	-7.296955	-2.840529
25-Oct		-0.519619	-1.130489	0.418843	-11.61776	-1.010476	1.063705	-2.18572	10.31519	-3.850489	2.40748
26-Oct		-0.125882	1.448872	1.222752	-3.801792	0.613674	1.693447	-0.280972	8.882017	-2.485939	0.010307
27-Oct		-0.330017	0.146631	-0.274689	9.570009	-0.476655	4.429542	-2.581636	9.524562	-4.009422	3.07481
28-Oct		-0.704383	-2.073708	0.383161	-17.87373	-4.344626	3.31571	-4.615721	3.943417	-7.019235	-4.628899
29-Oct		-0.887931	0.036647	0.272349	-1.04878	-0.578599	9.47303	-1.486045	7.228919	-3.085973	1.218374
30-Oct		-0.910628	0.043777	-0.08697	17.59105	-0.497261	10.22852	-2.371094	6.364421	-2.755716	2.217826
31-Oct		-1.44991	1.622741	0.418086	1.37519	-4.366279	14.30053	0.609315	3.718651	2.765842	6.827091

Table E-3: Data showing the drift per day in Sensors #1-10, Y-Axis. Daily initial and final half hour averages are shown with the difference throughout the day.

Y-axis

Sensors in Temperature Chamber											
Drift per Day in mV - average of 1/2 hour											
		Sensor 1	Sensor 2	Sensor 3	Sensor 4	Sensor 5	Sensor 6	Sensor 7	Sensor 8	Sensor 9	Sensor 10
19-Oct	initial	61.94437	146.5352	0.763891	29.38015	1083.395	357.2849	601.3753	-770.3872	-289.1396	-64.16108
	final	66.73476	151.1747	-0.53362	54.89297	1012.242	353.8955	588.0231	-761.8018	-291.062	-64.88499
	difference	4.79039	4.639452	-1.297511	25.51282	-71.15297	-3.389394	-13.35218	8.585391	-1.922324	-0.723908
20-Oct	initial	66.73476	151.1395	-0.581019	52.76477	1011.51	353.8979	587.8669	-761.8452	-291.0732	-64.88708
	final	67.35408	151.4834	-1.420931	64.53012	993.4089	352.4462	582.7747	-769.2836	-293.5355	-64.28621
	difference	0.619324	0.343916	-0.839913	11.76535	-18.10127	-1.451793	-5.092247	-7.438426	-2.462224	0.600878
21-Oct	initial	67.42231	151.1997	-1.447878	65.48815	993.322	352.4188	582.6745	-769.5571	-293.5717	-64.28163
	final	66.80021	151.0925	-2.900567	70.29105	987.9465	349.0308	580.8266	-781.9038	-295.1454	-64.19082
	difference	-0.622103	-0.107188	-1.452688	4.802898	-5.375505	-3.388016	-1.847905	-12.34669	-1.57375	0.09081
22-Oct	initial	62.19095	150.0044	-3.487209	69.11429	981.2576	347.6861	580.2909	-781.6448	-293.9259	-64.86621
	final	68.00775	151.1785	-3.102215	89.13446	988.0961	347.6597	581.143	-797.4927	-295.2675	-62.95656
	difference	5.816805	1.174114	0.384994	20.02016	6.838513	-0.026331	0.852117	-15.84783	-1.341641	1.909651
23-Oct	initial	68.05193	151.1884	-3.090162	90.45986	988.4498	347.633	581.1907	-798.2382	-295.3938	-62.90432
	final	69.42898	152.5251	-2.73238	95.9406	997.0212	345.731	581.3044	-814.6994	-296.7868	-62.93132
	difference	1.377047	1.336722	0.357782	5.480744	8.57142	-1.902052	0.113771	-16.46122	-1.392988	-0.027004
24-Oct	initial	69.42156	152.5284	-2.765879	95.52153	997.1733	345.734	581.3233	-814.9114	-296.6547	-62.86066
	final	66.99629	151.944	-3.285665	102.875	1003.705	344.814	581.0993	-829.5761	-298.2424	-63.7432
	difference	-2.425268	-0.584382	-0.519787	7.353491	6.532042	-0.919975	-0.224035	-14.66471	-1.58766	-0.88254
25-Oct	initial	67.15378	151.9825	-3.259305	103.4177	1004.184	344.8982	581.2027	-829.8243	-298.2594	-63.75388
	final	66.86948	152.1594	-4.821363	99.91633	1012.344	345.0439	581.4351	-844.595	-300.8958	-65.43534
	difference	-0.284294	0.176933	-1.562058	-3.501391	8.159591	0.145682	0.232303	-14.77067	-2.636386	-1.681464
26-Oct	initial	69.35483	152.7807	-4.527057	100.4519	1015.65	345.8504	581.8335	-845.1952	-301.5865	-65.03618
	final	69.20209	152.578	-5.418383	106.8628	1022.198	349.8922	583.1381	-854.3669	-301.5436	-63.16819
	difference	-0.152746	-0.202698	-0.891326	6.410836	6.547526	4.041799	1.304584	-9.171663	0.042925	1.86799
27-Oct	initial	69.18788	152.5781	-5.466956	107.3844	1022.264	350.0208	583.1073	-854.385	-301.5769	-63.22366
	final	69.93853	153.8979	-5.757399	124.8532	1034.389	355.8469	586.1922	-864.4003	-301.8145	-62.26415
	difference	0.750647	1.319853	-0.290443	17.46885	12.12448	5.826023	3.084884	-10.01531	-0.237602	0.959509
28-Oct	initial	70.10994	153.8985	-5.747306	125.2853	1034.581	356.0336	586.2389	-864.5731	-301.7795	-62.25465
	final	68.99633	154.6529	-5.010977	120.0914	1043.41	360.6592	587.3974	-874.402	-302.1476	-62.35837
	difference	-1.113609	0.754403	0.736329	-5.193839	8.829703	4.625517	1.158452	-9.828856	-0.368129	-0.103717
29-Oct	initial	71.6325	155.2627	-4.675881	120.2629	1046.679	361.6181	587.736	-874.7261	-302.8342	-61.93833
	final	71.75425	155.3888	-5.626195	132.6567	1057.557	367.4947	588.7933	-883.8707	-304.5507	-62.91165
	difference	0.121747	0.126071	-0.950314	12.39387	10.8772	5.876513	1.057386	-9.144543	-1.716494	-0.973321
30-Oct	initial	71.87111	155.3956	-5.663283	132.3657	1057.779	367.7345	588.8669	-884.4802	-304.5754	-62.82496
	final	71.40554	155.2605	-6.719851	152.6176	1066.709	374.7079	589.1435	-892.7194	-305.9942	-63.37952
	difference	-0.465573	-0.135074	-1.056568	20.25192	8.930086	6.973416	0.276565	-8.239238	-1.41887	-0.55456
31-Oct	initial	66.74299	154.1193	-7.330279	150.9632	1061.231	373.4216	588.5223	-892.4195	-304.6503	-64.18305
	final	69.51498	154.6494	-7.664106	159.353	1086.1	382.832	592.3414	-889.4009	-305.2716	-61.89666
	difference	2.771989	0.530064	-0.333827	8.389761	24.86903	9.410324	3.819037	3.018596	-0.621277	2.286389

Table E-4: Summarized drift per day for Sensors #1-10, Y-Axis.

Sensors in Temperature Chamber											
Drift per Day in mV - average of 1/2 hour											
		Sensor 1	Sensor 2	Sensor 3	Sensor 4	Sensor 5	Sensor 6	Sensor 7	Sensor 8	Sensor 9	Sensor 10
19-Oct	Difference	4.79039	4.639452	-1.297511	25.51282	-71.15297	-3.389394	-13.35218	8.585391	-1.922324	-0.723908
20-Oct		0.619324	0.343916	-0.839913	11.76535	-18.10127	-1.451793	-5.092247	-7.438426	-2.462224	0.600878
21-Oct		-0.622103	-0.107188	-1.452688	4.802898	-5.375505	-3.388016	-1.847905	-12.34669	-1.57375	0.09081
22-Oct		5.816805	1.174114	0.384994	20.02016	6.838513	-0.026331	0.852117	-15.84783	-1.341641	1.909651
23-Oct		1.377047	1.336722	0.357782	5.480744	8.57142	-1.902052	0.113771	-16.46122	-1.392988	-0.027004
24-Oct		-2.425268	-0.584382	-0.519787	7.353491	6.532042	-0.919975	-0.224035	-14.66471	-1.58766	-0.88254
25-Oct		-0.284294	0.176933	-1.562058	-3.501391	8.159591	0.145682	0.232303	-14.77067	-2.636386	-1.681464
26-Oct		-0.152746	-0.202698	-0.891326	6.410836	6.547526	4.041799	1.304584	-9.171663	0.042925	1.86799
27-Oct		0.750647	1.319853	-0.290443	17.46885	12.12448	5.826023	3.084884	-10.01531	-0.237602	0.959509
28-Oct		-1.113609	0.754403	0.736329	-5.193839	8.829703	4.625517	1.158452	-9.828856	-0.368129	-0.103717
29-Oct		0.121747	0.126071	-0.950314	12.39387	10.8772	5.876513	1.057386	-9.144543	-1.716494	-0.973321
30-Oct		-0.465573	-0.135074	-1.056568	20.25192	8.930086	6.973416	0.276565	-8.239238	-1.41887	-0.55456
31-Oct		2.771989	0.530064	-0.333827	8.389761	24.86903	9.410324	3.819037	3.018596	-0.621277	2.286389

Appendix F. Slowly Varying Angle Changes

Table E-5: Statistics from the entire test using Sensors #2, 3 and 5-10, X-Axis.

Entire Test (11/1 12:32 - 11/3 15:25)								
	Sensor 2	Sensor 3	Sensor 5	Sensor 6	Sensor 7	Sensor 8	Sensor 9	Sensor 10
average (mV)	-500.000	-792.957	-635.439	269.832	-491.926	552.822	-568.338	499.954
maximum (mV)	-483.299	-777.783	-617.765	282.550	-487.581	560.972	-563.381	501.413
minimum (mV)	-522.540	-812.053	-662.504	249.379	-495.148	543.420	-578.958	496.731
STD (mV)	9.234	8.467	10.296	7.569	1.885	4.353	2.679	0.629
variance (mV^2)	85.274	71.693	106.013	57.283	3.552	18.952	7.180	0.396

Note: Excluding errant data points

Table E-6: Statistics from one 48 hour period using Sensors #2, 3 and 5-10, X-Axis.

1 - 48 hour period (11/1 12:35 - 11/3 12:34)								
	Sensor 2	Sensor 3	Sensor 5	Sensor 6	Sensor 7	Sensor 8	Sensor 9	Sensor 10
average (mV)	-498.865	-792.002	-634.414	269.130	-491.782	552.428	-568.072	499.914
maximum (mV)	-483.299	-777.783	-617.765	281.810	-487.581	559.874	-563.381	501.413
minimum (mV)	-516.845	-809.568	-662.504	252.043	-495.029	543.744	-577.205	496.731
STD (mV)	8.225	7.731	9.681	7.153	1.836	4.140	2.519	0.623
variance (mV^2)	67.644	59.769	93.712	51.167	3.372	17.136	6.347	0.388

Table E-7: Statistics from two 24 hour periods using Sensors #2, 3 and 5-10, X-Axis.

2 - 24 hour periods								
	Sensor 2	Sensor 3	Sensor 5	Sensor 6	Sensor 7	Sensor 8	Sensor 9	Sensor 10
average (mV)	-496.938	-790.488	-632.920	262.858	-490.329	548.814	-566.002	499.634
	-500.792	-793.516	-635.909	275.401	-493.235	556.042	-570.141	500.193
maximum (mV)	-483.299	-777.783	-617.765	269.731	-487.581	553.711	-563.381	501.413
	-484.321	-777.894	-618.522	281.810	-491.292	559.874	-567.288	500.945
minimum (mV)	-516.845	-809.568	-662.504	252.043	-492.629	543.744	-577.205	496.731
	-514.045	-805.329	-648.919	268.693	-495.029	551.660	-573.578	497.046
STD (mV)	9.743	9.400	12.275	3.418	1.389	2.123	1.608	0.646
	5.743	5.160	5.687	3.459	0.768	1.908	1.241	0.450
variance (mV^2)	94.924	88.366	150.681	11.679	1.930	4.506	2.586	0.418
	32.979	26.627	32.339	11.964	0.590	3.639	1.540	0.203

Table E-8: Statistics from four 12 hour periods using Sensors #2, 3 and 5-10, X-Axis.

4 - 12 hour periods								
	Sensor 2	**Sensor 3**	**Sensor 5**	**Sensor 6**	**Sensor 7**	**Sensor 8**	**Sensor 9**	**Sensor 10**
average (mV)	-504.040	-797.285	-641.092	259.948	-489.153	546.999	-565.119	499.983
	-489.826	-783.682	-624.736	265.771	-491.507	550.632	-566.886	499.285
	-497.690	-790.772	-632.756	272.420	-492.560	554.422	-569.115	499.906
	-503.890	-796.256	-639.057	278.379	-493.909	557.660	-571.166	500.480
maximum (mV)	-490.526	-783.793	-624.438	263.177	-487.581	549.379	-563.381	501.413
	-483.299	-777.783	-617.765	269.731	-490.739	553.711	-565.594	500.443
	-484.321	-777.894	-618.522	275.340	-491.292	557.380	-567.288	500.477
	-502.026	-794.527	-636.032	281.810	-493.258	559.874	-570.046	500.945
minimum (mV)	-516.845	-809.568	-662.504	252.043	-490.926	543.744	-577.205	496.731
	-491.233	-785.070	-626.685	262.538	-492.629	548.110	-569.731	497.012
	-502.358	-795.335	-637.828	268.693	-493.463	551.660	-570.361	497.046
	-514.045	-805.329	-648.919	275.298	-495.029	555.635	-573.578	498.936
STD (mV)	9.118	8.877	12.679	1.654	0.969	0.932	1.749	0.738
	2.372	2.315	2.603	1.914	0.385	1.242	0.742	0.216
	5.929	5.534	6.061	1.829	0.440	1.037	0.771	0.452
	3.408	2.760	2.851	1.679	0.274	0.979	0.618	0.190
variance (mV^2)	83.145	78.794	160.746	2.737	0.938	0.869	3.060	0.545
	5.624	5.359	6.775	3.662	0.148	1.543	0.551	0.047
	35.157	30.625	36.734	3.346	0.194	1.075	0.594	0.204
	11.614	7.620	8.128	2.819	0.075	0.958	0.382	0.036

Table E-9: Statistics from eight 6 hour periods using Sensors #2, 3 and 5-10, X-Axis.

8 - 6 hour periods								
	Sensor 2	Sensor 3	Sensor 5	Sensor 6	Sensor 7	Sensor 8	Sensor 9	Sensor 10
average (mV)	-512.091	-805.202	-652.147	258.668	-488.313	546.339	-565.376	500.499
	-495.967	-789.346	-630.005	261.232	-489.994	547.662	-564.863	499.466
	-490.966	-784.839	-625.990	264.143	-491.173	549.605	-566.246	499.257
	-488.693	-782.531	-623.489	267.390	-491.838	551.653	-567.523	499.313
	-493.314	-786.620	-628.178	270.867	-492.217	553.686	-568.482	499.598
	-502.115	-794.970	-637.386	273.990	-492.907	555.167	-569.755	500.218
	-502.153	-794.978	-637.693	276.930	-493.701	556.908	-570.675	500.424
	-505.614	-797.524	-640.410	279.816	-494.115	558.406	-571.653	500.535
maximum (mV)	-503.354	-797.080	-638.917	262.368	-487.581	548.025	-563.381	501.413
	-490.526	-783.793	-624.438	263.177	-488.670	549.379	-563.534	500.647
	-490.577	-784.661	-624.736	265.603	-490.739	551.234	-565.594	499.447
	-483.299	-777.783	-617.765	269.731	-491.335	553.711	-566.982	500.443
	-484.321	-777.894	-618.522	272.915	-491.292	555.550	-567.288	500.434
	-501.839	-794.603	-636.789	275.340	-492.577	557.380	-568.854	500.477
	-502.026	-794.595	-636.032	278.235	-493.258	558.580	-570.046	500.689
	-502.060	-794.527	-637.419	281.810	-493.514	559.874	-571.246	500.945
minimum (mV)	-516.845	-809.568	-662.504	252.043	-489.854	543.744	-577.205	496.731
	-504.886	-798.281	-639.130	260.036	-490.926	546.238	-566.811	496.740
	-491.233	-784.976	-626.524	262.538	-491.743	548.110	-567.245	499.030
	-491.216	-785.070	-626.685	265.552	-492.629	550.179	-569.731	497.012
	-502.034	-794.927	-636.951	268.693	-493.139	551.660	-570.208	497.046
	-502.358	-795.335	-637.828	272.319	-493.463	553.899	-570.361	499.847
	-502.358	-795.233	-637.998	275.298	-494.033	555.635	-571.476	500.060
	-514.045	-805.329	-648.919	278.175	-495.029	557.082	-573.578	498.936
STD (mV)	3.979	3.561	7.564	1.294	0.404	0.729	2.396	0.590
	4.510	4.366	4.342	0.714	0.547	0.576	0.497	0.455
	0.096	0.048	0.185	0.941	0.195	0.643	0.390	0.056
	2.939	2.835	3.220	1.077	0.193	0.757	0.367	0.297
	5.603	5.119	5.550	1.016	0.296	0.844	0.490	0.443
	0.075	0.146	0.289	0.881	0.246	0.582	0.372	0.138
	0.051	0.102	0.205	0.811	0.193	0.654	0.433	0.152
	4.145	3.457	3.533	0.900	0.165	0.604	0.314	0.207
variance (mV^2)	15.830	12.683	57.209	1.674	0.163	0.531	5.741	0.348
	20.340	19.065	18.850	0.510	0.300	0.331	0.247	0.207
	0.009	0.002	0.034	0.886	0.038	0.413	0.152	0.003
	8.640	8.038	10.367	1.160	0.037	0.573	0.135	0.088
	31.395	26.209	30.804	1.032	0.088	0.713	0.240	0.197
	0.006	0.021	0.084	0.775	0.061	0.339	0.138	0.019
	0.003	0.010	0.042	0.657	0.037	0.428	0.188	0.023
	17.181	11.949	12.482	0.810	0.027	0.364	0.098	0.043

Table E-10: Color-coded summary of statistics during each period.

Standard Deviation (mV)								
	Sensor 2	Sensor 3	Sensor 5	Sensor 6	Sensor 7	Sensor 8	Sensor 9	Sensor 10
Entire Test (11/1 12:32 - 11/3 15:25)	9.234	8.467	10.296	7.569	1.885	4.353	2.679	0.629
1 - 48 hour period (11/1 12:35 - 11/3 12:34)	8.225	7.731	9.681	7.153	1.836	4.140	2.519	0.623
2 - 24 hour periods	9.743	9.400	12.275	---	1.389	2.123	---	0.646
	5.743	5.160	5.687	3.459	0.768	1.908	1.241	0.450
4 - 12 hour periods	9.118	8.877	12.679	---	0.969	0.932	---	0.738
	2.372	2.315	2.603	1.914	0.385	1.242	0.742	0.216
	5.929	5.534	6.061	1.829	0.440	1.037	0.771	0.452
	3.408	2.760	2.851	1.679	0.274	0.979	0.618	0.190
8 - 6 hour periods	3.979	3.561	7.564	---	0.404	0.729	---	0.590
	4.510	4.366	4.342	0.714	0.547	0.576	0.497	0.455
	0.096	0.048	0.185	0.941	0.195	0.643	0.390	0.056
	2.939	2.835	3.220	1.077	0.193	0.757	0.367	0.297
	5.603	5.119	5.550	1.016	0.296	0.844	0.490	0.443
	0.075	0.146	0.289	0.881	0.246	0.582	0.372	0.138
	0.051	0.102	0.205	0.811	0.193	0.654	0.433	0.152
	4.145	3.457	3.533	0.900	0.165	0.604	0.314	0.207

Note: Blue - stationary sensors, Green - Sensors moved, Red - Sensors NOT moved

Note: --- Invalid point do to start-up time

Table E-11: Data showing statistics that verify the distinction between stationary drift and slight movement.

Statistics for Standard Deviation from 8 - 6 hour periods					
	Average (mV)	Maximum (mV)	Minimum (mV)	STD (mV)	Variance (mV^2)
Stationary Sensors (blue)	0.504	1.077	0.056	0.272	0.074
Sensors NOT Moved (red)	0.133	0.289	0.048	0.081	0.007
Sensors Moved (green)	4.315	7.564	2.835	1.247	1.555

REFERENCES

"The Angle between two Planes." from http://members.tripod.com/vector_applications/angle_between_two_planes/.

Alampalli, S. (2005). N. Y. S. D. o. Transportation.

FHWA (2001). Evaluating Scour at Bridges. F. H. Administration. **HEC-18**.

Iskander, M. A., W; Gouvin, P (2001). "Instrumentation and Monitoring of a Distressed Multi-story Underground Parking Garage." Journal of Performance of Constructed Facilities **15**(3).

Marron, D. (2000). Remote Monitoring of Structural Stability Using Electronic Inclinometers. Structural Materials Technology IV - An NDT Conference

Mueller, D. S., Wagner, C.R. (2005). Field Observations and Evaluations of Streambed Scour at Bridges. DTFH61-93-Y-00050. Washington, D.C., Federal Highway Administration**:** 134.

NYSDOT (2005). Structural Forensic Investigation Report: BIN 109299A, Ramp AC, Dunn Memorial Bridge Interchange. Albany, New York.

Olson, L. D. (2004). Determination of Unknown Depths of Bridge Foundations for Scour Safety. Structural Materials Technology V: An NDE Conference. Cincinnati, OH, American Society for Nondestructive Evaluation.

Richardson, E. C., H-C; Briaud, J-L (2002). Instruments to Measure and Monitor Bridge Scour. First International Conference on Scour of Foundations.

Richardson, E. P.-O., JE; Schall, JD; Price, GR (2003). Monitoring and Plans for Action For Bridge Scour: Instruments and State Departments of Transportation Experiences. 9th International Bridge Management Conference

Schall, J. P., GR (2004). "Portable Scour Monitoring Equipment." NCHRP Report(515).

Schuyler, J. N. (2000). Automated Tiltmeter Monitoring of Bridge Response To Compaction Grouting. International Symposium on Smart Structures and Materials, Newport Beach, California.

Virto, A. L. (2000). Testing Tiltmeters for the Alignment System of the CMS Experiment. Santander, Spain, University of Cantabria.